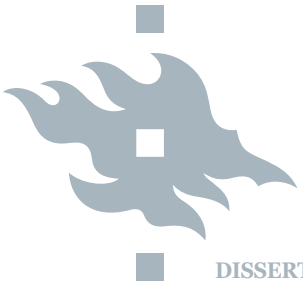

DISSERTATIONES SCHOLAE DOCTORALIS AD SANITATEM INVESTIGANDAM
UNIVERSITATIS HELSINKIENSIS

67/2017

MÓNICA FERREIRA

Multifunctional Nanoparticles for Targeted Drug Delivery and Imaging for Ischemic Myocardial Injury

DRUG RESEARCH PROGRAM
DIVISION OF PHARMACEUTICAL CHEMISTRY AND TECHNOLOGY
FACULTY OF PHARMACY
DOCTORAL PROGRAMME IN DRUG RESEARCH
UNIVERSITY OF HELSINKI

Division of Pharmaceutical Chemistry and Technology
Faculty of Pharmacy
University of Helsinki
Finland

Multifunctional Nanoparticles for Targeted Drug Delivery and Imaging for Ischemic Myocardial Injury

by

Mónica Ferreira

ACADEMIC DISSERTATION

To be presented, with the permission of the Faculty of Pharmacy of the University of Helsinki, for public examination in Auditorium 2 at Infocenter Korona (Viikinkaari 11, Helsinki) on December 15th, 2017, at 12.00 noon.

Helsinki 2017

Supervisors Associate Professor Dr. Hélder A. Santos
Drug Research Program
Division of Pharmaceutical Chemistry and Technology
Faculty of Pharmacy
Helsinki Institute of Life Science (HiLIFE)
University of Helsinki
Finland

Professor Dr. Heikki Ruskoaho
Drug Research Program
Division of Pharmacology and Pharmacotherapy
Faculty of Pharmacy
University of Helsinki
Finland

Professor and Dean Dr. Jouni Hirvonen
Drug Research Program
Division of Pharmaceutical Chemistry and Technology
Faculty of Pharmacy
University of Helsinki
Finland

Reviewers Professor Dr. Twan Lammers
Department of Experimental Molecular Imaging, University Clinic and Helmholtz Institute for Biomedical Engineering
RWTH Aachen University
Germany

Professor Dr. Ester Segal
Department of Biotechnology and Food Engineering and the Russell Berrie Nanotechnology Institute
Technion – Israel Institute of Technology
Israel

Opponent Professor Dr. Christel Bergström
Department of Pharmacy
Uppsala Biomedical Center
Uppsala University
Sweden

ISBN 978-951-51-3863-7 (Paperback)
ISBN 978-951-51-3864-4 (PDF)
ISSN 2342-3161

Helsinki University Printing House
Helsinki 2017

Abstract

Ferreira M., 2017. **Multifunctional nanoparticles for targeted drug delivery and imaging to the ischemic heart**

Dissertationes Scholae Doctoralis Ad Sanitatem Investigandam Universitatis Helsinkiensis, 67/2017, pp. 70
ISBN 978-951-51-3863-7 (Paperback), ISBN 978-951-51-3864-4 (PDF, http://ethesis.helsinki.fi), ISSN 2342-3161

Currently, there is no major discovery of an effective cure to restore the function of an injured heart, despite of the existing and developeing therapies. While existing options ameliorate the care of myocardial infarction (MI) and heart failure patients, cardiac stem cell therapy has only recently shown positive results in clinical trials, and thus there is an urgent medical need to develop advanced therapeutic entities to reverse this disease burden. The employment of biomaterials as potential therapeutics for MI is at the pre-clinical stage. Particulate systems are arising as a promising tool to provide minimally invasive treatment, an important aspect to take into account for clinical translation and patient compliance.

Porous silicon (PSi) and spermine-acetalated dextran (AcDXSp) are emerging biomaterials for applications in varying biomedical fields. Drug delivery is one of these fields benefiting from the materials' properties, such as biocompatibility, biodegradability, customized particle preparation, surface functionalization, simple yet efficient drug loading, and tunable release of the therapeutic cargos. Therefore, the aim of this thesis was to develop multifunctional PSi and AcDXSp platforms for targeted drug delivery to and imaging of the ischemic heart. Initially, the biocompatibility of PSi-based carriers of different sizes and surface chemistries was evaluated. Thermally hydrocarbonized PSi microparticles and thermally oxidized PSi nanoparticles showed better cytocompatibility *in vitro*, while *in vivo,* the thermally hydrocarbonized PSi microparticles activated pro-inflammatory and pro-fibrotic genes. However, all the particles showed no alterations in the cardiac function in both healthy and MI rats. Secondly, three different PSi-based nanosystems were developed, functionalized with a metal chelator for radiolabeling and three different peptides (atrial natriuretic peptide (ANP) and two other heart-homing peptides), with the aim to screen the targetability of the nanoparticles to the ischemic heart. All the nanosystems showed no toxicity up to 50 μg/mL concentration, and cell–nanoparticle interaction studies in cardiomyocytes and non-myocytes revealed a preferential cellular interaction with ANP-functionalized nanoparticles in both the cell types, through the natriuretic peptide receptors (NPRs) present at the cell surface. Thirdly, the ANP-PSi functionalized nanoparticles were PEGylated in order to improve the colloidal stability and enhance the circulation time, in isotonic 5.4% glucose solution and in human plasma. Upon labeling with radioisotope Indium-111, the ANP-PSi nanoparticles displayed a preferential accumulation and selectivity towards the endocardial layer of the ischemic heart. *In vivo* delivery of a cardioprotective small drug molecule from the ANP-PSi showed attenuation of the extracellular signal-regulated kinase pathway that is involved in the hypertrophic signaling of the injured heart. Lastly, and in parallel, the development of functionalized and dual-loaded AcDXSp nanoparticles for potential application in cellular reprogramming was proven successful, by utilizing acidic pH-triggered drug delivery of the two poorly water-soluble cargos. The incubation of non-myocytes with ANP-functionalized AcDXSp nanoparticles showed therapeutic modulation of key signaling pathways involved in the direct fibroblast reprogramming into cardiomyocytes. Overall, PSi and AcDXSp-based (nano)particulate systems were developed, bringing new insights about potential therapeutic advances in the applicability of imaging and targeted delivery of relevant pharmacological molecules to the ischemic heart with a minimally invasive therapeutic approach.

Acknowledgements

The last 4 years were an incredible and plentiful voyage of exciting experiences, professional and personal growth. Great people, from different cultural (and professional) backgrounds, a handful of really good friends, many lessons learned, uncountable failures and a few successes mark this now-ending chapter of my life. It is time to thank those that contributed to making this journey unforgettable. There is no physical space to express my gratitude to all those that contributed and were present, in every way, during this part of my life. I will try to be brief in the next couple of pages.

I start by acknowledging the University of Helsinki Doctoral Program in Drug Research for conceding me a grant to pursue my doctoral studies and develop the work presented in this thesis at the Division of Pharmaceutical Chemistry and Technology, Faculty of Pharmacy, University of Helsinki.

It was a privilege and an honor to be mentored by my three supervisors. I want to express my deepest gratitude to my supervisor Associate Professor Dr. Hélder Santos for everything he did for me. Hélder, you gave me the opportunity to start my doctoral studies at your group. Your kindness, ambition, and passion about great science truly inspire me. Your close guidance and unlimited professional (and personal) support contributed largely to the person and professional I am today. Most of all, you believed in me since day 1 and you pushed me forward when I thought I couldn't go any further. I will always admire you and look up to you. Obrigada por tudo!

I want to sincerely thank my supervisor Professor Dr. Heikki Ruskoaho for his valuable guidance and scientific input throughout my studies. Heikki, you are an encyclopedia of the Heart, and you truly inspired me in all our conversations. While after our meetings my brain was completely melted with so much information, your kindness and joyful attitude towards science, as well as our discussions helped me grow to who I am today. Literally, from the bottom of my heart, I hereby express my forever gratitude to you, for everything. Kiitos!

I also extend my sincere appreciation to my supervisor Professor and Dean Dr. Jouni Hirvonen, for allowing me to pursue my studies at his group and at this great institution. In addition, your scientific input, always supportive, thoughtful and understanding attitude helped me a lot throughout my studies. I will always be very grateful to you. Kiitos!

The series of acknowledgments follows with a big THANK YOU to all my co-authors, who provided me with their priceless help, cooperation, and great discussions. Your contributions made our work and this thesis possible, and without you, I would have never reached here. I start by thanking the Docent Dr. Jarno Salonen and Ermei Mäkilä, for our productive collaboration and discussions that largely contributed to this work. Ermei, you were always available to reply to my panic e-mails with questions about porous silicon and FTIR. Thank you! I also want to thank Dr. Marja Tölli and all the people from the University of Oulu that contributed for the first part of this thesis. In addition, I want to express a word of appreciation to Docent Dr. Anu Airaksinen and Dr. Sanjeev Ranjan for the fruitful cooperation and discussions, which also resulted in a large contribution for this thesis. Special thanks to Sini Kinnunen and Dr. Virpi Talman for teaching me everything I know about the isolation of heart cells, cell culture and related experiments, and above all, for being always so kind, supportive and patient with me. Sini, you were one of the first people that I worked with in the UH. Your kindness and welcoming attitude helped me to adapt to my new reality at that time. Thank you for teaching me about the isolation of heart cells and for our friendly conversations. Virpi, you are another encyclopedia and you truly fascinated me with so much knowledge and sense of organization. More than teaching me different techniques in the lab, your calmness and supportive words convinced me that I could do it. It was a real pleasure to work with the

two of you and I will never forget you. Kiitos! In addition, I acknowledge all the rats I had to work with, wishing that I have treated each one of them with the very much deserved care and respect.

A special word of gratitude to Professor Dr. Twan Lammers (Aachen University, Germany) and to Professor Dr. Ester Segal (Technion, Israel), who reviewed this thesis and provided constructive suggestions to improve this book. Your comments were extremely valuable and awaken my critical thinking.

I would like to express my thankfulness to all of those that are and were my colleagues and friends (in alphabetical order), Alexandra Correia, Dr. Barbara Herranz-Blanco, Dr. Dongfei Liu, Dr. Hongbo Zhang, Dr. Mohammed-Ali Shahbazi, Dr. Neha Shrestha, Patrick Almeida and Sérgio Almeida. You guys were there when I arrived to Finland and to the lab, provided the best atmosphere for my adaptation in the group and were my role models in the lab. I learned a lot from all of you. Thank you so much! I also want to express my gratitude to my other colleagues and friends Dr. Antti Rahikkala, Dr. Elisa Lazaro-Ibañez, Flavia Fontana, Giulia Torrieri, Jernej Štukelj, João Pedro Martins, Jukka Saarinen, Dr. Marlene Lopes, Patrícia Figueiredo, Dr. Sami Svanbäck, Tomás Ramos, Dr. Vimalkumar Balasubramanian and so many others (you are simply too many to mention here) with whom I shared and learned so much. You all were very important throughout these years and your words of motivation, time spend in and outside the lab, lunches, dinners, coffee breaks and other equally fun events made my stay in Santos' Lab so enjoyable. In particular, Alexandra, with you I gave my "first steps" in the lab and your help was precious throughout my studies. Ali, your friendship is priceless. You brought me to the core of your family and allowed me to be there with you when Anna was born. You and your family will always have a place in my heart. Sérgio, together with Alexandra, you and your funny humor were essential for my adaptation to the new life in Finland and your friendship throughout the years is unique. I am the luckiest person for having such a friend and brother-in-law! Obrigada, cunhado! Giulia, you were fundamental for the last part of this thesis. Your companionship, kind heart, and positive attitude were a key factor for this achievement. Thank you so much for your help, for your always motivating words and for being there. Grazie! João, you are such a kind person and always there when I needed a hug! You were holding my hand when I finally submitted this thesis and I will never forget that. You will always have a place in my heart, my friend! Obrigada, miúdo! Sami, mun rakas ystävä... You marked this chapter of my life in so many ways... I feel so lucky for having someone like you as a friend! "Friends will be friends..." Kiitos! I also thank all my colleagues at the division of Pharmaceutical Chemistry and Technology for the friendly and pleasant atmosphere, good company and for unreservedly sharing their technical support and knowledge. To all the people that I did not mention here but somehow crossed my life in this period, please be aware that I am so glad to have interacted with you in some way during this time. A big thanks to you all.

To my friends Miia, Riky, Behrouz and Islam, for the lovely and fun times we spent together. You made me feel closer to home. To my Portuguese friends Ana Rita, Ivo, Joana Guedes and Nuno, Joana Pereira, Joana Viseu, Liliana, Marta and Diogo, Patrícia, Tânia, Xu and Mário, I thank you all for being always there even though you were far. Your words of support and never-ending friendship made me realize that distance is just a detail and brought joy to my days ever since I met you. Amélias, obrigada por estes anos de amizade e apoio incondicional, pela companhia e partilha de todas as coisas, e por me fazerem sempre rir. Minha Joaninha, a nossa longa amizade e o teu apoio contínuo dão e deram-me muita força para continuar. Gmdti! Tânia, não há palavras para descrever o quão importante és na minha vida e em especial durante esta fase em que nunca me deixaste dizer "declaro que desisto".

Your friendship is priceless and I have no words to describe how grateful I am for having you in my life.

I need to deeply thank my family for the inconditional love and support, not only during these years but throughout my entire life. Sara, és a melhor irmã que alguém pode ter. Cumplicidade, amor de irmãs, amizade e apoio incondicionais são apenas algumas das palavras que descrevem tudo aquilo que és para mim. I extend my gratitude to my parents, José and Dulcí. Pai, Mãe, obrigada por tudo. O vosso amor, apoio e constante presença são a força que me inspira e me faz continuar sempre em frente. Tudo o que sou hoje devo a vocês e à excelente educação e valores que sempre me incurtiram. Espero estar à altura e fazer-vos muito orgulhosos. Obrigada por tudo! Dad, mom and Sara are the pilars that keep me standing strong. I cannot thank you enough.

Last but not the least, I want to show my deepest appreciation and love to my beloved Teemu, my boyfriend, my comrade, my best friend. You came into my life in the middle of this chapter like a pleasant breeze of fresh air, and you presented me with an infinite patience, unconditional support and love in the most demanding and difficult moments of this Ph.D. The successful end of this journey would not have been possible without you. I also thank Riitta, Petri and Juuso for taking me into your family in such a warming way, it definitely made me feel like home. My love, since we met you have been there all the time, for the good and bad times, and so I cannot thank you enough, ever. Life is best with you in it. Olet paras, mun rakkaani.

Helsinki, December 2017.

Mónica Ferreira

Life doesn't have to be perfect to be wonderful" – Annette Funicello

“Para ser grande, sê inteiro: nada
Teu exagera ou exclui.
Sê todo em cada coisa. Põe quanto és
No mínimo que fazes.
Assim em cada lago a lua toda
Brilha, porque alta vive”

– Fernando Pessoa

"Nas resilientes asas da Fénix
O meu voo
Qual renascer constante de um amor
Que assim se denuncia
Por uma busca permanente
Por um despertar diferente
A cada passo
Em cada dia
Nem sempre fácil
Nem sempre difícil
Mas sempre com igual propósito…
O de chegar mais além
Em conhecimento e sabedoria.

No voo rasante da Fénix
O meu voo infinito
Na vontade de ser e de vencer."

– Dulcí Ferreira

To my parents Zé and Dulcí, and to my sister Sara

Table of contents

List of original publications

This thesis is based on the following publications, which are referred to in the text by their respective roman numerals (**I–IV**).

I Tölli M.A.*, **Ferreira M.P.A.***, Kinnunen S., Rysä J., Mäkilä E., Szabó Z., Serpi R., Ohukainen P., Välimäki M., Correia A., Salonen J., Hirvonen J., Ruskoaho H., Santos H.A., *In Vivo* Biocompatibility of Porous Silicon Biomaterials for Drug Delivery to the Heart, Biomaterials, 2014, 35(29), 8394.

II **Ferreira M.P.A.**, Ranjan S., Correia A., Mäkilä E., Kinnunen S., Zhang H., Shahbazi M.-A., Almeida P., Salonen J., Ruskoaho H., Airaksinen A., Hirvonen J., Santos H.A., *In Vitro* and *In Vivo* Assessment of Heart-Homing Porous Silicon Nanoparticles, Biomaterials, 2016, 94, 93.

III **Ferreira M.P.A.***, Ranjan S.*, Kinnunen S., Correia A., Talman V., Mäkilä E., Barrios-Lopez B., Kemell M., Balasubramanian V., Salonen J., Hirvonen J., Ruskoaho H., Airaksinen A.J., Santos H.A., Drug-Loaded Multifunctional Nanoparticles Targeted to the Endocardial Layer of the Injured Heart Modulate Hypertrophic Signaling, Small, 2017, 13(33), 1701276.

IV **Ferreira M.P.A.**, Talman V., Torrieri G., Liu D., Marques G., Moslova K., Liu Z., Pinto J., Hirvonen J., Ruskoaho H., Santos H.A., Dual-drug Delivery using Dextran-functionalized Nanoparticles Targeting Cardiac Fibroblasts for Cellular Reprogramming. (*Submitted*)

*In publications **I** and **III**, the first two authors had equal contribution to the work.

Abbreviations and symbols

AcDX	Acetalated dextran
AcDXSp	Spermine-Acetalated Dextran
AcDXSp-P	AcDXSp-PEG
ACN	Acetonitrile
AF488	AlexaFluor 488®
ANP	Atrial natriuretic peptide
ATP	Adenosine triphosphate
ATR	Attenuated total reflectance
BNP	Brain natriuretic peptide
C1	Trisubsituted-3,4,5-isoxazole
$CoCl_2$	Cobalt chloride
Col Ia1	Collagen Iα1
CSFM	Complete serum-free medium
CS	CHIR99021 + SB431542
CVD	Cardiovascular diseases
DAPI	4',6-diamidino-2-phenylindole dihydrochloride
DDS	Drug delivery systems
DLS	Dynamic light scattering
DOTA	S-2-(4-aminobenzil)-1, 4, 7, 10-tetraazacyclododecane-1,4,7,10-tetrater-butyl acetate
DMEM	Dulbecco's Modified Eagle's Medium
DMEM/F12	DMEM + Nutrient Mixture F-12
DMSO	Dimethyl sulfoxide
EDC	1-ethyl-3-(3-dimethylaminopropyl)carbodiimide hydrochloride
EDX	Energy-dispersive X-ray spectroscopy
EE	Encapsulation efficiency
EGF	Epidermal growth factor
ELS	Electrophoretic light scattering
Endo/Epi	Endocardial/Epicardial ratio
ERK 1/2	Extracellular signal–regulated kinase 1/2
FTIR	Fourier transform infrared spectroscopy
GADPH	Glyceraldehyde 3-phosphate dehydrogenase
GSK3B	Glycogen synthase kinase 3β
H&E	Hematoxylin and eosin
HBSS	Hank's balanced salt solution
HEPES	4-(2- hydroxyethyl)-1-piperazineethanesulfonic acid
hiFBS	Heat inactivated fetal bovine serum
HPLC	High performance liquid chromatography
IHD	Ischemic heart disease
i.v.	Intravenous
IL-6	Interleukin-6
LAD	Left anterior descending coronary artery
LD	Loading degree
LV	Left ventricle
MAPK	Mitogen-activated protein kinase
MEK1	MAPK kinase-1
MES	2-(N-morpholino)ethanesulfonic acid

MI	Myocardial infarction
miRNA	Micro RNA
MTT	Thyazolil blue tetrazolium bromide
NHS	N-hydroxysulfosuccinimide
NPR-A/C	Natriuretic peptide receptor A/C
OSP	Osteopontin
o/w	oil-in-water
PBS	Phosphate buffered saline
PEG	Polyethylene glycol
PET	Positron emission tomography
PLGA	Poly(lactic-co-glycolic acid)
PS	Penicillin/Streptomycin
PSi	Porous silicon
PVA	Polyvinyl alcohol
P2	CSTSMLKAC
P3	CRSWNKADNRSC
RGD	Arginyl-glycyl-aspartic acid peptide
ROI	Region of interest
SC	Stem cells
SEM	Scanning electron microscopy
S.E.M.	Standard error of the mean
SPECT/CT	Single-photon emission computed tomography
SPIO	Superparamagnetic iron oxide
SUV	Standardized uptake value
TC	Thermal carbonization
TCPSi	Thermally carbonized porous silicon
TEA	Triethylamine
TEM	Transmission electron microscopy
TFA	Trifluoroacetic acid
TGF-β	Transforming growth factor beta
TH	Thermal hydrocarbonization
THCPSi	Thermally hydrocarbonized porous silicon
TIPS	Triisopropylsilane
TNF-α	Tumor necrosis factor-α
TO	Thermal oxidation
TOPSi	Thermally oxidized porous silicon
Un-D	UnTHCPSi-DOTA
Un-D-ANP	UnTHCPSi-DOTA-ANP
Un-D-P2	UnTHCPSi-DOTA-P2
Un-D-P3	UnTHCPSi-DOTA-P3
Un-P	UnTHCPSi-PEG
Un-P-D	UnTHCPSi-PEG-DOTA
Un-P-D-ANP	UnTHCPSi-PEG-DOTA-ANP
UnTHCPSi	Undecylenic acid modified THCPSi
w/o/w	water-in-oil-in-water
α-SMA	Alpha smooth muscle actin
ζ-potential	Zeta-potential

1. Introduction

Cardiovascular diseases (CVD) cause the highest mortality rates globally, and over one-third of the CVD-related casualties are due to the ischemic heart disease (IHD).[1, 2] Because IHD causes injury to the myocardium, and the heart has extremely limited capacity to recover from the ischemic insult,[3] the progress of the initial ischemic event – myocardial infarction (MI) – leads to a decompensated state characterized by scar formation, ventricular wall dilation, thinning and hypertrophy.[4-6] This pathological state – heart failure – is irreversible, having no cure up to date. While the currently available therapeutics do not perform towards curing the disease, but rather treat the symptoms and/or try to stop the progression of the disease, they only provide a certain improvement in the state of care of heart failure patients. Therefore, there is an unmet need to find a permanent solution for these patients.

The understanding of the basic mechanisms that lead to the development and progression towards heart failure has emphasized the vast complexity of the molecular and cellular mechanisms that govern the pathological process of this disease and, over time, more and more of this puzzle is uncovered. The clarification about the characteristic pathological processes of heart failure leads to the identification of new therapeutic targets.[7] Alternatively to the pharmacological medicines and implantable devices available in the clinic for heart failure patients, other therapeutic approaches are currently being investigated and developed. To name a few, cell therapy, cardiac tissue engineering and particulate systems have been increasingly studied to tackle the problematic of cardioprotection and cardio restoration that the current therapies lack.[8-11]

While pharmacological medication may be administered orally or intravenously, implantable devices require risky surgical procedures that many times put the lives of patients at stake. In both cases, the benefits are temporary and only amelioration of the patients quality of life is achieved. For newly developing therapeutics strategies, such as cell therapy or cardiac tissue engineering, the administration routes required are always highly invasive.[12, 13] Ideally, intravenous (*i.v.*) or oral administration routes are preferred for patient compliance and are regarded as an important factor to take into account when considering clinical translation.[14] Thus, nanoparticulate systems are more suitable for administration by minimally invasive routes, such as the *i.v.* route. Besides the advantageous possibility of *i.v.* administration, nanocarriers are versatile platforms for the creation of functional nanosystems. This is due to their tunable properties, which are for example dictated by the type of material, size, surface chemistry, porosity, or surface area. This brings up the possibility to deliver one or more payloads with similar or different physicochemical properties, allowing the creation of functional carriers for specific targeting, stimuli responsiveness, imaging or more than one feature in the same nanocarrier, leading to versatile applications in different pathologies.[15, 16]

Porous silicon (PSi) and acetalated dextran (AcDX) are two of the many different examples of biomaterials available for the production and development of nanoparticulate systems. On one hand, PSi materials have been widely studied for different applications in the biomedical field, due to their attractive properties, such as tunable porosity and surface chemistry, stability, high surface area, biocompatibility, and biodegradability.[17-30] On the other hand, AcDX tackles some problems of PSi materials, such as the leakage of cargos, as the polymeric matrix only allows drug release below certain pH values, featuring a triggered cargo release upon exposition to an acidic pH stimulus.[31] Thus, there exists evident potential for both the biomaterials with increasing interest to be explored for new applications for these biomaterials, such as the treatment of MI and heart failure.

This thesis project began by investigating the biocompatibility of different surface chemistries and sizes of PSi-based particles, a biomaterial that had not been employed for MI

therapy before. Upon favorable biocompatibility features, the surface functionalization of the PSi nanoparticulate systems was done with a metal chelator for radiolabeling purposes, followed by attachment of different heart-homing peptides to enhance therapeutic efficacy. Next, the different nanosystems developed were screened to find out the most promising nanosystem(s) for targeted drug delivery and imaging, and for clarification of the mechanism of the cell–nanoparticle interactions. Additional stability protection was provided by coating the most promising nanosystem with polyethylene glycol (PEG), followed by detailed *in vivo* characterization and evaluation of the biodistribution and heart accumulation. In addition, proof-of-concept studies of the potential bioeffect upon delivery of a cardioprotective compound to MI diseased hearts were investigated. In parallel, the polymeric nanocarrier (AcDX) was investigated for the ability to deliver two relevant pharmacological small molecules, involved in the direct cellular reprogramming of fibroblasts to cardiomyocytes, with similar physicochemical properties in a pH-dependent fashion, for combination drug therapy. The release of the two drugs was evaluated in physiologically relevant environments, such as the intracellular acidic (pH 5) and the extracellular (pH 7.4) compartments. Furthermore, the *in vitro* drug delivery and biological effects of the developed functionalized nanoparticles were assessed, for further application in the direct pharmacological reprogramming of cardiac fibroblasts.

2. Literature overview

2.1. Ischemic heart diseases and therapeutic approaches

2.1.1. Cardiovascular diseases

Cardiovascular diseases (CVD) are characterized by a group of disorders of the heart and blood vessels, including hypertension, coronary heart disease, cerebrovascular disease, peripheral vascular disease, heart failure, rheumatic heart disease, congenital heart disease, and cardiomyopathies, according to the World Health Organization.[2] They are mainly the result of improved public health measures over the 20th century, shifting from causing less than 10% of deaths in the early 1900's to the reality of becoming the leading cause of death, and a great economic and resource burden on public health systems in the present days.[32-34] Official reports state that CVD are the number 1 cause of death globally, which in 2015 represented 17.7 million casualties (31% of all global deaths) caused by some form of CVD. Out of this colossal number, 7.4 million deaths were due to coronary heart disease, causing 1 out of 6 deaths in the USA in 2010.[34, 35] The 5-year survival rate for heart failure patients is disturbing, worse than for most cancer patients. Remarkably, the costs of care exceed US$30 billion per year in the United States.[36] In Europe, CVD cause 3.9 million deaths each year. The number of existing cases is astonishing, more than 85 million people live with this burden and about 11.3 million new cases of CVD arose in 2015. The overall costs of CVD to the European Union economy are estimated as €210 billion a year.[35] In Finland, ischemic heart diseases (IHD) are still a major cause of death, despite a substantial decrease over the years. IHDs caused 1 out of 5 deaths in Finland in the year 2014.[37]

2.1.1.1. The heart and its cellular composition

The heart is a structurally complex organ divided into four chambers, namely two atria and two ventricles. The right atrium and right ventricle pump venous blood to the pulmonary circulation to be oxygenated. When returning to the heart, oxygenated blood enters the left atrium and is pumped out to the systemic circulation by the left ventricle (LV). While the atria are characterized by a thin wall and function as large reservoir conduits of blood for their respective ventricles, the ventricles in turn act as pumping agents for the propulsion of blood.[38] **Figure 1** shows a simplified anatomical structure of the heart.

The heart architecture is composed of cell types of different features, which contribute to the heart structure, as well as for the mechanical, biochemical and electrical properties. The three main cardiac cell types with respect to the number of cells are cardiomyocytes, endothelial cells (forming the endocardium, the interior of blood vessels and cardiac valves), and fibroblasts. With regards to the relative numbers, the cell counts differ substantially and depend not only on the species, age, and gender but also on, for example, the lack of a unique and comprehensive marker for fibroblasts, hindering the precision analysis of the cardiac cell types and relative abundances, as fibroblasts are composed of heterogeneous cell populations.[39, 40] For this reason, several publications have listed fibroblasts as one of the most abundant cardiac cells.[39-42] Yet, recent reports acknowledge endothelial cells and cardiomyocytes as the most abundant cell types in adult murine and human hearts, followed by fibroblasts.[5, 43] Other important cell groups are the smooth muscle cells, epicardial cells, and the electrical impulse conductors, pacemaker cells and Purkinje fibers (**Figure 1**).[3] All the

cardiac cells work harmoniously to allow the heart to do its job: to provide a continuous blood circulation to the whole body.

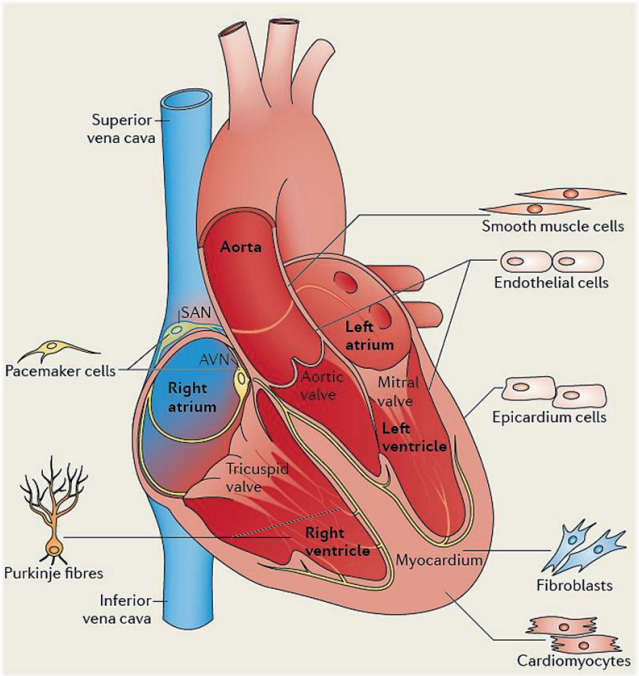

Figure 1. The heart structure and its constitutive cardiac cell types. Copyright © 2013 Nature Publishing Group. Abbreviations: AVN, atrioventricular node; SAN, sinoatrial node. Adapted with permission from ref.[3].

2.1.1.2. Myocardial infarction and hypertrophic signaling

Myocardial infarction (MI) is defined by the loss of viable cardiomyocytes in response to a prolonged shortage in blood supply in the heart muscle, causing a deprivation of oxygen and glucose needed for cellular metabolism. MI can be the manifestation of coronary artery disease for the first time, or occur repeatedly in patients with established disease.[44] Upon an ischemic event, the development of histological cell death begins as early as in 20 min,[45] and complete necrosis may be identified after 2–4 h, or even longer, after the onset of MI. This depends on several factors, such as the existence/abundance of collateral blood circulation in the ischemic area, individual oxygen and nutrient demands, the application of preconditioning (where repetitive short episodes of ischemia protect the myocardium against a later ischemic insult), sensitivity of the myocytes to ischemia, and permanent or intermittent occlusion of the coronary artery.[46] In particular, the LV wall encompasses three different layers that include the endocardial layer (inner oblique), myocardium (middle circular) and the epicardial layer (outer oblique), which translate into differences in the deformation and function patterns across the LV wall. In systole, the endocardial layer is subjected to greater straining dimentional deformations than any other transmural layer of the LV, having a major contribution to the the heart function. However, in MI, this inner oblique layer is the most

vulnerable and the first affected area upon an insult caused by ischemia,[47] characterized by evident morphologic and functional changes, leading to a detrimental function of the heart.[48]

In response to an ischemic insult and consequent increase in loading conditions and ventricular wall stress, the heart will develop reparative phenotypic alterations, triggering a cascade of biochemical intracellular signaling processes. The initial post-MI phase of LV remodeling results from fibrotic repair of the necrotic area with collagen scar formation, elongation, and thinning of the infarcted zone. This is an adaptive attempt of the heart to normalize the stroke volume and cardiac output.[49] Due to wall stress, this early adaptation can progress into a decompensated state with deep changes in gene expression, contractile dysfunction, and extracellular remodeling.[50, 51]

In addition, the remodeling process is also driven by myocyte hypertrophic enlargement in the non-infarcted areas, resulting in an overall increased wall mass, ventricular dilation and shape adjustment towards spherical chamber configuration.[52, 53] LV remodeling may last for several weeks or months, and will depend, among others, on the size, location, transmural extent of the infarct, and/or local trophic factors.[54] This remodeling results in progressive deterioration of ventricular performance and can ultimately lead to heart failure (**Figure 2**).[55, 56]

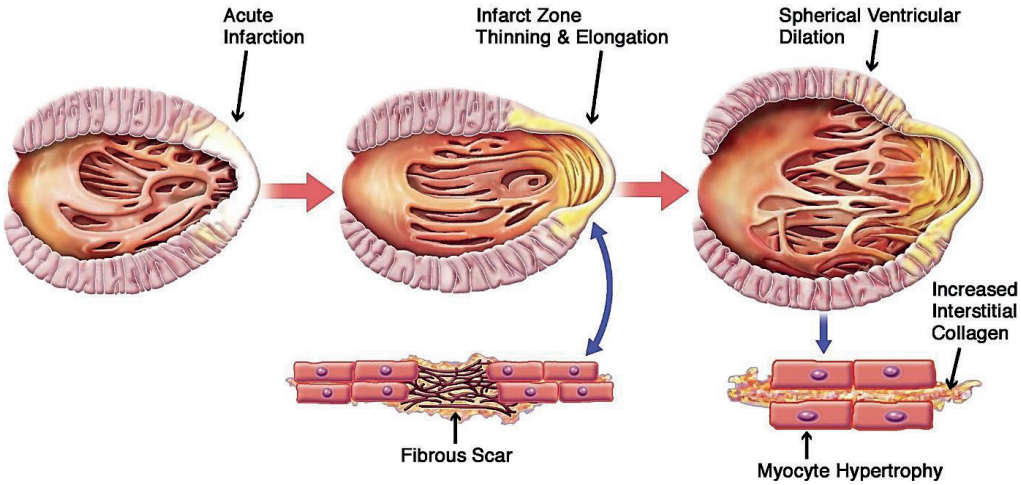

Figure 2. Schematic representation of post-myocardial infarction left ventricular remodeling. The early phase is characterized by thinning and elongation of the fibrous scar within the infarcted zone. Subsequent LV dilation, with a transition from an elliptical to a more spherical configuration, is driven essentially by diffuse myocyte hypertrophy associated with increased apoptosis (not shown) and increases in interstitial collagen. Copyright © 2011 American College of Cardiology Foundation, Elsevier Inc. Reprinted with permission from ref.[56].

Hypertrophic signaling is heavily influenced and stimulated by ventricular wall distress. Many transcriptional and growth factors are upregulated in hypertrophy and serve as potential therapeutic targets. Among them, this thesis gives emphasis to the extracellular signal–regulated kinases (ERK) from the mitogen-activated protein kinase (MAPK) family as

a therapeutic target and natriuretic peptides (in particular, atrial natriuretic peptide (ANP)) as a potential targeting moiety.

Cardiac hypertrophy and ERK1/2 pathway as a therapeutic target

ERK 1/2 belongs to one of the 4 MAPK subfamilies and has important roles in heart development and pathological processes, such as hypertrophy, cardioprotection *vs*. myocardial cell death, or other cardiac remodeling events, including chamber dilation, fibrosis, and changes in structural proteins and ion channels.[57] ERK 1/2 hypertrophic signaling is characterized by phosphorylation of the ERK 1/2 protein, which in turn activates transcription factors in the nucleus and leads to the hypertrophied phenotype of cardiomyocytes.[58] Previous reports have shown the involvement of ERK pathway with hypertrophy in the myocardium.[59-62] For example, Bueno *et al.*[62] demonstrated that MAPK kinase-1 (or MEK1) transgenic mice with established concentric hypertrophy and MEK1 adenovirus-infected neonatal cardiomyocytes had ERK1/2 activation, revealing that the MEK1–ERK1/2 signaling pathway is involved in hypertrophy. Thus, the observation that the inhibition of ERK 1/2 pathway attenuates hypertrophy and makes researchers believe that this could constitute a therapeutic target. Peng *et al.*[63] observed that angiotensin II and epidermal growth factor (EGF) increase the phosphorylation of ERK and lead to hypertrophy in myoblastic H9c2 cells. By using pharmacological inhibitors and gene silencing, they observed decreased phosphorylation of ERK, demonstrating a protective effect of these therapeutics against hypertrophy induced by angiotensin II.[63] Another study supported the use of peptides to inhibit Ca^{2+}/calmodulin protein kinase II to reduce cardiac hypertrophy both in *in vitro* and *in vivo* models, with the observation of significantly reduced ERK phosphorylation.[64] Thus, exploring the possibility of reducing the phosphorylation of ERK *in vivo* using heart-targeted nanoparticles is one of the aims of this thesis.

Natriuretic peptides and natriuretic peptide receptors

Natriuretic peptides are circulating hormones produced mainly in the heart. In humans, the natriuretic family consists of atrial natriuretic peptide (ANP), brain natriuretic peptide (BNP), and C-type natriuretic peptides.[65-67] Natriuretic peptides have a pivotal role in the regulation of intravascular plasma volume, fluid retention, and vascular tonicity, by increasing renal excretion of salt and water, vasodilation, and vascular permeability.[68-70] Moreover, ANP has been demonstrated to have a paracrine role in the regulation of fibroblast growth and mitogenesis during cardiac hypertrophy,[71] cardioprotective properties, antiapoptotic effects, and inhibited hypertrophy of cardiomyocytes.[72] In the event of MI and in heart failure, the plasma levels of ANP and BNP are significantly elevated, and their upregulation takes place during hypertrophy.[73-75] In particular, studies suggest that the expression of both ANP and BNP are increased in hypertrophy, in the margins of the infarcted zone of the LV, and ANP was particularly produced in the fibroblasts that invaded the infarcted myocardium and along with their transition to myofibroblasts.[76] Therefore, the detection of ANP and BNP serum levels is currently used as a biomarker in the diagnostics and prognostics of hypertrophy and heart failure.[75, 77, 78]

Natriuretic peptide actions are mediated by natriuretic peptide receptors (NPR), in particular, the NPR-A or guanylyl cyclase-A, and the NPR-B. There is a third NPR, responsible for the clearance natriuretic peptides, the NPR-C. ANP is a ligand for the NPR-A, exerting its known natriuretic effects by catalyzing the synthesis of cyclic guanosine monophosphate

(cGMP). ANP also binds to the clearance NPR-C, being cleared from the extracellular environment through receptor-mediated internalization and degradation.[79] This receptor, together with neutral endopeptidases, is responsible for the very short half-life of ANP (1.7–3.1 min) (**Figure 3**).[80-83] Although NPR-A is widely expressed in different organs, such as lungs, kidney, adrenal gland, brain, testis and vascular smooth muscle tissue, it has been described to be expressed in several regions of the heart. NPR-C is also reported to be expressed in the endocardium of primate hearts and in rat hearts.[84, 85] In humans, NPR-A mRNA is present in the LV, while NPR-C has an even distribution in both the ventricles.[86] At the cellular level, both NPR-A and NPR-C are present in cardiac cells. Cardiac fibroblasts seem to express all NPR, but predominantly the NPR-C (approximately 80%), while all NPR are observed for cardiomyocytes, although the most significant NPRs were predominantly NPR-A and possibly NPR-C.[71, 85]

Based on the presence of NPR-A and NPR-C in cardiac cells, in this thesis, it was explored the possibility of homing drugs inside nanoparticles into the cardiac cells and the heart using the ANP peptide as a targeting moiety.

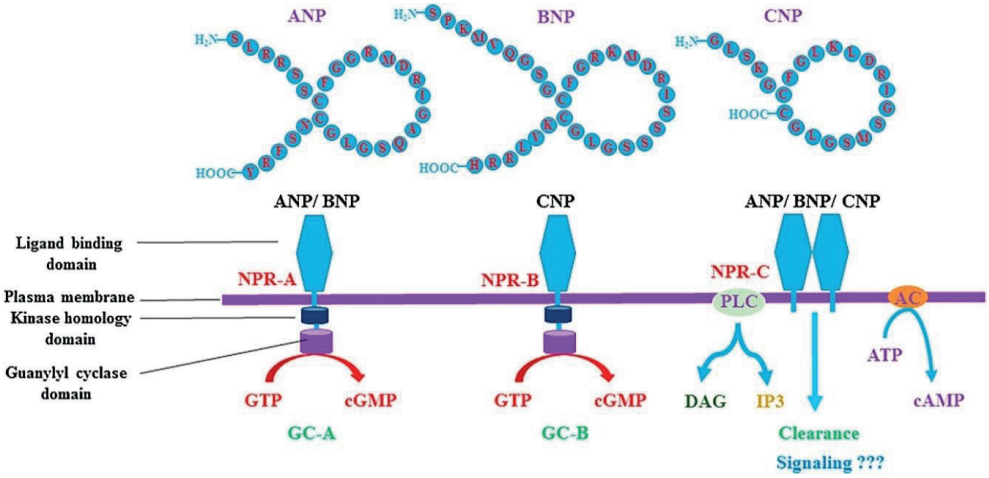

Figure 3. The three main types of natriuretic peptides and the NPRs. Reprinted with permission from ref. [87].

2.1.1.3. Small animal models for myocardial ischemia

Animal models of MI are necessary to validate the finding on *in vitro* cell models, providing a better understanding of the pathological mechanisms of the disease. In addition, they serve as tools for investigation of possible therapeutic interventions and are useful for studying the biodistribution and bioeffects of drug delivery systems (DDS) in a real context. In the case of small animal models, such as rodents and rabbits, the most common methods to induce MI are either by the left anterior descending artery (LAD) surgical ligation, genetic modifications (for mice), and chemical induction.[88] In this thesis, both LAD and chemically induced MI in rodent models were used.

LAD ligation is the most used surgical induction of acute MI by blocking the LAD either permanently or for a limited amount of time.[89] Infarctions can be induced by ligating different

regions of the coronary artery and provide a localized, although with variable sizes, infarction in the LV.[90] In addition, the use of catecholamines, such as isoprenaline, (β-receptor adrenergic agonist) is a well-established non-surgical method to induce MI chemically in animal models like rats.[91] This model is more advantageous than the LAD model due to the fewer mortality rates of animals. It has been reported that the hearts of isoprenaline MI animal models display a rise in cardiac marker enzymes, and metabolic and morphologic abnormalities similar to those observed in human MI, as it causes severe stress and produces necrosis in the ventricular subendocardial region and the inter-ventricular septum.[92, 93] Isoprenaline induces acute diffuse myocyte damage upon a single subcutaneous or intraperitoneal injection. The principle of injury is based on the infliction of alterations in intracellular Ca^{2+} leakage, due to hyperphosphorylation of the ryanodine receptor 2 of the sarcoplasmic reticulum.[94] The acute increased levels of isoprenaline are cardiotoxic, leading to significant myocyte loss and hypertrophy in the long term.[95-97] Both animal models are widely used in the assessment of the therapeutic cardioprotective potential of natural and synthetic entities.[88, 98, 99]

2.1.2. Treatment of myocardial infarction and heart failure

2.1.2.1. Current therapeutics

The LV remodeling is closely related to the activation of a series of upregulated factors after MI, hemodynamic imbalance and augmented LV wall stress. Paracrine, neuroendocrine, and autocrine factors include the adrenergic nervous system, renin-angiotensin-aldosterone axis, increased oxidative stress, as well as pro-inflammatory cytokines and endothelin-1.[56] Thus, the current therapeutic interventions for MI patients mainly attempt to prevent recurrent ischemic events, reduce congestion, delay pathological remodeling, and preserve myocardial contractile function by maintaining myocyte viability.[100] At present, the therapeutic options clinically available for MI patients only ameliorate their survival, care, and thus, the prevalence of the disease.[101] To date, no cure has been found for this burden. The main therapies for MI include changes in the lifestyle, reduction of afterload, and β-adrenergic and renin–angiotensin–aldosterone blockage. For patients with advanced disease, the use of mechanical support devices is considered and, ultimately, heart transplantation.[55, 102] A brief list of the currently used pharmacological groups [99] and implantable heart devices/surgical procedures [103, 104] are summarized in **Table 1**.

Table 1. *Pharmacological therapeutic approaches and surgically implantable devices used for the therapy of MI and heart failure.*

Pharmacological therapy	***Surgically implantable devices***	***Refs.***
Angiotensin-converting enzyme inhibitors Angiotensin-receptor blockers β-blockers Mineralocorticoid-receptor antagonists Ivabradine Diuretics Digoxin Hydralazine, Isosorbide dinitrate	Ventricular assist devices Pacemakers (cardiac resynchronization therapy) Cardioverter-defibrillators Coronary artery bypass Angioplasty Stent	55, 101-104

2.1.2.2. Therapeutics under development

As the existing therapeutic options do not stop the high mortality rates and morbidity of heart failure, this complex pathology is now actively investigated, in order to better understand the pathophysiological mechanisms, as well as to discover new therapeutic targets and approaches for the prevention of remodeling or at least improvement of patient care. Different therapeutic approaches are investigated, either for cardioprotective or cardio restorative purposes, leading to the development of most diverse strategies to tackle the burden of heart failure.[105] Discovery and use of small drug molecules and biologics, gene therapy, cell therapy, tissue engineering, particulate systems, or a combination of them are the main research considerations of today.

Cardiac regeneration provides new hope for the treatment and cure of heart failure. While zebrafish heart can fully regenerate after amputation of the heart apex, the mammalian adult heart has limited regenerative potential,[106] despite a certain degree of cell renewal capacity of cardiomyocytes in both mice [107] and humans.[108] However, the heart regeneration extent is still under active discussion,[109, 110] as the turnover and source of cardiomyocytes are not clarified, attributed to endogenous and exogenous progenitor cell niches,[111-112] or even to the division of existing cardiomyocytes.[113] Thus, research efforts are intensively continued towards the development of novel cardiac regeneration therapies.

Small drug molecules and biologics

Small drug molecules and biologics constitute promising deliverables for MI therapy. Particular advantages make these entities attractive, such as often inexpensive fabrication and storage. Advances in synthetic chemistry have led to large libraries of structurally diverse molecules that are screened for efficacy, identification of new molecular targets and elucidation of unknown signaling pathways involved in the pathology of MI. For example, stabilization of the calcium cycling process in cardiomyocytes is regarded a new therapeutic target, bringing up to light new drug molecules, such as derivatives of 1,4-benzothiazepine for stabilization of the type 2 ryanodine receptors,[114] or omecamtiv mecarbil, a compound that enhances the sensitivity of cardiac myosin to calcium to improve cardiac function.[115] Another example, pyrivinium pamoate, which is specifically cytotoxic for fibroblasts, has been investigated as a potential drug for anti-fibrotic therapy.[116]

There is an increasing interest in the screening and development of small drug molecules for myocardial regeneration purposes.[117] Enhancement of cardiomyocyte proliferation was previously achieved with the administration of fibroblast growth factors, neuregulin 1, periostin or prostaglandin E2.[118-121] In contrast, direct reprogramming of cells into cardiomyocyte-like cells is another strategy to repair the injured myocardium. Sole or combinational therapy with small drug molecules has also shown successful in cell reprogramming. A list of small molecules used for cardiac reprogramming is listed by Xie *et al.*[122] As an example, a combination of CHIR 99021 (glycogen synthase kinase 3β (GSK3B)), SB431542 (transforming growth factor (TGF)-β signaling inhibitor), parnate ((LSD1/KDM1 inhibitor) and forskolin (adenylyl cyclase activator), in combination with the transcription factor Oct4, led to the direct reprogramming of mouse fibroblasts into induced cardiomyocytes.[123] This is a trivial demonstration of the great potential of small drug molecules towards the achievement of cardiac regeneration, a sub-field of the therapy for CVD that is emerging fast.

MicroRNA therapy

Among the different gene therapeutic approaches, microRNA (miRNA) is currently in the spotlight regarding the gene therapy for MI.[124] They can be used, for example, in the inhibition of hypertrophy[125, 126] or as cardioprotection of apoptotic effects of β-blockers.[127] Cardiac reprogramming has been also achieved using miRNAs. The administration of different miRNAs (1, 133, 208 and 499) induced a low-efficiency reprogramming of murine fibroblasts into cardiomyocyte-like cells.[128] A recent study showed that combination of transcription factors (Gata4, Hand1, Tbx5, and myocardin) and miRNAs-1 and -133 successfully induced the reprogramming of human fibroblasts into cardiomyocyte-like cells.[129]

Cell therapy

Transplantation of stem or progenitor cells into the injured heart brings up hope that new cardiac tissue is regenerated with, therefore, improved cardiac function. Thus, scientists and healthcare professionals see great potential in cell therapy for MI patients. A high number of cell types has been investigated for cardiac regeneration purposes in vast preclinical and clinical trials.[130] The included cell types are skeletal myoblasts, embryonic stem cells (SCs), bone marrow-derived mesenchymal SCs, adipose-derived mesenchymal SCs, embryonic SCs and cardiac SCs. Although the different cell types tested have shown potential benefits *in vitro* and in pre-clinical trials,[131-138] only cardiac and cardiopoietic SCs demonstrated the most promising results regarding efficacy.[139-143] For example, the C-CURE clinical trial investigated the transplantation of cardiopoietic mesenchymal SCs to MI patients, with demonstrations of improved safety and efficacy results, such as 7% increase in LV ejection fraction, improved exercise tolerance and positive effects on hemodynamics.[143]

Tissue engineering

A major problem in the clinical translation of cell therapy is the delivery and retention of cells in the cardiac tissue, as the majority of the transplanted cells do not preserve viability and are not able to provide a therapeutic effect. The administration strategy of cells can also constitute a problem, implying the suspension of cells in saline for systemic infusion, perfusion into the coronary vessels and direct injection into the injured myocardium, strategies that do not provide a proper environment for cell survival, or have the ability to localize and retain the cells at the target site.[110, 144-147] Biomaterial scaffolds and carriers were brought up as a solution for cell delivery to the target site, engraftment of cells to the injured tissue, and maintenance of cell viability, by engineering them to provide a favorable environment for cell survival and proliferation. In addition, they may promote the production of beneficial paracrine factors, and have additional effects by exerting mechanical therapy and offering physical support. These systems are mainly formulated as cell-loaded *in situ* polymerizable injectable hydrogels or pre-formed cell-seeded scaffolds, attachable to the epicardium.[130, 148, 149] Moreover, cardiac scaffolds and hydrogels can be applied as cell-free substrates for promoting mechanical reinforcement, tissue bulking in the scar zone, and serve as protective and drug delivery systems. In the field of cardiac tissue engineering, several natural or synthetic materials have been applied to form the backbone of the engineered substrate. Examples of cell-loaded and cell-free biomaterials for cardiac tissue engineering applications comprise hydrogels made of fibrin,[150-152] polyethyleneglycol,[153, 154] alginate [155] or chitosan.[156, 157] Pre-formed scaffolds may be composed of, for instance, collagen,[158, 159] chitosan,[160] and hemoglobin/gelatin/fibrinogen.[161]

Particulate systems

Over time, the research focus of CVD treatment has been expanded to different areas, some of them already reviewed above. The use of particulate systems for the treatment and diagnostics/imaging of MI has arisen in recent years to overcome important obstacles of traditional and developing therapies: to target the injured myocardium, to overcome the problems of extremely invasive administration routes, to provide protection for short half-life biologicals, to improve the physical properties of drug cargos, such as the solubility and stability, and to promote controlled delivery of one or more therapeutic drugs.[10, 162] Although some literature references still describe the use of (micro) particulate systems for local administration into the myocardium, micro- and nanoparticles have been developed to avoid this invasive need, an important factor to take into account when considering clinical translation.[14, 163]

The next section will be devoted to reviewing previous reports on micro- and nanoparticulate systems developed for the therapy and diagnostics/imaging of MI. The main developing therapeutic strategies for MI are presented in **Figure 4**.

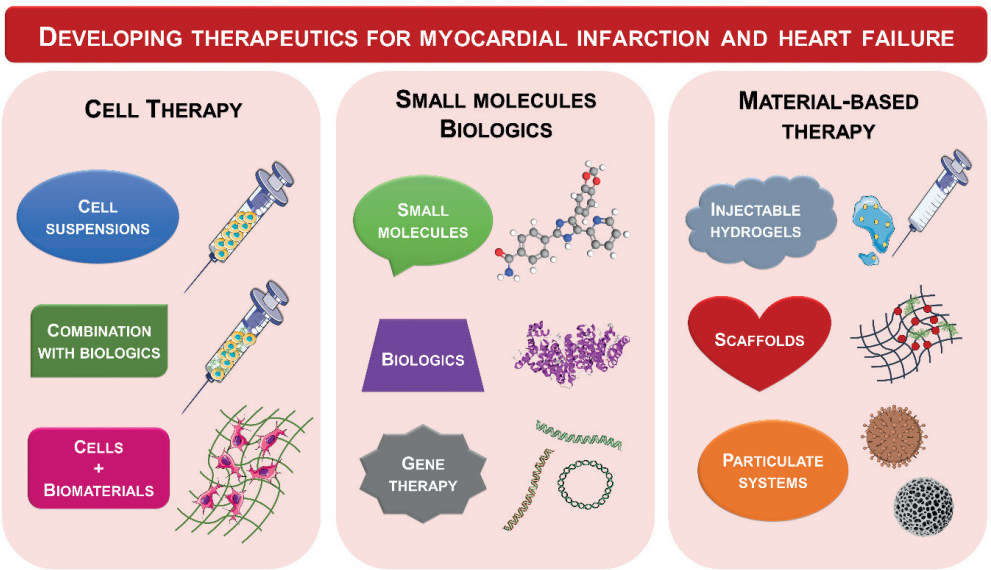

Figure 4. Summary of the different therapies used for the treatment of MI under investigation. The figure was constructed partly using Servier Medical Art.

2.2. Overview of micro- and nanoparticulate-based medicines for cardiovascular diseases

Although there are several therapeutic options for MI patients, there is no cure for this burden. As mentioned above, the prevalence of mortality and morbidity cases is plentiful, and the limited efficacy and harmful side effects of therapeutics and invasive procedures greatly affect the patients' quality of life. Along with other investigated therapeutic strategies, the development and application of micro- and nanomedicines for CVD is now increasing.[9]

Regarded as versatile tools, particulate carriers possess tailoring properties by changing the material's shape, chemically modifying and attaching the particle surfaces with targeting, imaging, and therapeutic moieties, or simply loading them with therapeutic and/or imaging entities (**Figure 5**).[164] For example, liposomes have the ability to entrap high amounts of payloads,[165] and polymeric and metal oxides may be functionalized with a variety of ligands for different purposes.[166] Particles may also be functionalized to improve the biodistribution,[167-169] act as therapeutic entities themselves, [170] or serve as DDS for poorly-water soluble drugs, thus improving their dissolution rate due to the particle's high surface-to-volume ratio.[171, 172]

Researchers are now gathering all these features to the availability of comprehensive information about the cardiac pathological processes at the cellular and molecular levels. As a result, micro- and nanomedicine are evolving as a multidisciplinary field to circumvent the limitations of conventional therapy, which is truly important in the diagnostics and treatment of CVD.[173] Examples of particulate-based carriers for therapeutic and imaging purposes are summarized **in Table 2**.

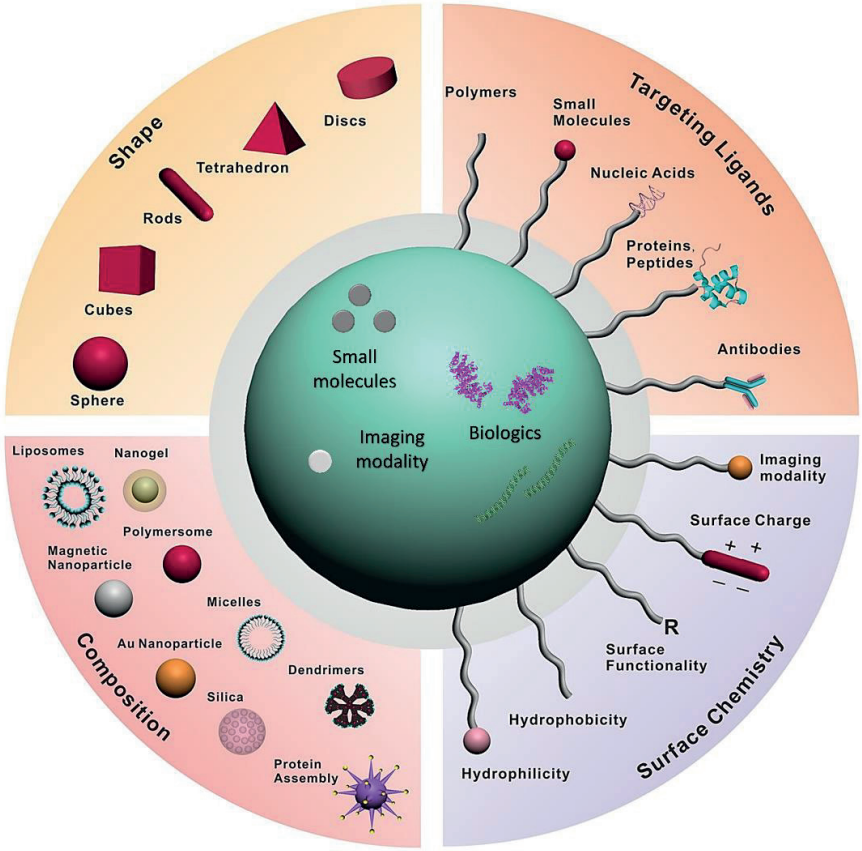

Figure 5. Parameters for micro- and nanoformulation design. Properties of the carrier can be tailored from the perspective of size, material composition, shape, surface chemistry, targeting ligand conjugation, and payload, in order to overcome the sequential physiological barriers for precise drug delivery. Copyright © 2017 the American Physiological Society. Adapted and reprinted with permission from ref.[164].

Table 2. Micro- and nanoparticulate systems developed for the therapy and imaging of MI.

Micro- and nanosystems	*Purpose*	*Administration route*	*Targeting strategy*	*Refs.*
PLGA NPs	*Therapeutics delivery*	*Intramyocardial*	–	174-176
Chitosan–alginate NPs	*Therapeutics delivery*	*Intramyocardial*	–	177, 178
Chitosan hydrogel NPs	*Imaging*	*Intramyocardial*	–	177, 178
Gelatin MPs	*Imaging*	*Intramyocardial*	–	179-181
Acetalated dextran MPs	*Gene delivery*	*Intramyocardial*	–	182, 183
siRNA Polyketal NPs	*Gene delivery*	*Intramyocardial*	–	184, 185
siRNA-dendrimers	*Gene delivery*	*Intramyocardial*	–	184, 185
Poly(glycoamidoamine) oligodeoxynucleotide polyplexes	*Gene delivery*	*Pericardial sac*	–	186
Peptide-polymer amphiphile nanoparticles	*Therapeutic delivery*	*Intramyocardial Intravenous*	*Passive*	187
Liposomes	*Therapeutics delivery*	*Intracoronary*	–	188
PEGylated polystyrene NPs	*Potential application in MI therapy*	*Intravenous*	*Passive*	189
PEGylated micelles	*Potential application in MI therapy*	*Intravenous*	*Passive*	190
PEGylated liposomes	*Therapeutics delivery Imaging*	*Intravenous*	*Passive Active*	163, 191-195
Micelles, Liposomes	*Therapeutics delivery Imaging*	*Intravenous*	*Passive Active*	163, 191-195
Liposomes	*Therapeutics delivery Imaging Gene delivery*	*Intravenous*	*Passive Active*	99, 196-203
Immunoliposomes	*Therapeutics delivery Imaging Gene delivery*	*Intravenous*	*Passive Active*	99, 196-203
Platelet-like proteoliposomes	*Therapeutics delivery Imaging Gene delivery*	*Intravenous*	*Passive Active*	99, 196-203
Solid lipid nanoparticles	*Therapy and therapeutics delivery*	*Intravenous*	*Passive Active*	204
Peptide-PEG-polylactic acid	*Therapy and therapeutics delivery*	*Intravenous*	*Passive Active*	205
Gold NPs	*Therapeutics delivery*	*Oral gavage*	–	206
Polyelectrolyte-coated gold nanorods	*Antifibrotic therapy*	–	–	170
Silica nanoparticles	*Therapeutics delivery*	*Intravenous infusion*	*Passive*	207
Iron nanoparticles	*Imaging Therapy*	*Intravenous*	*Active*	208
USPIO NPs	*Imaging Therapy*	*Bolus*	*Active*	209, 210
SPIO nanoparticles	*Imaging*	*Intravenous*	*Active*	211, 212
Perfluorocarbon nanoemulsions	*Therapy*	*Intravenous*	*Passive*	213

Abbreviations: MPs, microparticles; NPs, nanoparticles; PEG, polyethylene glycol; PLGA, poly(lactic-co-glycolic acid); USPIO, ultrasmall superparamagnetic iron oxide.

2.2.1. Administration routes

The administration routes often employed for micro- and nanomedicines for the therapy of MI are local intramyocardial, pericardial, intracoronary and *i.v.* administration. Oral administration is a rare route of administration of particulate carriers for MI therapy but has also been attempted.[206] Some examples of locally administered micro-and nanomedicines are presented next and included in **Table 2**. Chang *et al.* demonstrated that a single intramyocardial administration of insulin growth factor (GF)-loaded poly lactic-co-glycolic acid (PLGA) nanoparticles prolonged Akt phosphorylation and provided cardioprotection for up to 24 h, which was sufficient to improve cardiac systolic function, reduce infarct size, and prevent ventricular remodeling 21 days after MI in mice.[174] Similarly, Binsalamah *et al.* have injected placental GF-loaded chitosan-alginate nanoparticles intramyocardially in MI-induced rats. Besides a sustained release of the cargo over several days, the outcomes observed were significantly increased LV function, vascular density and serum levels of the anti-inflammatory cytokine interleukin-10, together with decreased scar area formation and reduced amounts of pro-inflammatory cytokines.[177] Other reports have also demonstrated the use of particulate systems made of different materials for intramyocardial injection in injured hearts.[175, 176, 179-182, 184, 185]

Tranter *et al.* administered low toxic glycopolymer-based polyplexes carrying oligodeoxynucleotide decoys in the pericardial sac, for the transfection of ventricular cardiomyocytes *in vivo*.[186] Intracoronary administration was based on the direct infusion of therapeutics into the coronary arteries. Verma *et al.* administered adenosine triphosphate (ATP)-loaded liposomes directly to the coronary artery in a rabbit MI model as a source of exogenous ATP for the protection of ischemically damaged cells.[188] Oral gavage was attempted by Vinodhini *et al.* for cardioprotective therapy using gold nanoparticles loaded with antioxidant proanthocyanidin.[206]

To tackle the need of surgery for the administration of cell-based therapy,[12] cardiac scaffolds,[13] or microparticulate medicines into the injured heart, the tendency is to develop nanoparticles that are possible to be administered by minimally invasive routes such as the *i.v.* route. In the 1970s, a study using plain radiolabeled liposomes of different surface charges showed that liposomes have the ability to accumulate in the infarcted zones and could serve as potential vehicles for delivery of therapeutics for the treatment of MI.[214] From this point on, an increasing research towards the development of nanomedicines for *i.v.* injection took off.[10, 162, 189, 191, 215, 216] More examples of developed particulate systems are given in the next section.

2.2.2. Targeting approaches

Targeting is considered when the main purpose is to develop a drug delivery nanocarrier to be administered by less invasive administration routes, such as oral, nasal or *i.v* administration. Focusing on *i.v.* administration, either active or passive targeting are the mainstream approaches for the delivery of cargos to prevent, alleviate and treat several diseases, such as cancer and MI. While passive targeting is based on the enhanced retention of the nanocarriers in the diseased tissue due to the increased microvascular permeability, active targeting relies on the interaction between a particular ligand attached on the surface of the carrier and a distinctive disease marker (over)expressed on the cell membrane. Both approaches theoretically lead to an increased amount of delivered therapeutics into the injured tissue area compared to the healthy tissue. [217]

2.2.2.1. Passive targeting

Similarly to solid tumors,[218] it has been shown that the vascular permeability is transiently increased upon an ischemic event in the myocardium.[219] This fact allows the exploitation of passive targeting of nanomedicines to the injured heart, although it is known that in many cases, a leaky vasculature is not enough to allow optimal delivery of therapeutic compounds.[220] Taking advantage of this, Lundy *et al.* investigated the ideal particle size for rapid passive targeting of the myocardium by systemic administration of polyethylene glycol (PEG)-polystyrene nanoparticles soon after ischemia–reperfusion injury. They observed that a wide range of particle sizes is able to accumulate in the injured LV compared to sham-operated models, ranging from core diameters of 20–200 nm, while 500 nm particles (and bigger) showed also accumulation in the injured LV, and also a much greater off-target retention in the spleen.[189] Liposomes have been used widely for passively targeted drug delivery, as their accumulation in regions of experimental MI has been demonstrated.[188, 190, 191, 221] Nguyen *et al.* developed enzyme-responsive nanoparticles for targeted accumulation in the infarcted heart upon MI. These nanoparticles, made for passive targeting due to their small size and relying on the leaky vasculature of the injured myocardium, were made of peptide-polymer amphiphiles and contained specific peptide sequences for the recognition of matrix metalloproteinases 2 and 9, which are upregulated in MI. They demonstrated, both by intramyocardial and *i.v.* injections, a change in nanoparticle conformation upon reacting to the presence of matrix metalloproteinase 9 in the infarcted myocardium, to an aggregate-like scaffold, and a retention for up to one month. Although not showing loading of therapeutic cargos or beneficial functional outcomes, this study opens up new doors for potential prolonged therapeutics delivery.[187]

Other materials have been used as nanoparticulate vehicles for passive delivery. Examples include silica,[207] and perfluorocarbons.[213] The latter ones were used as oxygen carriers to the ischemic myocardium, as perfluorcarbons have high ability to carry great volumes of respiratory gases physiologically. They accumulated in the ischemic areas of the heart by passive targeting, due to their small size, and demonstrated infarct size reduction in a murine MI model.[213] These and other examples of nanosystems used for passive targeting to the ischemic heart are summarized in **Table 2**.

2.2.2.2. Active targeting

The development of targeted DDS is an urgent need to maximize the overall efficacy of the delivered drugs for cardioprotection. Poor targeting to the infarcted heart is an issue, because this may lead to both failure in treatment and also induce unwanted side-effects in other organs.[222] One example was the encapsulation of cyclosporine in PEG-coated (or PEGylated) liposomes and administration to patients with MI in a clinical trial, revealing a distribution of cyclosporine mainly in other organs rather than in the heart. The failure of this trial was due to the transitory leaky vasculature effect upon MI, contrarily to what happens in tumors, which showed a sustained enhanced permeability and retention effect. Thus, relying on a leaky vasculature is insufficient for meaningful therapeutic outcomes.[223] Furthermore, a specific cardiomyocyte marker suitable for targeting has not been yet found.[224] Therefore, *in vivo* phage display is typically used instead, for the discovery of potential peptide targeting ligands,[203] or peptides targeting the low extracellular pH of the infarcted myocardium.[225, 226]

In this case, different targeting moieties or strategies are attempted to home the drug(s) to the injured LV. Peptides and antibodies are some of the targeting moieties utilized to functionalize the surface of nanocarriers for targeted drug delivery to the injured myocardium. For the first time, $InCl_3$-radiolabeled liposomes functionalized with antibodies to cardiac myosin were used to visualize the infarcted heart in a dog experimental MI model. After transient blockade of the left coronary artery, immunoliposomes were administered *i.v.* and accumulated preferentially in the infarcted zone.[196] Dvir *et al.* targeted the MI heart by functionalizing liposomes with antibodies against angiotensin II type 1 receptor, overexpressed in the infarcted heart, showing successful *in vivo* targeting, however without incorporation of drug molecules into the functionalized liposomes, and not showing relevant biological effect.[99] Similar approaches have also been presented using antibodies as targeting moieties.[197-200, 227] Dasa *et al.* used the *in vivo* phage display tool for identification of peptides that would be specific for the different cardiac cells present in the heart, including among others, cardiomyocytes and cardiac progenitor c-Kit$^+$ cells found in the border zone of the infarct area. After further conjugation of the discovered peptides onto liposomes' surface, pharmacokinetic studies reveal significantly higher liposome accumulation in the heart and more efficient drug delivery.[201] Cheng *et al.* exploited the fact that splenic monocytes are highly recruited to the heart after an MI event, and are known to interact with platelets during circulation.[202] They developed platelet-like proteoliposomes, which biomimic platelet interactions with circulating monocytes. Their results showed affinity of the nanocarriers for monocytes, but not for endothelial cells *in vitro*, mimicking normal platelet activity. *In vivo*, the platelet-like proteoliposomes accumulated at the injury site 72 h postinfarction and provided targeted drug delivery to the heart in an enhanced vascular permeability-independent manner, demonstrated anti-inflammatory effects and overall improvement in cardiac function. A similar approach to target cardiac macrophages towards a reparative state was also used by Harel-Adar *et al.*,[201] by creating phosphatidylserine-presenting liposomes that mimic anti-inflammatory effects of apoptotic cells. This induced the expression of anti-inflammatory cytokines, resolved inflammation, and promoted angiogenesis, and prevented negative ventricular remodeling *in vivo* in a MI rat model. Cheng *et al.*[208] utilized iron oxide nanoparticles, functionalized with two types of antibodies (one type against CD45 found in bone marrow-derived SCs and the other against CD34 expressed in injured cardiomyocytes) for delivery of SCs to the injured myocardium and possibility of non-invasive imaging. Targeting could be further enhanced by magnetic attraction and functional improvements in the LV ejection fraction were observed after 4 weeks, however, the imaging could be compromised by the degradation and absorption of the iron nanoparticles. In addition, the therapeutic efficacy was limited by possible insufficient SCs in the circulation for capture by the nanoparticles, and the time of administration immediately after acute MI requires further investigation of later administration time points.[208] More recently, Huang *et al.* targeted highly expressed fibrin in the injured area of the myocardium.[205] For this, they attached the clot-binding peptide cysteine–arginine–glutamic acid–lysine–alanine to PEG-polylactic acid nanoparticles to mediate their interaction with fibrin in the infarcted zone. They demonstrated the accumulation in the infarcted zone and delivery of thymosin beta 4 *in vivo* upon *i.v.* administration, with a reduction in infarct size and scar formation (**Figure 6**).

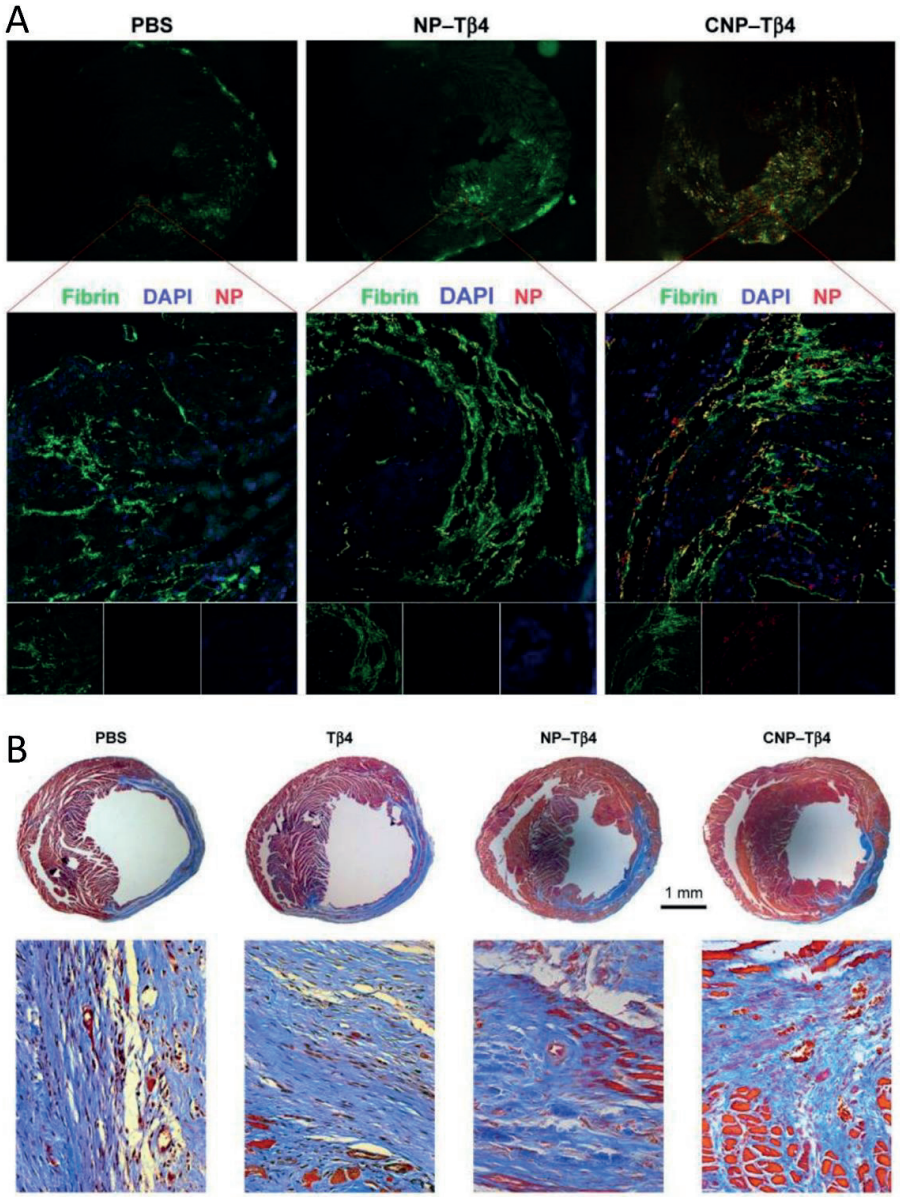

Figure 6. Fibrin-targeted CNP–Tβ4 accumulation in the infarcted heart (A) and reduction of the infarct size and scar formation with CNP–Tβ4 after MI in mice (B). Abbreviations: CNP–Tβ4, cysteine–arginine–glutamic acid–lysine–alanine and thymosin beta 4 conjugated to nanoparticles; PBS, phosphate-buffered saline; NP–Tβ4, thymosin beta 4 conjugated to nanoparticles; DAPI, 4′,6-diamidino-2-phenylindole; NP, nanoparticle. Copyright © 2017 Dove Medical Press Limited. Adapted and reprinted with permission from ref. [205].

2.2.2.3. Imaging of MI with nanoparticulate systems

Imaging of the infarcted area is another interest of the medical and scientific community, as conventional methods do not allow an optimal and detailed visualization of the different pathological states of the injured myocardium in patients at risk (such as myocardial edema and hemorrhage). Iron oxide nanoparticles have been widely studied as contrast agents for magnetic resonance imaging, and are the most common nanoparticulate-based approach studied for imaging of MI.[208, 228] In this context, and making use of both passive and active targeting approaches, ultrasmall superparamagnetic iron oxide nanoparticles (SPIOs) were developed and used in a phase III clinical trial with MI patients for cardiovascular magnetic resonance imaging. The principle of this study was based on the targeting of the infiltrating macrophages of the (peri-) infarct zone.[209] In addition, another study from the same group demonstrated the dual advantage of ultrasmall SPIO for theranostics.[208] Other studies included antibody and heat shock protein 70-functionalized iron oxide nanoparticles for magnetic resonance imaging of infarcted hearts,[211, 212] liposomes and micelles.[193, 194] Shevtsov et al. explored the use of heat shock protein 70-functionalized SPIO nanoparticles as contrast agents for MI imaging, since it has been demonstrated that the receptor for this ligand is expressed in cardiomyocytes.[229] They showed that the functionalized SPIO nanoparticles provided high contrast potential for diagnosis of injured areas of the rat MI heart (**Figure 7**), due to an elevated expression of the heat shock protein-70 receptor in the stressed MI tissue.[212] Other strategies to image the MI heart include radiolabeling of nanoparticles,[178] liposomes and micelles containing paramagnetic and fluorescent lipids,[163, 192] and gadolinium-labeled liposomes.[193, 194] These systems are summarized in **Table 2**.

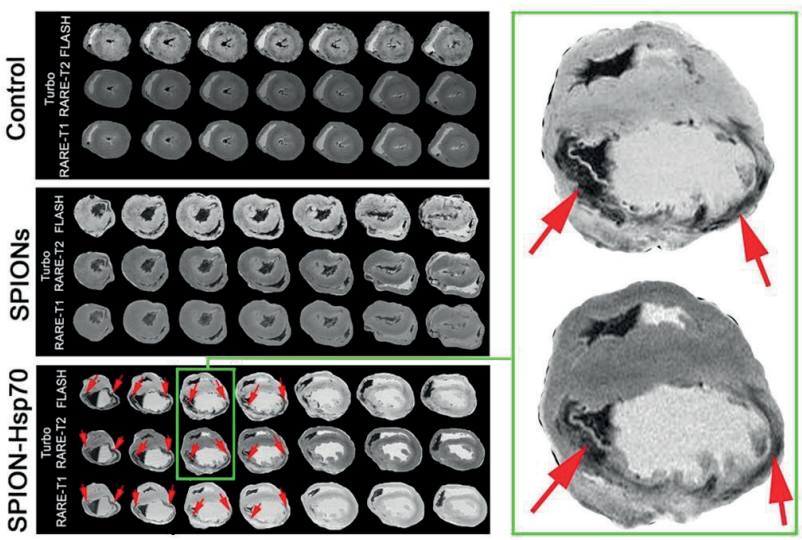

Figure 7. Imaging of the myocardial infarct. Magnetic resonance images were taken for control untreated animals, animals treated with SPIO nanoparticles, and heat-shock protein-70 (Hsp70)-SPIO nanoparticles. Copyright © 2015 Elsevier B. V. Adapted and reprinted with permission from ref.[212].

2.3. Drug delivery systems

2.3.1. Porous silicon

Porous silicon (PSi) was first reported by the Uhlirs in 1956 as an unwanted side product of electrolytic shaping of silicon.[230] This phenomenon was later investigated by Turner, who electrochemically dissolved silicon wafers in aqueous or ethanolic hydrofluoric acid solutions, and established the detachment of a dark layer from the silicon wafer after increasing the current density above a critical point – the electropolishing region.[231] However, only in 1971, Watanabe *et al.*[232] recognized the porous nature of this layer and an increasing interest for this material took-off. After Canham demonstrated the first hints of photoluminescence, bioactive properties, and the ability to convey bioinert and bioactive nature of PSi[233, 234], the application of PSi in biomedicine became extremely popular.[235-237]

2.3.1.1. Fabrication and surface stabilization of PSi materials

PSi is fabricated by a top-down approach, which makes it easy for scaling-up. The distinct properties of this material make it attractive and advantageous for biomedical applications. Among them, biocompatibility, biodegradability, high surface-to-volume ratio and surface area, porosity, pore size and volume, tunable surface chemistry, stability, shape and particle size make PSi interesting for use in therapeutic drug delivery and biosensing.[17, 23, 29, 238-240]

The most common fabrication method of PSi is electrochemical anodization in aqueous or ethanolic electrolytes of hydrofluoric acid.[18, 23, 241, 242] The silicon wafer is in contact with a conductive metal anode, and usually, platinum is used as a cathode. A porous structure layer is formed upon application of an etching current at the surface of the silicon wafer. The porosity, porous layer thickness, shape and size of the pores are tunable properties, determined by several factors and parameters during the electrochemical anodization process.[17, 241, 243]

The freshly etched PSi is hydrogen terminated (Si-H_x), and thus, very unstable and prone to oxidation, going from hydrophobic to hydrophilic oxidized surface over time, with loss of optical and structural properties of the material.[241, 244, 245] To avoid this phenomenon, there are strategies to stabilize the surface of PSi. Examples include controlled oxidation, thermal hydrocarbonization (THC), hydrosilylation and thermal carbonization (TC).[239] Thermal oxidation (TO) of PSi (TOPSi) provides a hydrophilic Si–O surface to the PSi material, by thermal, chemical, photo and anodic methods.[242, 244] TO facilitates wettability and degradation in physiological fluids. In addition, by imparting a relatively fast degradation in aqueous media, the stability of the material against dissolution is affected, and may not be always the best choice when longer-term dissolution profiles are required. In this case, surface functionalization with carbon is commonly used. Hydrosilylation gives a Si–C surface to the PSi material through a thermal, photo or Lewis-acid catalyzed reaction of alkene or alkyne with Si–H bond, and yielding better hydrolytic stability.[18, 242] TC and THC are based on the thermal addition of carbons from acetylene molecules onto the surface of PSi; the temperature differs from 450–680° C for THC and above 700° C for TC. TC and THC yield hydrophilic TCPSi and hydrophobic THCPSi.[246] The further functionalization of THCPSi with –COOH groups is possible by thermal treatment with undecylenic acid,[247] making it easier for the covalent attachment of ligands for diverse nanocarrier biofunctionalization. Due to the numerous properties and advantages of PSi material, stabilized PSi are turned into micro- and

nanoparticles, generally using lithography, imprinting method, ball milling or ultrasonic fracturing, followed by sieving and/or centrifugation or filtering, to separate the different size fractions of micro- and nanoparticles.[248-253]

2.3.1.2. Progress in porous silicon-based particulate systems for biomedical applications

PSi micro- and nanomaterials have been extensively studied and employed for biomedical applications due to the above above mentioned attractive properties. The different forms of PSi available, such as layers, membranes, micro- and nanoparticles, make this material versatile for different purposes.[239]

For drug delivery, micro- and nanoparticles are the most important and widely used forms of PSi. [17, 242] Enhancement of the dissolution rate of poorly water-soluble drugs is one advantage of using nanocarriers due to the high surface-to-volume ratio and surface area. [236] In addition, by being highly porous, PSi confines drug molecules in an amorphous-like state or nanocrystalline form, which impacts the dissolution rate of a drug compared to its crystalline form. [254] Meeting these criteria, PSi materials seem to be extremely helpful in the enhancement of the dissolution rate of various extremely poorly water-soluble drugs. [255, 256]

PSi micro- and nanoparticles have been proved to be suitable for different applications, such as the therapeutics and imaging of cancer,[26, 256-258] diabetes,[20, 25, 259, 260] immunotherapy,[21, 24, 261] and, recently, also as a nanoreactor,[262] to name a few. Investigation of PSi materials for different administration routes concludes that the hydrophobic THCPSi is the most suitable for oral drug delivery.[19] Surface modification was needed to improve retention time in the gastrointestinal tract, although not in an ideal fashion when the particles reach the small intestine.[263] Thus, as an application for diabetes therapy, to impart a prolonged gastric transit, PSi particles have been surface-modified with mucoadhesive chitosan and/or coated with enteric polymers, in order to resist the harsh conditions of the stomach and deliver peptide or protein therapeutics in the intestine.[20, 25, 259, 260, 264] Mucoadhesivity of PSi materials is also achieved for gastrointestinal related cancer therapy, with poly(methyl vinyl ether-co-maleic acid), to maximize the benefits of dual drug delivery of anticancer payloads.[27] In many cases, the parenteral application of PSi for anticancer drug delivery requires other types of functionalization, for example, to prevent payload leakage from the PSi pores, shielding from the reticuloendothelial system, or targeting the tumor site. Pore capping and nanoparticle shielding can be achieved by encapsulating or coating drug loaded-PSi carriers with bioinert lipids, DNA, polymers or cyclodextrins.[257, 265-267] Targeting of tumors may be accomplished by functionalizing the PSi carriers with specific ligands to target (over)expressed receptors or proteins at the cell surfaces.[22, 26, 268] PSi nanocarriers have been also explored for the applications in immunotherapy.[240] While screening of the different PSi nanoparticles was useful to determine which surface chemistries induced the higher immunostimulation,[24] it also allowed further investigation of functionalized PSi materials for targeted[261] cancer immunotherapy,[21] and insights in the development of particulate-based vaccines.[269] Finally, as next generation therapeutics, PSi nanoparticles have also been cell membrane-encapsulated with the aim to create bioinspired artificial organelles, in order to mimic subcellular organelle functions for supplementing pathological cellular dysfunctions.[262] In **Table 3** are provided examples of the applications of particulate PSi materials in the biomedical field.

Table 3. PSi micro- and nanoparticles for diverse biomedical applications.

Application	*PSi*	*In vitro cell model*	*In vivo model*	*Main conclusions*	*Refs.*
Oral drug delivery	*TCPSi TOPSi*	*In vitro dissolution*	–	*Hydrophilic drugs: sustained release*	255
			Healthy rat	*Hydrophobic drugs: improved dissolution*	254
	THCPSi	*Caco-2 RAW 264.7*	*Healthy rat*	*In vivo stability Biocompatibility Ideal for oral delivery In vivo imaging of the transit of particles in the GI tract*	19
		AGS		*Enhanced GI transit in stomach, not in intestine*	263
Cancer	*APTES–TCPSi*	*U87 MG EA.hy926*	–	*Dual drug delivery Improved dissolution rate Enhanced antiproliferation effect*	256
	LPSiNPs	*HeLa*	*MDA-MB-435 tumor bearing mice*	*Biodegradability Biocompatibility Tumor imaging*	29
	UnTHCPSi	*Caco-2 HT-29*	–	*pH-controlled dual drug delivery Mucoadhesion Antiproliferation effect*	27
		PC3MM2	*PC3-MM2 tumor bearing mice*	*Tumor accumulation and targeted drug delivery In vivo tumor imaging*	26
		MCF-7 MDA-MB-231	–	*Colloidal stability Sustained drug release Antiproliferation effect*	266
		MCF-7	–	*pH-dependent release Targeted antiproliferation effect*	22
		MDA-MB-231	–	*Superior intracellular multi-drug/theranostic delivery Endosomal escape*	257
	THCPSi	*HT-29 HepG2 RAW 264.7*	–	*Cytocompatibility Controlled release Colloidal stability*	265
		RAW 264.7 PC3MM2	–	*Production by microfluidics – homogeneous nanocarriers pH triggered drug release pH-dependent cytotoxicity Minimal macrophage interactions*	267

Diabetes	*UnTHCPSi*	*Caco-2* *HT-29* *AGS* *Raji B*	–	*Improved insulin/GLP-1 permeation across intestinal cell monolayers* *Protection of peptide cargo from acidic GI conditions.* *Dual drug delivery*	20, 25, 259
		–	*Type-2 diabetes rat model*	*Notable adhesion to rat intestinal epithelia* *Decrease in blood glucose levels* *Increase in pancreatic insulin content*	264
(Cancer) Immuno-therapy	*APM* *TOPSi* *UnP* *UnTHCPSi* *TCPSi* *THCPSi* *APTES-TCPSi*	*PBMC* *PBL*	–	*Surface chemistry-dependent immunomodulation*	24
	APTES oxidized PSi	*BMDC*	*BALB/c* *C57BL/6* *C57BL/6-Tg(TcraTcrb)*	*PSi phagocytosis* *BMDC activation and migration to lymph nodes* *Antigen-mediated T-cell activation*	269
	TOPSi	*KG1* *BDCM*	–	*Cytocompatibility* *Co-stimulatory signal induction* *Multistage nanovaccines with adjuvant properties*	21
Biomimetic organels	*UnTHCPSi*	*MDA-MB-231*	–	*High catalytic activity* *Cytocompatibility* *Govern the transport of molecules* *Intracellular stability* *Protection of payload leakage*	262

Abreviations: BDCM, B-cells with dendritic cells morphology; BMDC, bone marrow dentritic cells; GI, gastrointestinal; GLP-1, glucagon-like peptide-1; LPSiNPs, Luminescent PSi nanoparticles; PBMCs, peripheral blood mononuclear cells; PBL, peripheral blood lymphocytes; TCPSi, thermally carbonized PSi; APTES–TCPSi, (3-aminopropyl)triethoxysilane functionalized TCPSi; APM, poly(methyl vinyl ether-alt-maleic acid) conjugated APTES-TCPSi; THCPSi, thermally hydrocarbonized PSi; UnTHCPSi, undecylenic acid functionalized THCPSi; UnP, polyethyleneimine conjugated UnTHCPSi, TOPSi, thermally oxidized PSi.

2.3.2. Acetalated dextran

The biocompatible and FDA approved dextran is a polysaccharide used for decades, for example, as a plasma expander.[270] Reported first by Bachelder *et al.*,[271] the properties of this polysaccharide were tuned to modulate compound solubility in a pH-dependent manner, by modifying the hydroxyl groups with acetal moieties through reaction with 2-methoxypropene under acid catalysis. In this reaction, kinetically favorable acyclic acetals are initially formed, followed by the formation of more thermodynamically stable cyclic acetals. The resulting

polymer, acetalated dextran (AcDX), is insoluble in water and freely soluble in common organic solvents, such as dichloromethane, ethyl acetate or acetone. The acetal formation depends on the reaction time and leads to varying degrees of degradation rate, based on the ratio of cyclic to acyclic acetals.[271] This enables easy preparation of acid-sensitive particles, an attractive property for biomedical purposes, as acid-sensitive nanocarriers are of great interest for application in pathologies where mildly acidic conditions govern, such as in tumors and in inflammation, or even in lysosomal compartments of the targeted intracellular drug delivery.[272, 273]

Cohen *et al.* reported a variation of AcDX, by further functionalizing it with the polyamine spermine, to overcome the difficulties of encapsulating negatively charged cargos into the neutral AcDX. Spermine-AcDX (AcDXSp) is produced by a reductive amination chemistry, where spermine is covalently conjugated to aldehyde functional groups previously generated by oxidation of dextran using sodium periodate. Biocompatibility is reported, while the mildly acidic pH-dependent degradation is maintained.[274]

Micro- and nanoparticles made of polymeric materials are usually prepared by standard emulsification. An emulsion is formed by mixing an organic phase consisting of the polymer and hydrophobic cargo(s) to be entrapped, with a stabilizer or surfactant in the aqueous phase. When mixing together, the polymer starts to precipitate at the interface between the organic and aqueous phases. This mixing is done by applying external energy, breaking the organic phase into droplets and creating an oil-in-water (o/w) emulsion. After evaporation of the organic solvent, these droplets lead to the formation of micro- or nanoparticles, which contain the hydrophobic cargos entrapped. Different factors contribute to the particle size and encapsulation efficiency of loaded cargos, such as the type and concentration of surfactant, sonication, evaporation and centrifugation parameters.[275, 276] The most common preparation methods of AcDX micro- and nanoparticles are the o/w single emulsion and water-in-oil-in-water (w/o/w) double emulsion techniques, followed by solvent evaporation. The choice of a single or double emulsion depends on the cargos to be loaded. While the entrapment of hydrophobic cargos can be achieved by a single emulsion, the entrapment of hydrophilic drugs or biologics requires a double emulsion, confining the hydrophilic cargos in the aqueous core of the nanodroplets.[182, 183, 271, 277-280]

2.3.2.1. Progress in acetalated dextran-based particulate systems for biomedical applications

The biocompatibility of AcDX is related to its degradation products, which are dextran, methanol (harmless in small quantities)[281] and acetone (harmless metabolic intermediate). Toxicity tests of AcDX particles in different cell lines did also not show significant toxicity values.[271] Combined with the acid-sensitive degradation profile, it is justifiable that quite much research for application in biomedicine has been conducted with this polymer.

One of the undeniable applications of AcDX is in immunotherapy. Bachelder *et al.* assessed the feasibility of using AcDX for vaccine applications, by incubating the antigen ovalbumin. They observed a significantly enhanced antigen epitope presentation, suggesting the potential of this material in cancer immunotherapy.[271] Other studies followed, including AcDX and AcDXSp encapsulation and attachment of different antigens for immunostimulation, cancer immunotherapy,[21, 277, 279, 282, 283] and immunosuppression therapy, the latter one with the aim to reduce immunosuppressant side effects. [280] The modification of AcDX with spermine also brought up new opportunities for gene delivery. Cohen *et al.*

demonstrated that by functionalizing AcDX with spermine and making it cationic, it was possible to efficiently encapsulate and deliver siRNA.[274] Taking advantage of the mildly acidic degradation of AcDX and AcDXSp, several studies demonstrated the polymer's feasibility for cancer therapy,[258] either the combination of anticancer drugs with different physicochemical properties, or different therapeutic modalities.[284, 285] The potential use of AcDX for deep lung drug delivery was also explored, taking into consideration different degrees of acetalation to modulate the polymer degradation and the delivery of therapeutics at different pH conditions.[286, 287]

Finally, AcDX has also been employed for the delivery of biologics for MI therapy. Suarez *et al.* studied the biocompatibility of AcDX to the heart and demonstrated an efficient entrapment of the model proteins myoglobin and basic fibroblast growth factor, and a controllable release of the cargos in some cases for more than 30 days, depending on the acetalation degree of the polymer.[183] In another study, it was also evaluated the effect of hepatocyte growth factor-loaded AcDX microparticles on the efficacy in angiogenesis, cardiomyocyte apoptosis, and infarct size, in an MI animal model.[182] Despite the therapeutic advantages demonstrated and sustained release of biologics, these microparticulate systems needed to be delivered intramyocardially, a considerable drawback for clinical translation and patient compliance.

2.3.3. PEGylation for enhanced stability, biodistribution and targeting properties of nanosystems

One of the greatest obstacles of systemically administered nano DDS is when they face the mononuclear phagocyte system in the blood stream. The body recognizes and clears foreign entities by using neutrophils, monocytes, and macrophages in the blood, liver, spleen, and lymph nodes, making systemic nano drug delivery difficult, by shortening the blood circulating time and tissue/cell distribution, and this makes their translation into the clinics difficult.[288]

The most common approach to overcome this issue is to strategically coat the nanocarrier surface with an inert polymer, resistant to interactions with the constituents of blood and giving the nanocarrier "stealth" properties. [289] PEG has long been used as a stealth polymer, considered safe and approved by FDA. PEG has been reported for the first time for drug delivery purposes in the 1970s, after increasing the circulation time and decreasing the immunogenicity of proteins. [290] These positive observations escalated towards the investigation of PEG coatings of nanoparticles for systemic delivery. PEGylation is demonstrated to efficiently shield nanoparticles from aggregation, opsonization, phagocytosis, and increases the circulation time, providing a higher probability for the circulating nanosystems to find and distribute to the target tissues. After the example of FDA approved nanomedicine Doxil® "Stealth" liposomes, PEGylation became mainstream in nanoparticle formulation. The mechanism by which PEG shields nanoparticles from opsonization and makes them stable is related to the hydrophilic nature. [168] Nanoparticles coated with PEG generate a hydrated layer with a large excluded volume that sterically impedes nanoparticles from interacting with neighboring objects. [291] Additionally, because the PEG chains are highly flexible, the interpenetration of foreign matter into the PEG corona is not thermodynamically favorable. [292]

The use of PEGylation has been extended to nanomedicines for the treatment of MI. Studies described the use of different particulate systems coated with PEG to prolong the circulation time, maximize the effect of passive targeting, and improve the pharmacokinetics

of loaded cargos. [189-191, 195] As an example, Zhang *et al.* compared the effect of PEGylation of nanostructured lipid carriers bearing a short-lived payload in the plasma concentration and efficacy in an MI model. [195] They observed a 3-fold increase in the plasma concentration of the payload in PEGylated nanocarriers compared to non-PEGylated ones, as well as a higher heart drug concentration in the MI model, which in turn resulted in a significantly decreased infarct size. In other reports, PEGylation was combined with targeting moieties for prolonged circulation and maximized active targeting of MI. [99, 204] Dong *et al.* linked the targeting peptide arginyl-glycyl-aspartic acid (RGD) to PEGylated solid lipid nanoparticles for the targeting of $\alpha_v\beta3$ integrins, which was highly expressed in cardiac endothelial cells during angiogenesis for dual passive and active targeted drug delivery of an antioxidant and a reactive oxygen species scavenger. The passive targeting was owed to the small size of the solid lipid PEGylated nanocarriers, while the active targeting was reached with the RGD ligand at the carrier surface. The pharmacokinetics of the payloads were improved and the infarct size reduced. [204] In this thesis, PEG was also used as a tool to stabilize the developed nanosystems both *in vitro* and *in vivo*.

2.3.4. Functionalization and radiolabeling of nanoparticles for theranostics

The fast advancement of nanotechnology for biomedical applications calls upon the combination of different features in one nanocarrier for multifunctional purposes. The ideal vision of a nanomedicine today may include therapeutic and imaging components. This leads to the development of theranostics for simultaneous diagnosis and therapy. [293] Nanoparticles have demonstrated suitable features and properties for imaging, such as favorable pharmacokinetics and biodistribution behavior, diverse material composition and surface chemistry, regarded as flexible platforms for the addition of multiple functional ligands, such as targeting moieties, therapeutics, and/or contrast materials. [293-295]

Several materials can serve as contrast agents, either by directly having that property or upon loading or functionalization. Examples including iron oxide, quantum dots, gold nanoparticles, carbon nanotubes and silica/silicon nanoparticles have been reviewed elsewhere. [293] In particular, radiolabeling of nanoparticles seems to have gained some attention due to the applicability of powerful, quantitative, superior signal sensitive and enhanced spatial resolution imaging techniques, such as positron emission tomography (PET) and single photon emission computed tomography (SPECT). Nanocarrier radiolabeling can be accomplished in different ways, directly or indirectly, via prior functionalization, and depends on the type of material and radiotracer used. For example, chitosan hydrogel nanoparticles carrying vascular endothelial growth factor proteins or peptides were radiolabeled with ^{99}mTc for targeting the ischemic myocardium and monitoring the nanoparticle's accumulation.[178] Sarparanta *et al.* radiolabeled PSi particles directly with ^{18}F for nuclear imaging with PET without the need for prior functionalization of the PSi surface, because of the spontaneous Si-F bond formation. [296] Moreover, the use of ^{111}In for PSi radiolabeling for SPECT may require prior surface modification with metal chelators.[26] In the latter case, 1, 4, 7, 10-tetraazacyclododecanetetraacetic acid (DOTA), known to form kinetically and thermodynamically stable complexes with trivalent radionuclides, was used to react with trivalent radionuclides, such as ^{111}In or $^{67/68}$Ga. [297] Wang *et al.* made use of PSi-based nanomaterials, surface functionalized with DOTA and RGD targeting ligand, radiolabeled with ^{111}In for application in cancer theranostics, as illustrated in **Figure 8**.[26] In this thesis, the same

kind of metal chelator (DOTA) was used for radiolabeling purposes in similar PSi-based nanoparticles.

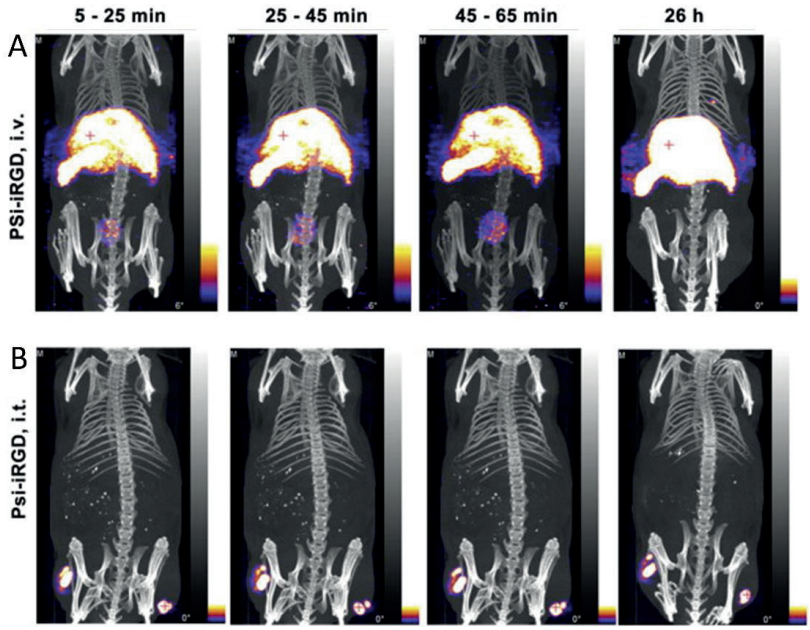

Figure 8. Nano-SPECT/CT fused images of the whole mouse. Images were taken in a dynamic mode during 1 h at 5 min post-injection and at 26 h for (A) PSi-iRGD *i.v.*, and (B) PSi-iRGD intratumoral (*i.t.*). Copyright © 2015 Elsevier B. V. Adapted and reprinted with permission from ref.[26].

3. Aims of the study

Particulate systems have been increasingly studied for the therapy and imaging of MI over the last decades. The search for better and more effective therapeutic strategies for treating the injured heart (unable to regenerate) is urgent. In this thesis, PSi and AcDXSp-based carriers, widely studied also for other biomedical applications, were investigated for their biocompatibility and targeted heart-homing and imaging potential through surface functionalization and labeling of the nanoparticles. In addition, heart-targeted drug delivery by loading of one or more therapeutic drugs is investigated.

More specifically, the goals of this study were to:

- Investigate the biocompatibility of PSi micro- and nanocarriers in heart tissue (**I**).
- Screen the ability to specifically home cardiac cells with PSi nanocarriers by functionalizing them with different heart-homing peptides (**II**).
- Reveal the mechanism of interactions of the most promising peptide-functionalized PSi nanosystem with cardiac cells (**II, III**).
- Enhance the colloidal stability and blood circulation, study the biodistribution, intracardiac accumulation and distribution, and *in vivo* therapeutic effect of peptide-functionalized PSi in heart targeting (**III**).
- Assess whether AcDXSp-based nanosystems could be used as pH-triggered drug delivery carriers in direct cardiac fibroblast reprogramming (**IV**).

4. Experimental

In this section, the experimental methods used for the studies described in the thesis are summarized. Experimental details can be found in the original publications (**I–IV**). The fabrication of the PSi micro- and nanomaterials was prepared by our collaborators at the Laboratory of Industrial Physics, Department of Physics and Astronomy, University of Turku, Finland. The *in vivo* experiments described in publication **I** were done by our collaborators at the University of Oulu. The radiolabeling of the nanoparticles, SPECT/CT, and autoradiography experiments were performed in collaboration with the Laboratory of Radiochemistry, Department of Chemistry, University of Helsinki, Finland (**II, III**).

4.1. Preparation and characterization of the PSi micro- and nanoparticles and the AcDXSp nanoparticles

4.1.1. Production of PSi micro- and nanoparticles (I–III)

The porous structures of the PSi micro- and nanoparticles were prepared using electrochemical anodization.[298] Multilayered free-standing PSi films were obtained from monocrystalline, boron-doped p-type Si ⟨100⟩ wafers with a resistivity of 0.01–0.02 Ω·cm, using a 1:1 (v/v) hydrofluoric acid (38%)–ethanol electrolyte solution. The free-standing silicon films were etched using a constant etching current of 50 mA/cm^2. The repeated pulse of low/high etching current applied led to porous films by fracturing the Si wafers. The multilayered porous film was lifted by elevating the current density, upon reaching the electropolishing region. The surface of PSi layers was stabilized by TO and THC. TOPSi was obtained by thermally oxidizing the multilayer films in ambient air for 2 h at 300 °C.[299] THCPSi was obtained by at first exposing PSi films to N_2 flow (1 L/min) for 30 min to remove residual moisture and oxygen before surface stabilization. Next, the surface was thermally hydrocarbonized by exposing the films to a mixture of N_2/acetylene (1:1 v/v) at room temperature during 15 min and at 500 °C for another 15 min, then cooling back to room temperature under N_2 flow.[19] Undecylenic acid thermal addition to THCPSi was done by immersing the films in neat acid for 16 h at 120 °C, [247] yielding undecylenic acid thermally hydrocarbonized porous silicon (UnTHCPSi). As for the final particle size, nanoparticles were fragmented from the multilayered PSi films by a wet milling in EtOH, and the size selection was done using centrifugation (**I–III**). To produce microparticles, the anodized films were dry milled and the particles were separated into different size classes by sieving followed by centrifugation (**I**).

4.1.2. Functionalization of UnTHCPSi nanoparticles (II, III)

The surface carboxyl groups of 3 mg of UnTHCPSi nanoparticles were activated by 1-ethyl-3-(3-dimethylaminopropyl) carbodiimide hydrochloride/N-hydroxysulfosuccinimide (EDC/NHS) chemistry during 2 h at room temperature in the dark and under stirring. After, the excess of EDC/NHS reagents were removed and S-2-(4-aminobenzil)-1, 4, 7, 10-tetraazacyclododecane-1,4,7,10-tetrater-butyl acetate molecules (DOTA, 150 μg/mL in 50% ethanol) was added to the activated UnTHCPSi nanoparticles in a ratio of 100:1 (*w/w*) (UnTHCPSi:DOTA). The obtained UnTHCPSi-DOTA nanoparticles (Un-D) were washed twice with 50% ethanol. The tert-butyl ester groups from DOTA were cleaved by treating the Un-D

nanoparticles with a standard solution of trifluoroacetic acid/triisopropylsilane/Milli-Q water (TFA/TIPS/H_2O) in a ratio of 95:2.5:2.5 [300] for 24 h at room temperature under vigorous stirring, after which two washing steps were done with ethanol. Three different peptides, ANP (United BioSystems Inc.), CSTSMLKAC (P2), and CRSWNKADNRSC (P3) (GenicBio Ltd.) were covalently attached to the Un-D nanoparticles. The free carboxyl groups of Un-D NPs were again activated for 2 h at room temperature under stirring, by using EDC/NHS chemistry. After removing the excess of crosslinking reagents, the peptide solutions (2 mg/mL in PBS pH < 7.2) were added to the activated surface of the Un-D nanoparticles in a ratio of 1:5 (Un-D:peptide). The reaction was allowed to occur for 3 h for P2 and P3, and overnight for ANP under stirring at room temperature. The resultant Un-D-ANP, Un-D-P2 or Un-D-P3 nanoparticles were washed twice with Milli-Q water (**II**). For publication **III**, the surface carboxyl groups of 3 mg of UnTHCPSi were first activated for 2 h with EDC/NHS chemistry, as described above. The activated nanoparticles were exposed to a 2 mg/mL of a 5 kDa heterobifunctional PEG (NH_2-PEG-COOH, Jenkem Technology) in PBS (pH 7.2) in a ratio of 1:2 w/w, (UnTHCPSi:PEG) overnight in the dark at room temperature and under stirring. UnTHCPSi-PEG (Un-P) nanoparticles were washed once with ethanol and twice with Milli-Q water. The functionalization with DOTA (yielding Un-P-D) and ANP (Un-P-D-ANP) was performed, as described above for publication **II**, except that the ratio of Un-P-D: ANP used was 1:5 (*w/w*).

4.1.3. Synthesis of spermine-acetalated dextran

Dextran (5 g, MW 9–11 kDa; Sigma-Aldrich) was dissolved in 20 mL of Milli-Q water. Sodium periodate (0.22 g; Sigma-Aldrich) was added to the dextran solution and the mixture was stirred at room temperature for 5 h to yield partially oxidized dextran. Upon washings and lyophilization, partially oxidized dextran (3 g) was modified with 2-methoxypropene (10.6 mL, Sigma–Aldrich) and pyridinium *p*-toluenesulfonate (46.8 mg; Sigma–Aldrich) in anhydrous dimethyl sulfoxide (30 mL, Sigma–Aldrich) during 1 h under a N_2 atmosphere to obtain the partially oxidized AcDX. Triethylamine (TEA, 1 mL; Sigma–Aldrich) was used to quench the reaction and precipitate the resulting AcDX, followed by a series of centrifugations (10 min, 68320*g*) and washings. The pellet was dried under vacuum at 40 °C to yield partially-oxidized acetalated dextran (AcDX) powder. The partially oxidized AcDX (2.0 g) was dissolved in 20 mL of DMSO and spermine (4.0 g, 19.8 mmol; Sigma-Aldrich) was added to the solution and kept stirring for 24 h at 50 °C. Sodium borohydride ($NaBH_4$, 1.0 g; Sigma-Aldrich) was added and the reduction reaction was allowed to occur at room temperature during at least 24 h. H_2O (80 mL) and methanol (10 mL) were added to the flask to precipitate the polymer and to dissolve the excess $NaBH_4$. Upon a series of centrifugations and washes and final lyophilization, the resultant AcDXSp comes as a white powder.[274, 277]

4.1.4. Preparation of spermine-acetalated dextran nanoparticles and surface functionalization (IV)

The AcDXSp nanoparticles were prepared by a standard single emulsion method. Briefly, AcDXSp polymer (6.5 mg) was dissolved in CH_2Cl_2 (0.125 mL). The compounds CHIR99021 (300 µg, Tocris) and SB431542 (500 µg, Sigma) (CRIH99021 + SB431542, CS) were added to the AcDXSp solution. An aqueous solution of polyvinyl alcohol (PVA, MW:

31000-50000 g/mol, Sigma–Adrich) (0.25 mL, 2.0%, w/v) was further added to the AcDXSp solution, and the mixture was mixed thoroughly and emulsified by sonication during 30 sec on ice, with an output setting of 5 and a duty cycle of 50%, using a probe sonicator (Sonics VCX 750). The resulting single emulsion was transferred immediately to another solution of PVA (0.75 mL, 0.2% w/v) and stirred for 3 h for solvent evaporation. The resulting CS@AcDXSp nanoparticles were pelletized by centrifugation (16100*g*, 5 min) and washed twice with Lutrol® F127 0.5 % pH 8 (BASF) and once with Milli-Q water. All supernatants were kept for the detection of CHIR and SB contents by high-performance liquid chromatography (HPLC). Empty nanoparticles were prepared similarly.

The surface of the AcDXSp nanoparticles was modified with PEG (CO_2H-PEG-CO_2H, 2 kDa, Sigma-Aldrich). In brief, a solution of PEG was prepared in EDC/NHS at pH 7.8. The EDC/NHS solution was prepared as described in section *4.1.2*. This solution was added to 2 mg AcDXSp NPs in a ratio of 10:1 (*w/w*) (PEG:AcDXSp). The mixture was allowed to stir at room temperature during 4 h in the dark, yielding AcDXSp-PEG (AcDXSp-P). For further functionalization with ANP, the AcDXSp-P nanoparticles were pelletized by centrifugation and the supernatant containing the remaining EDC, NHS, and excess of PEG was discarded. The AcDXSp-P nanoparticles were resuspended in a solution of ANP (pH 8, AcDXSp-P:ANP ratio 1:1 w/w) and prepared in the same solution and kept under stirring for 3 h at room temperature, in the dark. The resulting AcDXSp-P-ANP nanoparticles were washed twice with sucrose 2% (pH 8).

4.1.5. Fluorescence-labeling (II–IV)

For fluorescence labeling, the Un-D (**II**) or Un-P-D (**III**) nanoparticles were activated using EDC/NHS chemistry and after 1 h, AlexaFluor® 488 (AF488, Life Technologies) was added to the reaction in a ratio of 70:1 (*w/w*) (nanoparticles:AF488). The reaction was allowed to occur for 2 h and the fluorescently labeled nanoparticles were washed with 0.05 M HCl and twice with Milli-Q water (**II**), or the excess of AF488 was simply removed by centrifugation before modification with ANP (**III**). The labeled nanoparticles were further modified with the respective peptides, as described in section 4.1.4.. The same treatment was applied to Un-D or Un-P-D particles, excluding the addition of peptides. For fluorescence labeling of AcDXSp nanoparticles, the AcDXSp were activated using EDC/NHS chemistry and the addition of AF488 was at a ratio of 500:1 (w/w) (AcDXSp:AF488) during 1 h (**IV**). PEGylation and modification with ANP were performed the same way as described in section 4.1.4.

4.1.6. Physicochemical characterization (I–IV)

The hydrodynamic diameter (Z-average), PdI, and ζ-potential values of the different nanoparticles were determined by DLS and ELS using Zetasizer Nano ZS instrument (Malvern Instruments Ltd). The measurements were performed in Milli-Q water and/or 5.4% glucose (**II, III**) or 2% sucrose (**IV**). To evaluate the morphology and size distribution of THCPSi and TOPSi microparticles, the samples were suspended in EtOH and a droplet of each was added to a metallic sample holder, allowed to dry and sputter-coated with platinum. The imaging was done under a scanning electron microscope (SEM; Zeiss DSM 962) (**I**). The size distribution and morphology of nanoparticles (**I–IV**) was evaluated by transmission electron microscopy (TEM; FEI Tecnai F12). The samples for TEM were prepared by embedding carbon-coated

copper grids into nanoparticle suspensions and allowed to dry overnight. The morphological features of UnTHCPSi modified nanoparticles were also imaged with a high-resolution SEM (ZEISS Ultra-55) (**II**). The evaluation of the qualitative elemental composition of UnTHCPSi, Un-P, Un-P-D and Un-P-D-ANP nanoparticles was done by TEM – energy-dispersive X-ray (EDX) spectroscopy (Hitachi S-4800 field emission scanning transmission electron microscope equipped with a bright field TE detector and INCA 350 EDX spectrometer) (**III**). The amount of ANP peptide covalently conjugated to the Un-D nanoparticles was determined by HPLC by an indirect method (**II**). The quantification of ANP onto Un-P-D and AcDXSp-P-ANP nanoparticles was done by elemental analysis (EA) (Elementar Analysensysteme, GmbH), where the amount of peptide was calculated based on the percentage of each element (carbon (C), hydrogen (H), nitrogen (N) and sulfur (S)), and the chemical structure of the peptide (**III, IV**). The surface chemistry of the dry micro- and nanoparticles was evaluated by attenuated total reflectance Fourier transform infrared spectroscopy (ATR–FTIR), using a Bruker VERTEX 70 series FTIR spectrometer (Bruker Optics) and an ATR sampling accessory (MIRacle, Pike Technology, Inc.). The spectra were recorded in the wavenumber region of 4000–650 cm^{-1} with a resolution of 4 cm^{-1} using OPUS 5.5 software. Finally, the colloidal stability of the nanoparticles was assessed by DLS. The different nanoparticles were dispersed in 5.4% glucose, and their *Z*-average, PdI and ζ-potential values were measured over the course of 6 days. The samples were kept at +4 °C under static conditions (**III**). To evaluate the effect of human plasma (**II, III**) or cell medium (**IV**) on the size and the PdI, the nanoparticles were dispersed in 200 μL of Milli-Q water (**II**) and 5.4% glucose (**III**), or freshly prepared Milli-Q water at pH 8 (**IV**). Sequential samples were taken and the hydrodynamic diameter (nm), PdI and ζ-potential values were measured at different timepoints up to 120 min (**II, IV**) or 240 min (**III**). To evaluate the dissolution behavior of AcDXSp nanoparticles under different pH-conditions, the AcDXSp, AcDXSp-P, and AcDXSp-P-ANP were individually added into the buffer solution (pH 7.4 and 5.0) at a concentration of 1 mg/mL. Samples were taken at different time points (100 μL) to a TEA solution (0.01%, v/v; 1 mL, pH 8) to terminate the degradation process of AcDXSp, centrifuged (5 min, 16100*g*), and again redispersed in TEA solution. The sample preparation for TEM imaging was similar to the process described above.

4.1.7. Drug loading and encapsulation, encapsulation efficiency, loading degree and release studies (III, IV)

In **III**, Un-P-D-ANP nanoparticles (1.05 mg) were suspended in 10.5 mL of a solution of the small molecule compound trisubstituted-3,4,5-isoxazole (C1) [301, 302] in 90% EtOH (2 mg/mL) with stirring at room temperature for 2 h. The excess of the drug was removed by washing with PBS, after which 50 μg of nanoparticles were suspended in EtOH and stirred at room temperature for 1 h. The supernatant was collected and analyzed by HPLC for the detection of C1 and determination of the loading degree (LD). Drug release studies were conducted in human plasma for Un-P-D-ANP nanoparticles loaded with C1, as well as for the free C1 as a control. For that purpose, 300 μg of C1-loaded Un-P-D-ANP particles or C1 alone was suspended in human plasma with stirring at 37 °C and samples were collected over 4 h. An Agilent 1100 series HPLC system (Agilent Technologies) was used to quantify C1. A Gemini–NX 3 μm C_{18} 110Å reversed phase column (100 × 4.6 mm, Phenomenex) was used. The mobile phase was 0.1% phosphoric acid and MeOH (ratio of 65:35 v/v), the flow rate was 0.8 mL/min, the injection volume was 20 μL, and the wavelength was 280 nm. To detect the compound in human plasma, a Zorbax C_{18} (4.6 × 100 mm, 5 μm) column was used as the

stationary phase, with the same mobile phase. The flow rate was 1 mL/min, the injection volume was 50 µL, and the wavelength was 280 nm. The plasma samples were diluted 1:1 with acetonitrile beforehand to precipitate plasma proteins. In **IV**, a known amount of CS@AcDXSp, CS@AcDXSp-P or CS@AcDXSp-P-ANP nanoparticles were suspended in 1 mL of acetonitrile (ACN) for total dissolution of the nanoparticles. The resulting solution and all supernatants were measured for the detection of CHIR99021 and SB431542 contents. The encapsulation efficiency (EE) and LD were calculated as follows:

$$EE\ (\%) = \frac{\text{amount of drug encapsulated (µg)}}{\text{total amount of drug (µg)}} \times 100$$

$$LD\ (\%) = \frac{\text{mass of loaded drug (µg.}\ mL^{-1}) \times \text{volume (mL)}}{\text{total mass of drug encapsulated nanoparticles (µg)}} \times 100$$

The release of CHIR99021 and SB431542 from the different nanoparticles was assessed at physiologically relevant pH-values of 7.4 and 5.0. The drug-loaded nanoparticles were immersed into the appropriate release medium, stirring at 150 rpm and 37 ± 1°C. Pure CHIR99021 and SB431542 were used as controls. Samples of 200 mL were taken at specific time points, and the same volume of fresh pre-heated buffer was added for replacement. The withdrawn samples were centrifuged (5 min, 16100*g*), and analyzed by HPLC for quantification of the concentrations of the drugs. The same HPLC instrument was used to quantify the compounds encapsulated inside the bare and functionalized AcDXSp nanoparticles. A Discovery® 5 µm C_{18} reversed phase column (100 × 4.6 mm, Supelco) was used. The mobile phase was Na_2HPO_4:citric acid (2:1) (pH 6.0) and ACN (50:50, v/v). The flow rate used was 1.4 mL/min, the injection volume 5 µL, and the wavelength 274 ± 20 nm.

4.2. *In vitro* studies

4.2.1. Isolation of primary cardiomyocytes and non-myocytes (I–IV) and continuous cell lines (II, III)

The isolation of cardiac cells from neonatal rats was adopted from Pikkarainen *et al.*[303] Wistar rats (1–4 days old) were euthanized by decapitation, and the cardiac ventricles were excised and cut into small pieces. The tissue pieces were enzymatically digested by incubating at 37 °C with gentle mixing for about 1:45 h in collagenase type 2 and pancreatin solution. The cells in suspension were collected by centrifugation. The supernatant and the top layer containing damaged cells were discarded, and the remaining cells were suspended in Dulbecco's Modified Eagle's Medium (DMEM)/F12 supplemented with 2.5 mM L-glutamine, penicillin (100 IU/mL), streptomycin (100 mg/mL) (PS, 1% v/v) and 10% heat inactivated fetal bovine serum (hiFBS). The cells were pre-plated for 60-80 min onto cell culture plates, and unattached cells (enriched cardiomyocytes)[304, 305] were plated at a desired density. The day after plating, cardiomyocytes media was replaced by complete serum-free medium (CSFM). Non-myocytes were cultured in supplemented DMEM/F12 until confluency and plated for the experiments. The cells were maintained at 37 °C with 5% CO_2 and 95% air in a humidified atmosphere. H9c2 (2-1) (American Type Culture Collection® CRL-1446™) myoblast cells (**II**)

were cultured in DMEM supplemented with 10% hiFBS and 1% PS. The cells were maintained at 37 °C with 5% CO_2 and 95% air in a humidified atmosphere.

4.2.2. Chemically induced hypoxic conditions (II, III)

Healthy primary cardiomyocytes and non-myocytes were pre-treated with cobalt chloride ($CoCl_2$) (**II, III**) at a concentration of 100 μM, 18–24 h before the experiments, in order to mimic the hypoxic conditions in the ischemic heart tissue.[306, 307] The $CoCl_2$ was maintained during the experiments.

4.2.3. Cytocompatibility (I–IV)

The cells were primarily seeded into 96-well plates. Primary cardiomyocytes were seeded at a cell density of $2–5\times10^4$ cells per well. After reaching confluency, primary non-myocytes were seeded at a cell density of $1–3.5\times10^4$ cells per well (**II–IV**). H9c2 cells were seeded at a density of 3.5×10^4 cells per well and both were allowed to attach overnight (**II, III**). For publications **I** and **II**, the cell viability upon incubation with the different particles was assessed in 10 mM Hank's balanced salt solution (HBSS)-4-(2-hydroxyethyl)-1-piperazineethanesulfonic acid (HEPES) buffer solution at pH 7.4. The suspensions of micro- and nanoparticles were prepared at concentrations ranging from 25 to 1000 mg/mL. Prior to the addition of the particle suspensions to the cells, the wells were washed with 100 μL of HBSS–HEPES (pH 7.4) buffer and 100 μL of the PSi suspensions (in HBSS–HEPES, pH 7.4) were added to each well. For publications **III** and **IV**, the cell viability was assessed in CSFM for cardiomyocytes and in DMEM/F12 (complete and serum-free (**IV**)) for non-myocytes. The cells were then incubated at 37 °C for 3 h (**I**), 4 h (**III**), 6 h (**II, IV**) and 24 h (**III, IV**). After the incubation, the cells were washed twice with HBSS–HEPES (pH 7.4) buffer. 50 μL of HBSS–HEPES (pH 7.4) and 50 μL of CellTiter Glo® (Promega Corporation) were added to each well. In publication **IV**, the cytocompatibility of cardiomyocytes and non-myocytes in complete medium was assessed using thyazolyl blue tetrazolium bromide (MTT). After incubation at 37 °C for 24 h, 10 μL of MTT solution (2.5 mg/mL) were added to the cells and incubated for 2.5 h at +37°C. The supernatant was removed and 100 μL of DMSO were added to dissolve the water-insoluble formazan crystals formed. Negative (1% Triton X-100), positive (cell medium) and blank (only Cell Titer Glo reagent® or MTT solution) controls were used and treated similarly. The luminescence or absorbance (490 nm) were measured using a Varioskan Flash Multimode Reader (Thermo Fisher Scientific).

4.2.4. Cell–nanoparticle interactions and displacement studies (II–IV)

The cell–nanoparticle interactions were evaluated qualitatively by TEM (**II**) and confocal microscopy (**III**). Quantitative cell–nanoparticle interactions were measured by flow cytometry (**II–IV**). For the TEM imaging, cardiomyocytes, non-myocytes or H9c2 cells were seeded onto 13 mm round shape coverslips placed on 24-well plates at a density of 10^5 cells per well and incubated with each nanoparticle's suspension (50 mg/mL). After incubation over 6 h, the coverslips were washed twice with HBSS–HEPES (pH 7.4) and fixed with 2.5% glutaraldehyde for 30 min. For TEM sample preparation, the cells were post-fixed with 1% osmium tetroxide in 0.1 M NaCac buffer (pH 7.4), dehydrated and embedded in epoxy resin.

Ultrathin sections (60 nm) were cut parallel to the coverslip, post-stained with uranyl acetate and lead citrate, and the images were acquired using a TEM microscope (Jeol 1400).

For the confocal fluorescence microscopy imaging (**III**), cardiomyocytes were seeded onto 13-mm coverslips at a density of 10^5 cells per well. Non-myocytes were seeded at a density of 4×10^4 cells per well in Lab-Tek 8-chamber slides. Cells were pre-treated with $CoCl_2$ over 18–24 h prior to and for the duration of the experiments. Both the cell types were exposed to 50 μg/mL of AF488-labeled nanoparticles in their respective culture medium for 4 h and washed twice with HBSS–HEPES (pH 7.4). The plasma membrane was stained with CellMask® Deep Red (5 μg/mL, at 37 °C) and fixed with 4% paraformaldehyde for 20 min at room temperature. The coverslips containing the cardiomyocyte samples were mounted on glass slides using Vectashield antifade mounting medium with DAPI (Vector Laboratories). For the non-myocytes, the nuclei were stained with DAPI-405 (2.8 μg/mL) for 5 min at room temperature. Leica TCS SP5II HCS A confocal inverted microscope (Leica Microsystems) was used for imaging. The images were processed using LAS AF (2.6.0 build 7266) software.

For quantitative studies (**II–IV**), cardiomyocytes were seeded in 6-well plates at a density of $4–5\times10^5$ cells per well (**II, III**). Non-myocytes were seeded at a density of $1–3.5\times10^5$ cells per well (**II–IV**). Cells were kept under normoxic conditions (**II**), pre-treated with $CoCl_2$ over 18–24 h (**II, III**) or serum-starved for 18h (**IV**) prior to and for the duration of the experiments and incubated with AF488-labeled nanoparticles (50 μg/mL) for 6 h (**II**) and 4 h (**III**) and 1 h (25 μg/mL, **IV**) in the respective culture medium. For the displacement experiments, the cells were treated with free ANP at concentrations ranging from 1 to 100 μM, together with the nanoparticles (25–50 μg/mL) (**II–IV**). Cardiomyocytes were also pre-treated with concentrations of anantin [308] (Bachem) ranging from 0.1–10 μM, 30 min before the treatment with nanoparticles. Anantin was kept during the experiments (**II**). The cells were washed, collected and suspended in HBSS–HEPES. The measurements were performed using an LSR II flow cytometer with a laser excitation wavelength of 488 nm. The internalization of nanoparticles in the ANP displacement experiments was assessed by quenching the fluorescence of membrane-associated nanoparticles trypan blue (0.005% v/v). Approximately 10,000 events were obtained per sample. The data analysis was performed using FlowJo X 10.0.7r2 software.

4.2.5. Immunostainings and high content cell imaging and analysis (IV)

Non-myocytes were seeded at a density of 10^4 cells per well in 96-well plates and starved during 18 h prior to the experiments. The nanoparticle suspensions or free-drugs were added to each well at concentrations of 1 μM of CHIR99021 and 2 μM of SB431542,[123, 309] and incubated for 6 h. The serum-free conditions were kept during the experiments. Cells were washed twice with PBS and fixed with 4% paraformaldehyde for 20 min. The cells were permeabilized with 0.1% Triton X-100 during 10 min. The blocking step was done with 4% FBS in PBS for 45–60 min and incubated with primary antibodies (β-catenin, Smad3, alpha-smooth muscle actin (α-SMA) and vimentin) for 60 min at room temperature. Secondary antibodies were added to each well (anti-mouse 488, anti-mouse 647, anti-rabbit 488, anti-rabbit 647 and DAPI, and incubated for 45 min at room temperature. Cells were washed and stored at +4°C until imaged. The images captured using a Cellomics CellInsight high-content analysis platform (Thermo Scientific) with a 10x objective and analyzed simultaneously using a protocol based on Compartmental Analysis bioapplication. DAPI staining was used to define the nuclei and a 5-pixel ring around the nuclear mask was used to represent cytoplasm.

4.3. *In vivo studies*

4.3.1. Particle injections and experimental models of MI (I–III)

About 8-week old male Sprague-Dawley rats (250–300 g) were anesthetized and microparticles or nanoparticles were injected intramyocardially in the LV of exposed hearts prior to the induction of MI, produced by ligation of the left anterior descending coronary artery during anesthesia.[310] At one or four weeks post-infarction, echocardiographic measurements were performed, the rats decapitated and particular tissues were collected for analysis. (**I**) Myocardial ischemia was produced in rats by subcutaneous injection of a single dose of isoprenaline (5 mg/kg)[311] 24 h before the *i.v.* injection of nanoparticles. Male Wistar rats (233–330 g) received unlabeled and ^{111}In-radiolabeled PSi nanoparticles *i.v.* via the tail vein. The animals were anesthetized with isoflurane (Attane Vet., ScanVet Animal Health, Finland) in an air/oxygen carrier at 0.4/0.6 (L/min). The animals were sacrificed at specific time points with an overdose of isoflurane or CO_2 followed by cervical dislocation (**II, III**).

4.3.2. Echocardiographic measurements (I)

Transthoracic echocardiography was performed using the Acuson Ultrasound System (Sequoia™ 512) and a 15-MHz linear transducer (15L8) (Acuson, Mountain View) in anesthetized rats. Using two-dimensional imaging, a short axis view of the LV at the level of the papillary muscles was obtained and a two dimensionally guided M-mode recording through the anterior and posterior walls of the LV was obtained. LV end-systolic and end-diastolic dimensions, the thickness of the interventricular septum and posterior wall were measured from the M-mode tracings. LV fractional shortening (FS) and ejection fraction (EF) were calculated from the M-mode LV dimensions. All echocardiographic measurements were performed by a skilled sonographer blinded to the treatments.

4.3.3. Hematoxylin and eosin staining and histology (I, III)

After sacrificing the animals, the hearts were removed and transverse sections of the middle part of the heart were fixed in 10% neutral buffered formalin for 1–2 days, embedded in paraffin, cut into 5 mm-sections from the injection area and mounted on slides. To evaluate the presence of micro-/nanoparticles and inflammatory response, formalin-fixed, paraffin-embedded sections were deparaffinized in xylene and dehydrated in graded EtOH and stained with hematoxylin and eosin (H&E). Inflammation was scored from the H&E stained slides by evaluating the size of the inflamed granulation tissue area as either negative (–) or positive (+); no inflammation or very slight inflammation was scored as negative, substantial inflammation was scored as positive. Masson's trichrome technique was used to define the extent of fibrosis (fibrotic area/total LV area) in the LV by using Nikon NISElement 3.2 software. Histological analysis was performed by using a light microscope (Nikon Eclipse 50i). (**I**) After autoradiography, the heart sections were subsequently stained with H&E, and a full image of each heart section was taken with a Nikon D40 Digital SLR camera fitted on a Nikon bright field microscope for digital microphotography with high color fidelity and 1× magnification (**III**).

4.3.4. Gene expression analysis (I)

The total RNA from the apical heart tissue was isolated by the guanidine thiocyanate–CsCl method.[312] For quantitative real-time polymerase chain reaction (RT-PCR) analyzes, cDNA was synthesized from total RNA with a First-Strand cDNA Synthesis Kit (GE Healthcare Life Sciences) following the manufacturer's protocol. RNA was analyzed by RT-PCR on an ABI 7300 sequence detection system (Applied Biosystems). The results were quantified using the ΔΔCT method and normalized to 18S housekeeping gene from the same samples to correct the potential variation in sample loading.

4.3.5. *In vivo* SPECT/CT imaging and *ex vivo* biodistribution (II, III)

Small animal SPECT/CT equipment (Bioscan NanoSPECT/CT, Mediso) was used to study the *in vivo* biodistribution and live heart accumulation of the nanoparticles. The rats were administered with [^{111}In]-labeled nanoparticles intravenously, and the whole-body SPECT/CT images were acquired under isoflurane anesthesia immediately after injection for 10 and 20 min (in a dynamic scanning mode with 2×10 min frames and 16 projections at 30 sec per projection). Another scan was performed at 4 h after ^{111}In-labeled nanoparticle administration (16 projections and 60 sec per projection). A 45-kV inbuilt X-ray source was used to acquire CT images with a 500-msec exposure time in 180 projections and a pitch of 0.5 with an acquisition time of 5 min after the respective SPECT scan. All images were reconstructed using HiSPECT NG software (Scivis GmbG, Göttingen) and analyzed using InVivo Scope software (InviCRO LLC) (**II, III**). Several voxel-guided ROI were drawn from the apical to basal regions of the heart using the fused SPECT/CT-images, and the results were expressed as SUVs, which were calculated using the average radioactivity concentration of the ROI normalized with the injected radioactivity dose and animal weight [311] (**III**). After the last SPECT scan, the rats were sacrificed by cervical dislocation under anesthesia, and the samples from the blood, liver, spleen, lung, heart, kidney, bone with marrow, brain, and urine were collected and weighed for independent radioactivity measurements using an automated γ-counter (Perkin Elmer Wizard 3, Perkin Elmer). The results were calculated as the percentage of injected dose per gram of tissue (%ID/g).

4.3.6. Tissue autoradiography and image quantification (III)

The fresh hearts were snap-frozen in isopentane on dry ice after being washed in PBS, and thin sections of 10 μm were cut from the apical, medial and basal regions using a cryostat microtome (CM1950, Leica Microsystems). The sections were thaw-mounted on SuperFrost Plus microscope slides (VWR Collection, Finland), air dried for 3–4 h and stored at −20 °C until autoradiography. The cryosections were exposed to a digital imaging plate (Fujifilm) for 88 h, and the plate was scanned on a Fujifilm-5100 scanner. Images were analyzed with AIDA 2.0 imaging software (Raytest). ROIs were drawn on the endocardium and epicardium (apical, medial and basal regions) autoradiographs based on the identification of their respective heart sections from H&E-stained photographs.

4.3.7. Biological effects of drug-loaded ANP-modified nanoparticles *in vivo* (III)

The C1-loaded Un-P-D-ANP or unloaded Un-P-D-ANP nanoparticles were suspended in 5.4% glucose (500 μg/mL) and 200 μg aliquots were injected *i.v.* in rats with isoprenaline-induced MI. The animals were sacrificed by either isoflurane overdose or CO_2 and additional cervical dislocation at three different time points: 4, 24 and 72 h after the first NP injection. The nanoparticles were administered once in the 4-h and 24-h study groups, and three times (t = 0, 24 and 48 h) in the 72-h study group. Immediately after sacrifice, the hearts were collected and washed in PBS while still pumping. The LV was placed between two tweezer platforms, frozen in liquid N_2 and further stored at −80 °C. The LV was cut into 100-μm slices from the endocardial side. The first 12 slices were combined and considered the endocardium. A NucleoSpin RNA Midi Kit (Macherey-Nagel) was used to isolate RNA and protein. The tissue samples were homogenized in lysis buffer using a Gentle MACS dissociator with M-tubes (Mitenyi Biotec). The proteins were isolated from RNA, precipitated using Protein Precipitator (Macherey-Nagel), washed with 50% ethanol, pelletized and air-dried. Finally, the protein pellet was dissolved in TCEP buffer (Macherey-Nagel), and the protein concentration was determined using a BCA protein assay kit (Pierce). Ten micrograms of total protein were loaded onto a 10% TGX gel (Bio Rad), separated at 160 V for 70 min and transferred to a nitrocellulose membrane (Bio Rad) for 7 min using the Trans-Blot Turbo Transfer System (Bio-Rad). For membrane blocking and antibody dilutions, 5% BSA in TBS-Tween (0.1%) was used. The immune complexes were visualized using SuperSignal West Pico Chemiluminescent Substrate (ThermoFisher Scientific), and chemiluminescence was detected and digitalized with a Luminescent Image Analyzer LAS-3000 (Fujifilm). Two identical western blots were run from each sample group for detection of phosphor-ERK and total ERK 1/2, phosphor-p38 and p38 and glyceraldehyde 3-phosphate dehydrogenase (GADPH). The immunoreactive bands were quantified using Quantity One software (Bio-Rad), and the optical densities were normalized to the reference GAPDH.

4.4. Statistics (I–IV)

Results are expressed as the mean ± standard deviation (SD) or standard error of the mean (S.E.M.). Statistical analyses were performed using a SPSS version 19.0.0.1 (SPSS Inc., Chicago, IL, USA) and GraphPad Prism version 5.00 (GraphPad Software, San Diego, California, USA) (**I, III**). For evaluation of the extent of inflammation and granulation tissue caused by the micro/nanoparticle injection, Fisher's exact test was used (**I**). To determine the statistical difference between two groups, the independent samples Student's *t*-test was used. For multiple comparisons, the statistical significance was evaluated by one-way analysis of variance (ANOVA), followed by a Bonferroni or Tukey-Kramer post hoc tests (**I–IV**). The probability values of $^{*, \#, \S, \bullet}p < 0.05$, $^{**, \#\#}p < 0.01$, and $^{***, \S\S\S}p < 0.001$ were considered statistically significant.

4.5. Ethics (I–IV)

In publication **I**, experimental protocols with animals were approved by the Animal Use and Care Committee of the University of Oulu and the Regional State Administrative Agency for Southern Finland, and conform to the Guide for the Care and Use of Laboratory Animals published by the US National Institutes of Health. In publications **II** and **III**, all experimental protocols with animals were approved by the Laboratory Animal Center of the University of Helsinki and the National Animal Experiment Board of Finland according to the EU's Guidelines for Accommodation and Care of Animals, following the Act (497/2013) and the Decree (564/2013) on Animal Experimentation approved by the Finnish Ministry of Agriculture and Forestry, and the EU Directive (2010/63/EU). For the primary cell cultures for *in vitro* experiments in all the publications **I–IV**, the animals were used after an internal license was authorized and approved by the Laboratory Animal Centre, University of Helsinki.

5. Results and discussion

There is a limited amount of information available showing the advantages of nanoparticulate systems for the treatment of cardiac ischemic disease, which requests for more studies in order to deliver biologicals and poorly-soluble small drug molecules that would be able to reverse the remodeling process, the dysfunctional fibrotic scar formation and/or promote cardiac regeneration after a MI event. In this thesis, the potential of PSi-based and AcDXSp-based nanosystems was explored. At first, the biocompatibility of PSi to cardiac cells and tissues was evaluated, after which a screening of different peptide-modified PSi nanosystems was performed to investigate the potential targetability, subsequently followed by an extensive *in vivo* study of the biodistribution, heart accumulation, selectivity to the ischemic heart areas and drug delivery. In the same line, AcDXSp nanoparticles were functionalized for enhanced stability, compatibility and targeting, and their potential to deliver different payloads for combined cardiac therapy in a controlled fashion was assessed.

5.1. Cytocompatibility and biocompatibility of PSi nanoparticles of different surface chemistries (I)

The study of the biosafety of a synthetic material for a new biomedical application, such as drug delivery and targeting, is of utmost importance to ensure successful delivery of therapeutics without exerting significant deleterious effects.[314-317] Because limited information is available about the effects of nanostructured materials on the heart tissue,[318] and there is a lack of previous reports describing the application of PSi materials for the application in cardiovascular diseases, the focus of this study was to investigate the cyto- and biocompatibility of PSi micro- and nanoparticles of different surface chemistries in primary cardiomyocytes, as well as *in vivo* in healthy and in MI LAD rat models.

5.1.1. Characterization and cytocompatibility of THCPSi and TOPSi particles (I)

In this initial study, a brief physicochemical characterization of the used hydrophobic THCPSi microparticles and hydrophilic TOPSi micro- and nanoparticles was performed, and their cytocompatibility assessed. **Figure 9A–E** shows representative SEM images of THCPSi and TOPSi microparticles and a representative TEM image of the TOPSi nanoparticles, characterized by an average particle size of 7 and 19 μm for the THCPSi microparticles, 7 and 17 μm for the TOPSi microparticles, and 110 nm for the TOPSi nanoparticles, showing an irregular shape. The cytocompatibility of THCPSi and TOPSi micro- and nanoparticles was evaluated by incubating the micro- and nanoparticles with cardiomyocytes and measuring their metabolic activity. A possible reason for the TOPSi microparticle toxicity could lie in the differences in size, as the TOPSi microparticles induced higher toxic effect than the TOPSi nanoparticles. This observation is in agreement with a previous study, where TOPSi particles in a size range of 1–25 μm were found to induce the most toxic effects in Caco-2 and RAW 264.7 macrophage cells, compared to TOPSi nanoparticles.[299] Overall, THCPSi microparticles and TOPSi nanoparticles were less toxic towards the primary cardiomyocytes (**Figure 9F–G**).

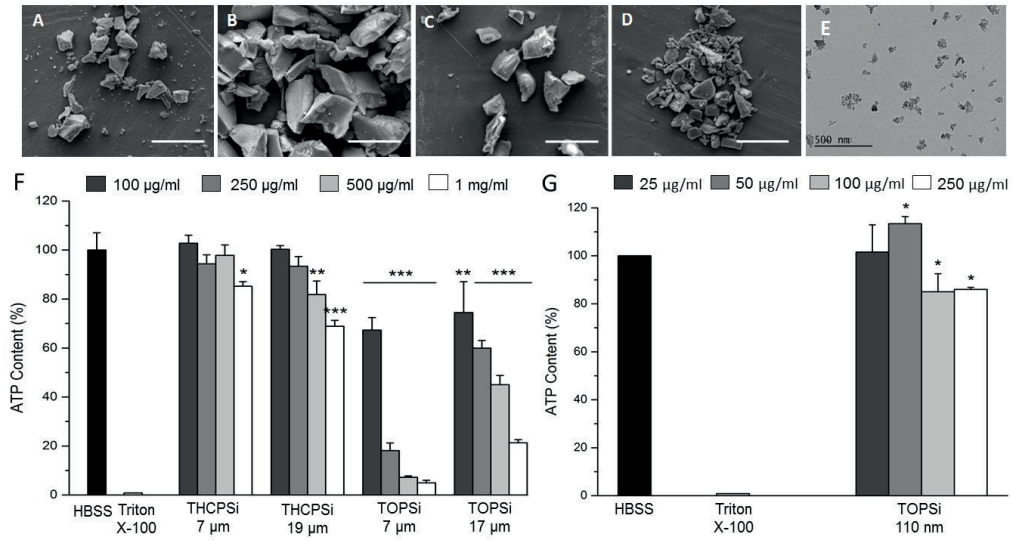

Figure 9. Characterization of TOPSi and THCPSi micro- and nanoparticles and cell viability studies used in publication (**I**). (A–D) SEM images of TOPSi 7 µm (A), TOPSi 17 µm (B), THCPSi 7 µm (C), THCPSi 19 µm (D) and TEM image of TOPSi 110 nm nanoparticles (E) used in this study. Scale bars are 40 µm and 500 nm for the SEM and TEM images, respectively. (F–G) Metabolic activity of primary cardiomyocyte cells determined by the CellTiter-Glo® Luminescence Cell Viability Assay after 3 h incubation at 37°C with THCPSi and TOPSi microparticles (F), and TOPSi nanoparticles (G). The results are expressed as mean ± S.E.M. (n = 3). *p<0.05, **p<0.01 and ***p<0.001 *vs.* control. Copyright © 2014 Elsevier B.V., adapted and reprinted with permission from publication (**I**).

5.1.2. Assessment of cardiac function

The *in vivo* biocompatibility of THCPSi microparticles and TOPSi micro- and nanoparticles was evaluated by injecting the particles intramyocardially. To study the effects of THCPSi and TOPSi micro- and nanoparticles on the function of the heart, cardiac function was assessed using echocardiography at 7 days or 4 weeks post-injection. THCPSi (7 and 19 µm) and TOPSi (7 and 17 µm) microparticle injections had no effect on LV systolic function (ejection fraction or fractional shortening) at one week or at 4 weeks compared to control injected animals (**Figure 10A** and 10**B**), showing a slight increase in LV ejection fraction (11%) and fractional shortening (13%) at one week in response to TOPSi 110 nm particles. Based on these observations, and to study whether the TOPSi particles can be a useful biomaterial in an experimental MI, LAD ligation was performed immediately after intramyocardial particle administration. Ligation of the LAD expectedly caused a decrease in the ejection fraction (**Figure 10C**) and fractional shortening (**Figure 10D**) in conjunction with the injection of TOPSi 7 µm during the one week's follow-up. Other parameters in both healthy and MI animals, such as cardiac output, stroke volume or heart rate, were not altered in consequence to any of the aforementioned treatments. Overall, no major alterations occurred in cardiac function after administration of THCPSi or TOPSi particles in the myocardium of normal rat hearts. In addition, no unexpected changes were observed after myocardial treatment with the

TOPSi in functional alterations after MI in rats, suggesting that PSi-based materials can be used and tested further in experimental MI models.

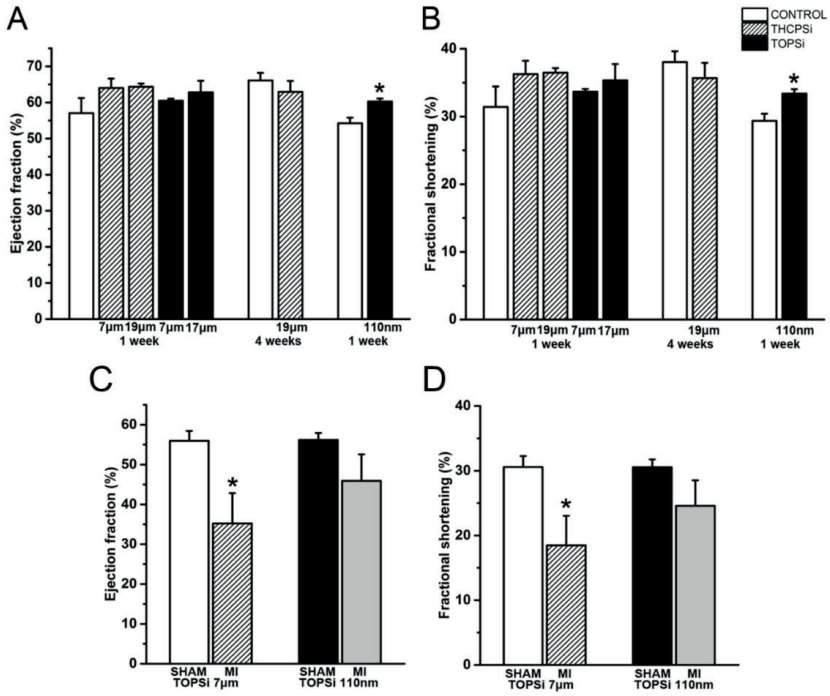

Figure 10. (A–B) Effect of intramyocardial delivery of THCPSi or TOPSi micro- and nanoparticles on cardiac function in normal rat heart. THCPSi and TOPSi microparticles had no effect on ejection fraction (A) and fractional shortening (B). The results are expressed as mean ± SEM (n = 3–4). *p<0.05 *vs.* control. (C–D) Effect of intramyocardial delivery of TOPSi micro- and nanoparticles on cardiac function in the rat heart after MI at one-week post-infarction and particle treatment. (C) Ejection fraction and (D) fractional shortening alterations are normal for an infarcted heart. The results are expressed as mean ± S.E.M. (n = 5–6). *p<0.05 *vs.* SHAM. Copyright © 2014 Elsevier B.V., adapted and reprinted with permission from publication (**I**).

5.1.3. Histology, inflammatory and fibrotic gene expression analyses

The inflammatory response and cytokine production play significant roles after MI. Cytokines, such as tumor necrosis factor-α (TNF-α) and interleukin-6 (IL-6), mediate cardiac repair and remodeling through activating matrix metalloproteinases, type I and III collagen formation, integrin regulation, angiogenesis, and progenitor cell mobilization. [4, 319, 320] To evaluate the inflammatory and fibrotic responses on a gene level, the mRNA levels of the pro-inflammatory cytokines IL-6 and TNF-α, and fibrosis promoting genes collagen Iα1 (Col Ia1)[320] and the pro-fibrogenic extracellular matrix protein and cytokine osteopontin (OSP), [319] were measured in MI rat hearts one week after TOPSi micro- and nanoparticles injections. One week after MI, it was observed a significant increase in IL-6 (**Figure 11A**), collagen Iα1 (**Figure**

11B) and osteopontin mRNA (**Figure 11D**) in the TOPSi 7 μm injected rat hearts. The same increasing trend was observed for IL-6, Col Ia1 and OSP gene expressions when TOPSi 110 nm particles were injected into rat hearts at one week after MI, although these changes were not statistically significant. The TNF-α mRNA levels did not differ (**Figure 11C**). This gene expression data is in agreement with the presented functional/echocardiographic data achieved from infarcted rat hearts (**Figure 10**), indicating that TOPSi micro- and nanoparticles can be considered a useful biomaterial for the treatment of MI in rats.

Additionally, histological sections were prepared from the THCPSi and TOPSi micro- and nanoparticles injected into healthy rat hearts, stained with H&E for inflammation and with Masson's trichrome for fibrosis detection. On one hand, at one week, fibrosis in the THCPSi and TOPSi micro-/nanoparticle -injected hearts did not differ significantly from the control hearts (**Figure 11E**). On the other hand, increased inflammation was observed in the myocardium after injection of THCPSi 7 μm microparticles (**Figure 11F**, black arrows), while only a minor inflammatory reaction was seen in control or THCPSi 19 μm and TOPSi-treated heart tissue sections. In the heart tissue sections after injections of THCPSi 7 and 19 μm, the particles constituted distinct zones, while only a few separate undissolved particles could be observed in heart sections after one-week post-injection by TOPSi 7 μm, 17 μm and 110 nm (**Figure 11F**). The surface chemistry properties of PSi particles play a key role in the resistance to degradation, so that hydrophilic TOPSi particles may degrade faster than corresponding THCPSi, which possess a hydrophobic surface.[29, 247, 299] In addition, it has been described that the presence of proteins might accelerate the degradation of PSi particles, [321] which could also explain the faster degradation rate of TOPSi from the myocardium compared to the THCPSi microparticles.

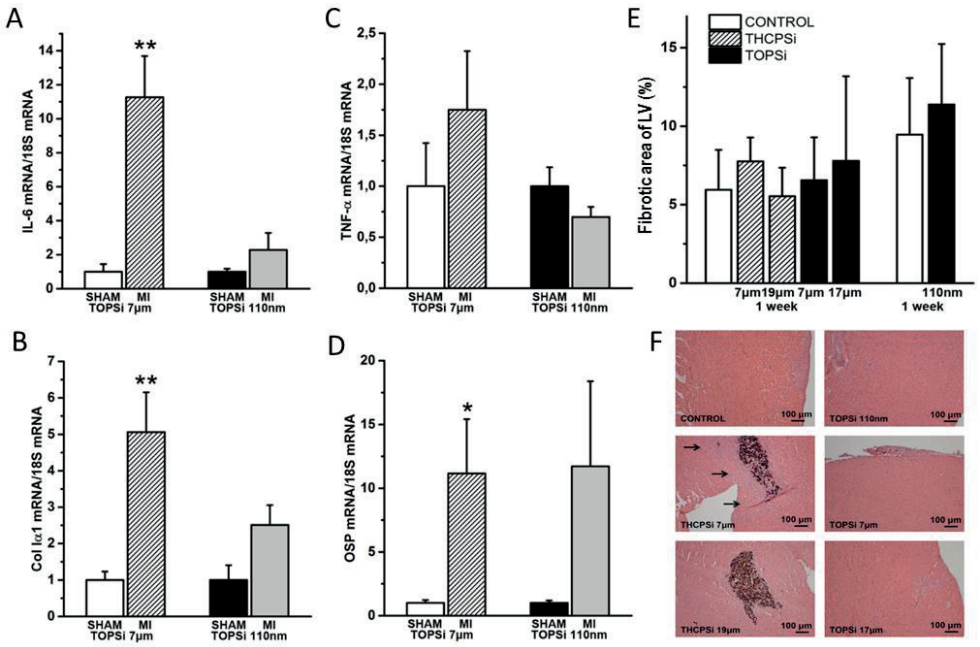

Figure 11. (A–D) The expression of inflammation related and pro-fibrotic genes in the rat heart after MI. TOPSi particles had no effect on gene expression alterations after MI. (A) IL-6 mRNA levels, (B) Collagen (Col) Iα1 mRNA levels, (C) TNF-α mRNA levels and (D)

osteopontin mRNA levels at one-week post-infarction and particle treatment. The results are expressed as mean ± S.E.M. (n = 5–6). *p < 0.05 and **p < 0.01 *vs*. SHAM. (E) Intramyocardial delivery of THCPSi or TOPSi micro- and nanoparticles has no significant effect on myocardial fibrosis at one week post-injection time point. The fibrotic area was assessed from Masson's trichrome-stained LV sections from the rat heart and expressed as mean ± S.E.M. (n = 3–4). (F) Local THCPSi 7 μm, but not THCPSi 19 μm, TOPSi 110 nm, TOPSi 7 μm and TOPSi 17 μm or control treatment increased myocardial inflamed granulation tissue (arrow) in the normal rat heart when injected into the LV myocardium. Paraffin-embedded histological sections were stained with H&E to define the area of inflammation at one-week post-injection (scale bar 100 μm). (**I**).

5.2. *In vitro* screening of heart-targeted UnTHCPSi nanoparticles (II)

Several therapeutic strategies have been used to decrease the myocardial remodeling after an ischemic event. The traditional approaches include pharmacological therapy [55] and/or more invasive methodologies, such as resynchronization therapy biventricular pacing [322, 323] and left ventricular assist devices,[324] while newer strategies comprise of cell therapy and cardiac tissue engineering.[325, 326] However, because the aforementioned approaches involve invasive administration into the damaged cardiac tissue, the employment of nanotechnology has been increasingly considered.[10, 173] The second and third studies of this thesis envisaged to investigate the possibility of development of nanosystems, which could target the heart tissue, via *i.v*. administration. PSi nanoparticles were chosen for their biocompatibility and possibility for *i.v*. administration, as well as for the screening of heart-homing peptides in primary cardiac cells, and mechanistic studies of the cardiac cells; nanoparticle interaction studies were performed to select the most promising system to be investigated *in vivo*.

5.2.1. Surface functionalization of UnTHCPSi nanoparticles

The functionalization of nanoparticles becomes of great importance when targeting a specific tissue. Thus, as an attempt to direct the PSi nanovectors to the heart, UnTHCPSi nanoparticles, originally with a hydrodynamic diameters of 159 ± 1 nm, PdI-values of 0.11 ± 0.02 and ζ-potential values of –31 ± 2 mV, were used and further modified with a metal chelator molecule, DOTA, that allowed the addition of radiolabeling isotopes for *in vivo* imaging studies. After that, the heart homing peptides (ANP, P2, and P3) were covalently attached. Both modifications were performed using EDC/NHS chemical reaction. Particle sizes of the nanosystems were slightly increased after surface modification, as expected, and only slight changes in PdI-values indicated homogeneous size distributions (**Table 4)**. The surface chemistry of the different peptide-modified nanoparticles was evaluated with ATR–FTIR, showing successful surface functionalization with the different peptides by the appearance (among other peaks) of amide I band at 1640 cm^{-1} and amide II band at 1550–1555 cm^{-1} (**Figure 12A**), in line with the formation of amide bonds. The changes of zeta-potential values from negative to positive after covalent attachment of the peptides are in agreement with FTIR observations, due to the presence of amine groups in ANP, P2 and P3, which attributed positive charges to the particle surfaces (**Figure 12B**). The morphology of the high resolution (HR)-

SEM and TEM microscopy were also used to evaluate the morphology of the nanosystems, represented in **Figure 12C–D**.

Table 4. Hydrodynamic diameter (nm) and PdI of the PSi nanoparticles developed in **II**.

Nanoparticle	Size (d.nm)	PdI
Un-D	169 ± 6	0.12 ± 0.05
Un-D-ANP	182 ± 10	0.09 ± 0.02
Un-D-P2	178 ± 7	0.14 ± 0.02
Un-D-P3	171 ± 11	0.13 ± 0.05

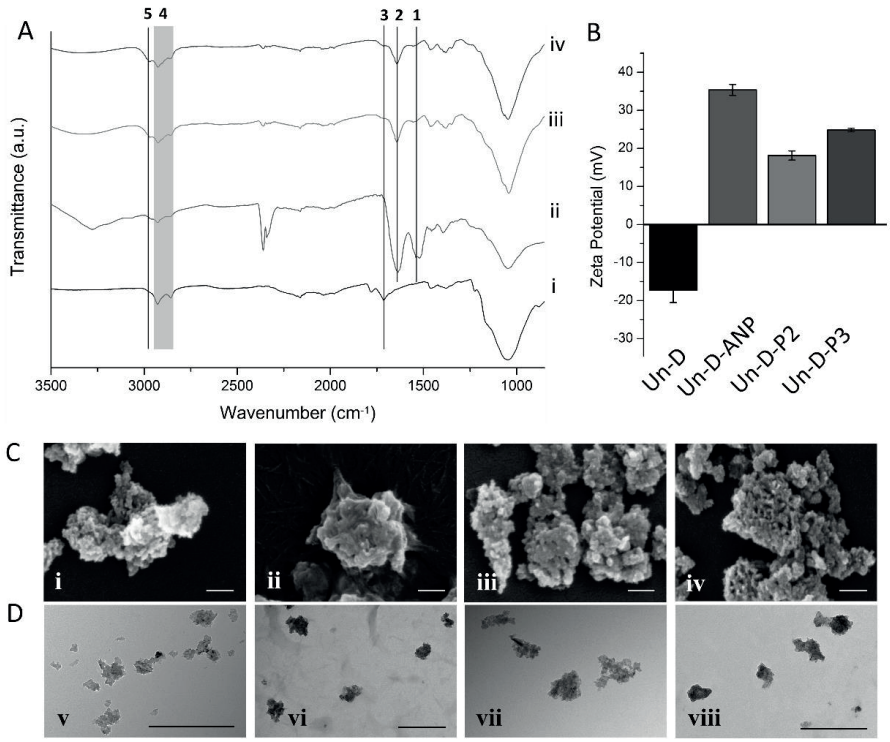

Figure 12. Characterization of the nanoparticles used in publication (**II**). (A) ATR–FTIR spectra. Amide I and II bands at 1550–1555 cm^{-1} (in-plane N–H bending and C–N stretching) and 1640 cm^{-1} (C=O stretching) (bands 1 and 2) of the peptide-modified Un-D NPs. Un-D spectra reveal the carbonyl C=O stretching band at 1713 cm^{-1} (band 3). C-H stretching bands belonging to the long linear aliphatic chain of the undecylenic acid of the NPs at 2929 and 2855 cm^{-1} for the Un-D NPs are visible (region 4) and the appearance of a third band at 2970 cm^{-1} (band 5) correspond to the C-H stretching vibration bands of the amino acids' side chains. (B) ζ-potential values of the NPs used in publication (**II**), mean ± s.d. (n = 3). (C) HR-SEM images of Un-D (i); Un-D-ANP (ii); Un-D-P2 (iii), Un-D-P3 (iv). Scale bars 100 nm. (D) TEM images of Un-D (v); Un-D-ANP (vi); Un-D-P2 (vii), Un-D-P3 (viii). Scale bars 500 nm.

5.2.2. Cytocompatibility studies in different cardiac cell types

The toxicity of nanoparticles is dependent on biological factors like cell type and exposure conditions, as well as on material-related variables, such as size and morphology, surface area, hydrophobicity, and surface charge. These factors can play a significant role in the reactive oxygen species-related toxicity and create potential sites of interaction with receptors, leading to variable degrees of cytotoxicity.[19, 327] In this study (**II**), the cytocompatibility of PSi-based nanomaterials functionalized with heart-homing peptides (25, 50, 100, and 250 μg/mL) was evaluated in primary cardiomyocytes, primary non-myocytes, and H9c2 cells after 6 h of incubation (**Figure 13**). For all the cell types tested, there was an increase in the nanoparticles'-induced toxicity in a concentration-dependent manner. The lower cell viability values were observed for the peptide-modified PSi nanoparticles because of their positive surface charge, in comparison with the negatively charged Un-D nanoparticles. The positive particles are more likely to have higher interactions with the cell membrane compared to nanoparticles with neutral or negative surface charge.[328, 329] Cardiomyocytes seemed to be more sensitive to Un-D-ANP nanoparticles (**Figure 13A**), which could be due to the high number of free amine groups present in ANP peptide, and thus, the more positive nanoparticle. In addition, the cardiomyocytes internalized more extensively Un-D-ANP (**Figure 14A** and **14D**) than Un-D-P2 or Un-D-P3. The greater cellular internalization may influence the cell viability, similarly as observed for other nanosystems.[330-332] H9c2 cells, in contrast, showed to be more resistant to the presence of all the nanoparticles tested (**Figure 13C**). In summary, a satisfactory cellular viability was achieved for nanoparticle concentrations up to 50 μg/mL, which was the concentration chosen for further cell studies.

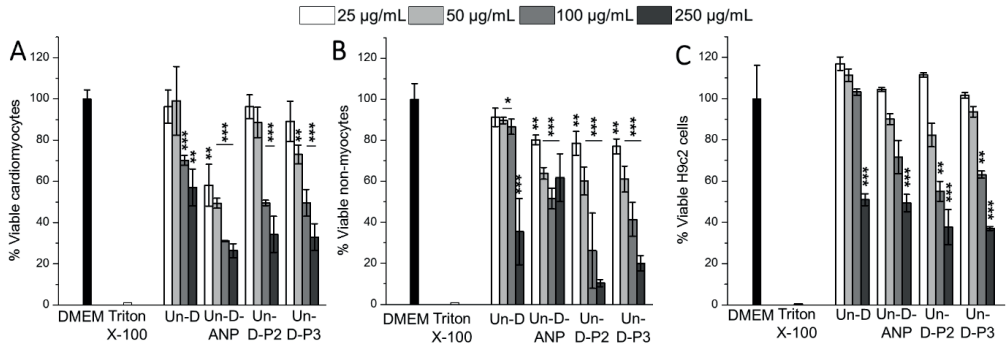

Figure 13. Cytotoxicity profiles of primary cardiomyocytes (A), primary non-myocytes (B), and H9c2 cells (C) after exposure to Un-D and peptide-functionalized Un-D NPs. The ATP-content was measured after 6 h incubation with different concentrations of PSi nanoparticles. The level of significance was set at probabilities of $*p < 0.05$, $**p < 0.01$, and $***p < 0.001$ *vs.* control (HBSS). Values are represented as mean ± s.d. ($n \geq 3$). Copyright © 2016 Elsevier Inc., reprinted with permission from publication (**II**).

5.2.3. Cell–nanoparticle interactions and mechanistic studies (II, III)

The ultimate goal of the biofunctionalization of the NPs with targeting moieties is to ensure a more direct and specific interaction between the nanocarrier and the tissue of interest at the cellular level, and eventually, internalization of the nanocarrier to the cytoplasm, where it may release one or several therapeutic payloads. However, besides the surface chemical composition, there are other factors that can affect the uptake of the nanoparticles and their interactions with the cells. Size, shape, surface charge and hydrophobicity are some of the physical properties that can dictate the interactions of a nanovector with cells.[333] In publications (**II**) and (**III**), primary cardiomyocytes and non-myocytes (mainly cardiac fibroblasts)[3] were used to study the cell–nanoparticle interactions and their main mechanism in hypoxia-like conditions. To induce hypoxia, cells were pre-treated with $CoCl_2$, a compound that stabilizes the hypoxia inducible transcription factor 1a. Cobalt is a metal that has the ability to inhibit key enzymes that participate in the oxygen dependent degradation of the transcription factor, thus upregulating the hypoxic signaling pathway.[306, 307] Because the nanoparticles tested had approximately the same sizes and irregular shapes, it was hypothesized that most of the differences in the cell–nanoparticle interactions were probably explained by the different surface charge and surface chemical composition of the nanoparticles.

Primarily, the screenings of the different peptide-modified nanoparticles were performed by incubating them with primary cardiomyocytes (**Figure 14A**) and non-myocytes (**Figure 14B**), using flow cytometry analysis. In both the cell cultures, the Un-D-ANP nanoparticles had higher cellular uptake percentages compared to the other peptide-modified nanoparticles. It is well-known that positively-charged nanosystems interact more readily with negatively charged groups on the cell surface through electrostatic interactions and translocate across the plasma membrane.[334] Un-D-ANP nanoparticles had the most positively charged surface (**Figure 12B)**. ANP is a 28 amino acids peptide that contains 5 arginines, 1 asparagine and 1 glutamine amino acids that possess primary amines.[68] Such amine groups protonate at pH values lower than the isoelectric point of ANP (pH 11), which largely contribute to the positively charged surface of Un-D-ANP at physiological pH. Thus, Un-D-ANP could be unspecifically internalized due to the interaction with random negative domains of the cell membrane. However, to elucidate this point, it was observed that the cellular internalization of Un-D-ANP occurred at least in part via the NPR-A receptor, which is expressed at the cell membrane level both in cardiomyocytes and non-myocytes.[335-337] Cardiomyocytes were pre-treated with the NPR-A specific antagonist anantin,[338, 339] which was kept during the incubation with Un-D-ANP nanoparticles. The inclusion of anantin showed inhibition of the interaction between cardiomyocytes and Un-D-ANP. This observation confirmed the specificity of the interaction between cardiac cells and ANP-functionalized nanosystems and supported the targetability role of ANP in the nanoparticles (**Figure 14C**). For the P2 and P3-functionalized nanoparticles, their internalization could be due to amine groups at the surface of the Un-D-P2 and Un-D-P3 nanoparticles, granting them a positive charge (**Figure 14B**); however, the mechanisms by which the peptides homed in the ischemic myocardium are not yet fully understood.[340, 341] Due to the lack of information on the binding mechanism for these peptides to cardiac cells, they were not tested in the competitive cellular displacement studies. This, in addition to the fact that ANP nanoparticles had higher interactions with cardiac cells, led us to further studies performed using the ANP-functionalized nanoparticles.

In publication (**III**), it was again demonstrated that Un-P-D-ANP nanoparticles interacted to a very high extent with both cardiomyocytes and non-myocytes as compared to

Un-P-D nanoparticles (**Figure 14D** and **14F**), and the addition of PEG to the formulation did not alter the specificity of the ANP functionalized nanoparticles. Additionally, it was observed a competitive interaction between Un-P-D-ANP nanoparticles and free ANP leading to decreased cell–nanoparticle interactions, both in cardiomyocytes and non-myocytes, in a concentration dependent manner (**Figure 14E** and **14G**). This data proved the preferential specific interaction of the Un-P-D-ANP with membrane NPR rather than non-specific interactions, which is in agreement with previous observations[340] and reports about ANP–NPR specific interactions.[336]

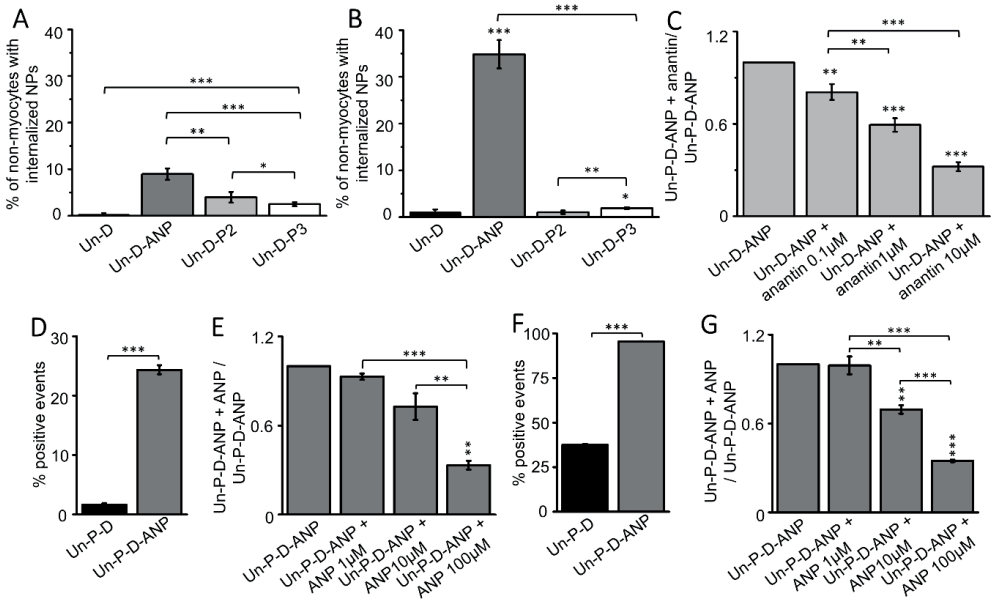

Figure 14. Quantitative and mechanistic determination of the cell–nanoparticles association and internalization. (A–B) Cellular internalization screening of different peptide-modified Un-D nanoparticles in (A) hypoxic cardiomyocytes and (B) non-myocytes. (C) Cardiomyocytes were incubated with Un-D-ANP nanoparticles + the NPR-A specific antagonist anantin (**II**). (D–G) Cellular interactions of Un-P-D and Un-P-D-ANP in (D) hypoxic cardiomyocytes and (F) non-myocytes. Cellular competition assay studies were performed by incubating free ANP and ANP-modified nanoparticles with (E) hypoxic cardiomyocytes and (G) non-myocytes (**III**). About 10,000 events were evaluated for each measurement. To determine the statistical difference between two groups, the independent samples Student's *t*-test was used. For multiple comparisons, one-way ANOVA, followed by Bonferroni post hoc test was performed. The level of the significant differences relative to the control nanoparticles and among the different peptide-conjugated PSi NPs was set at probabilities of $*p < 0.05$, $**p < 0.01$, and $***p < 0.001$. Values are represented as mean ± s.d. ($n \geq 3$). Adapted and reprinted with permission from publications **II** and **III**.

5.3. Drug delivery with multifunctional PSi nanoparticles to the endocardial layer of the injured heart (III)

After investigating the biocompatibility of PSi-based materials towards the heart tissue and screening different surface modifications for the enhanced specificity to cardiac cells, in publication (**III**) the most promising formulation was further evaluated *in vivo*. In this work, the heart regional accumulation and selectivity of the intravenously administered nanoparticles was assessed, followed by the delivery of a lead cardioprotective compound[302] (C1) and observations, if any, of relevant biological effects.

5.3.1. PEGylation and stability of UnTHCPSi nanoparticles

In publication (**III**), it was developed PEGylated and indium ^{111}In-labeled PSi nanoparticles functionalized with ANP to specifically target the myocardial NPRs.[297, 343, 344] To achieve a sufficient colloidal stability and prolonged blood circulation time, the UnTHCPSi nanoparticles [247] were surface-functionalized with NH_2-PEG-CO_2H using EDC/NHS chemistry, to obtain PEGylated PSi (Un-P) nanoparticles. The Un-P nanoparticles were further modified with the trivalent metal chelator DOTA (Un-P-D) for radiolabeling and *in vivo* imaging purposes and finally functionalized with the heart targeting ANP (Un-P-D-ANP). The size, size distribution and charge of the nanoparticles were analyzed by DLS and ζ-potential measurements after each modification step. For *in vivo* administration, the nanoparticles were dispersed in an isotonic solution of 5.4% glucose before and after simulated radiolabeling, and the physicochemical properties were comparable to those observed in Milli-Q water, as presented in **Table 5**.

Table 5: Hydrodynamic diameter (nm), polydispersity index (PdI) and zeta (ζ)-potential value of the nanosystems in Milli-Q Water and in 5.4% glucose solution, at the different stages of development and after simulated radiolabeling.

Sample	Size (d.nm)		PdI		ζ-potential (mV)	
	Milli-Q water	*5.4% glucose*	*Milli-Q water*	*5.4% glucose*	*Milli-Q water*	*5.4% glucose*
UnTHCPSi	165 ± 3	193 ± 10	0.10 ± 0.01	0.16 ± 0.03	−32.3 ± 0.2	−26.5 ± 1.3
Un-P	185 ± 8	205 ± 10	0.14 ± 0.04	0.13 ± 0.07	−35.7 ± 5.0	−32.1 ± 1.7
Un-P-D	173 ± 9	202 ± 10	0.12 ± 0.02	0.10 ± 0.03	−23.0 ± 4.4	−8.5 ± 0.7
Un-P-D-ANP	201 ± 10	229 ± 1	0.14 ± 0.02	0.15 ± 0.03	+27.3 ± 2.6	+23.1 ± 2.6
Simulated radiolabeling						
Un-P-D	–	204 ± 24	–	0.13 ± 0.05	–	−34.4 ± 5.8
Un-P-D-ANP		225 ± 4		0.35 ± 0.09		+6.2 ± 1.5

A considerable improvement in the colloidal stability of the nanoparticles was observed after PEGylation, which is necessary to improve the blood circulation time and prevent the aggregation of the particles after *i.v.* administration, by decreasing the occurrence of protein opsonization.[169] The colloidal stability of the multifunctional nanoparticles was screened in human plasma over 4 h at 37 °C for each surface modification step. The PEGylation was effective in stabilizing the nanoparticles, as the size of the Un-P nanoparticles remained almost unaltered and the PdI-values were only slightly increased over 4 h of incubation with human plasma when compared to UnTHCPSi nanoparticles, demonstrating the role of PEG in the

formulation as a stealth promoting and hydrophilic coating (**Figure 15A** and **15B**).[343] A slight increase in the hydrodynamic diameter and PdI were observed after DOTA and ANP additions to the nanoparticle's surface, suggesting weaker stealth properties, probably caused by at least partial coverage of the surface PEG polymer and alteration of the surface ζ-potential values of the nanosystems, favoring the formation of protein corona onto the nanoparticles' surface.[344] Still, the colloidal stability in human plasma was improved compared to the bare hydrophobic UnTHCPSi nanoparticles, where the sudden increase in size was followed by a decrease over time, suggesting a possible transient protein corona formation and disaggregation of roughly attached proteins on the surface of the UnTHCPSi particles.[346-348]

To investigate the long-term aqueous colloidal stability in the injection solution, the Un-P-D and Un-P-D-ANP nanoparticles were suspended in 5.4% glucose, and their size and PdI values were measured over 6 days. The Un-P-D-ANP nanoparticles exhibited more stable size and PdI than the Un-P-D nanoparticles over time (**Figure 15C** and **15D**), suggesting that the surface functionalization with ANP had a further stabilizing effect on the nanoparticles.

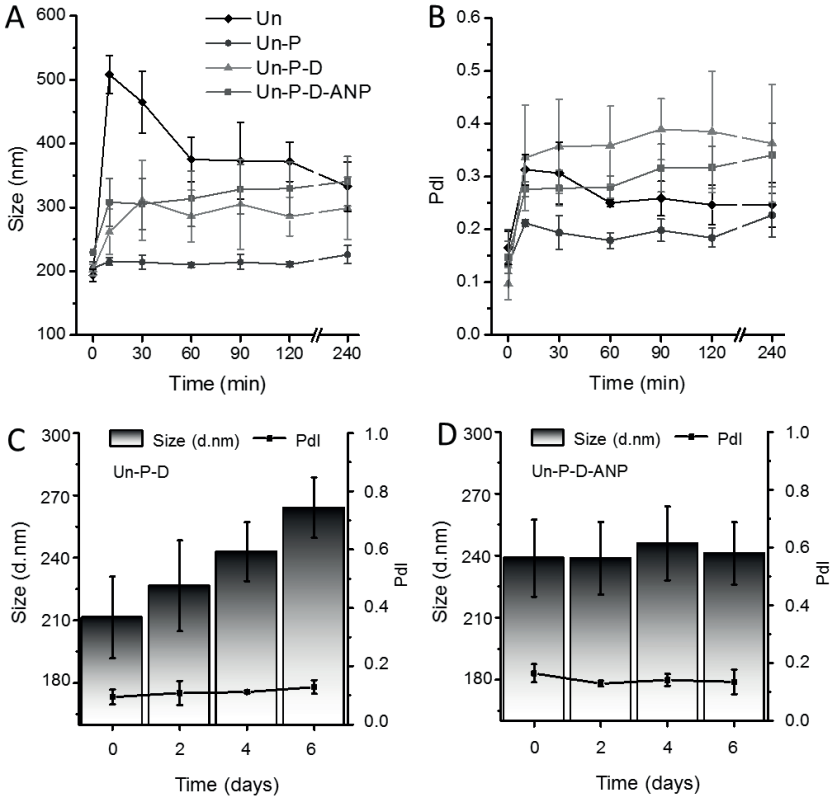

Figure 15. Assessment of the impact of human plasma proteins on the hydrodynamic diameter (A) and PdI (B) of UnTHCPSi, Un-P, Un-P-D and Un-P-D-ANP nanoparticles after incubation for 240 min at 37 °C. Values are represented as the mean ± s.d. (n = 3). Colloidal stability of Un-P-D (C) and Un-P-D-ANP (D) nanoparticles in the injection buffer (5.4% glucose). The hydrodynamic diameter and PdI of the nanoparticle suspensions were evaluated every 2 days for 6 days. The nanoparticle suspensions were stored under static conditions at 4 °C. Values are represented as the mean ± s.d. ($n \geq 2$).

5.3.2. *In vivo* biodistribution and intramyocardial location

To determine the targeting efficacy *in vivo*, the Un-P-D and Un-P-D-ANP nanoparticles were successfully radiolabeled with ^{111}In (a γ-emitter with a half-life of 67.2 h). Isoprenaline (5 mg/kg) was administered to the rats subcutaneously 24 h before nanoparticle injections to induce myocardial ischemia,[311] followed by a dose of 4.1±0.8 MBq of either Un-P-D or Un-P-D-ANP nanoparticles dispersed in 5.4% glucose, administered *i.v.* (0.5 mg/mL), detected by SPECT/CT scanning or autoradiography. The SPECT/CT scans were acquired for the whole body at 10 min, 20 min, and 4 h after the injection. SPECT/CT image quantification, represented as standardized uptake value (SUV), demonstrated that the Un-P-D-ANP nanoparticles were significantly accumulated in the heart area ($p < 0.01$), with the highest SUV at 10 and 20 min (**Figure 16A** and **16B**). Next, the regional location of the Un-P-D-ANP nanoparticles was investigated, and it was observed that the ANP-functionalized nanoparticles exhibited higher accumulation towards the endocardial layer of the left ventricle. The autoradiographic quantification of the Un-P-D-ANP and Un-P-D nanoparticles and free $InCl_3$ in the heart cryosections showed that the ratio of activity between the endocardium and epicardium (Endo/Epi) was significantly higher ($p < 0.01$) for Un-P-D-ANP nanoparticles in the ischemic heart, as observed from the autoradiographs (**Figures 16C** and **16D**). Further characterization of the transmural accumulation of nanoparticles demonstrated that the Endo/Epi ratio activity was higher ($p < 0.05$) for the Un-P-D-ANP nanoparticles in the apical and medial regions of the ischemic myocardium, as compared with the normal heart (**Figure 16E**). These results indicated that the Un-P-D-ANP nanoparticles were predominantly homed to the most vulnerable region of the heart after an ischemic event, the endocardial layer, likely due to the increase in NPR expression.[71, 349] To confirm the presence of the nanoparticles in the endocardial region of the heart, thin sections of regions of interest (ROI) were imaged by TEM and energy-dispersive X-ray (TEM–EDX). The images demonstrated the presence of the nanoparticles inside the cells 10 min after *i.v.* administration (**Figure 16F**). The identification of atomic elements by TEM–EDX showed the presence of silicon (Si) (**Figure 16G**), confirming the presence of PSi nanoparticles in the endocardial layer of ischemic hearts.

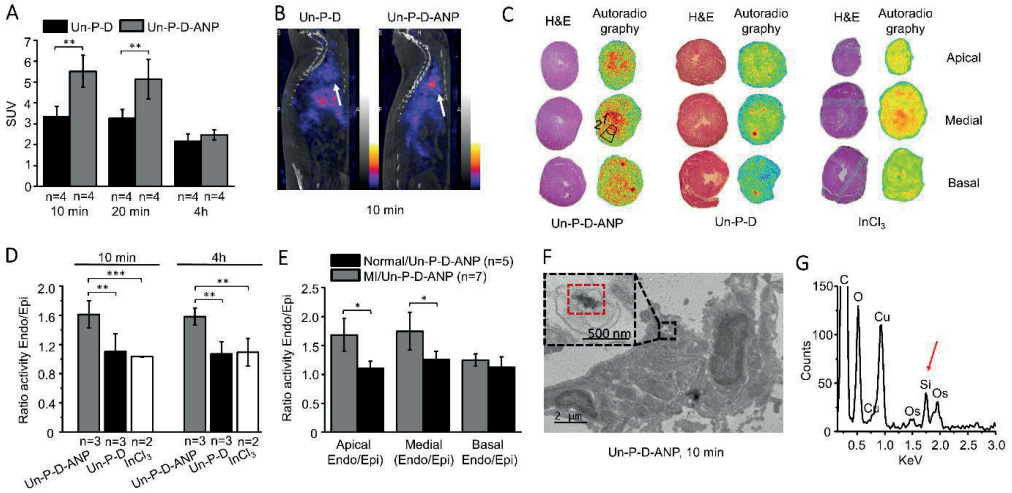

Figure 16. *In vivo* assessment of the accumulation, specificity and regional location of the nanoparticles in the infarcted myocardium after systemic administration in rats. (A) SPECT/CT image quantification of the SUVs in the rat heart at 10 min, 20 min, and 4 h after *i.v.* administration of the nanoparticles. (B) Representative sagittal SPECT/CT images showing the biodistribution of the nanoparticles at 10 min after *i.v.* administration. Arrows indicate the location of the heart. (C) Representative H&E stainings and autoradiograms of apical, basal and medial rat heart sections (from a single heart for each treatment: Un-P-D-ANP, Un-P-D, and $^{111}InCl_3$ control), showing the localization of radioactivity 10 min after the injection of nanoparticles or $^{111}InCl_3$. Delineated regions 1 and 2 represent examples of the regions of interest (ROI) used for activity quantifications. (D) Autoradiographic quantification of radioactivity in the endocardium (Endo) and epicardium (Epi) for Un-P-D-ANP, Un-P-D nanoparticles, and $^{111}InCl_3$ presented as a ratio of Endo to Epi. The results are shown for the whole heart 10 min and 4 h after the injection of nanoparticles into rats with isoprenaline-induced MI. (E) Autoradiographic quantification of the radioactivity in the Endo and Epi regions of the heart in the apical, medial and basal sections in isoprenaline-induced MI and normal rat groups, presented as a ratio of Endo to Epi. (F) Representative TEM image of a Un-P-D-ANP nanoparticle in the endocardial region of a heart section. (G) Elemental composition of the selected area (F, red box) by EDX analysis showing the presence of the Si element (red arrow). Copyright © 2017 WILEY-VCH Verlag GmbH & Co. KGaA, Weinheim, reprinted with permission from publication (**III**)

5.3.3. Drug loading, release, and *in vivo* modulation of hypertrophic signaling

To demonstrate the therapeutic potential of the Un-P-D-ANP nanoparticles towards the infarcted myocardium, the trisubstituted-3,4,5-isoxazole (C1)[301, 302] was loaded into the ANP-modified nanoparticles. The administration of C1 (30 mg/kg, intraperitoneally) in MI models (mice and rats with angiotensin II-mediated hypertension) significantly increased the left ventricular ejection fraction and fractional shortening.[301, 302] The loading degree of C1 in the Un-P-D-ANP nanoparticles was 16±5%. **Figure 17A** shows the release profile of C1 in human plasma. It was observed an improvement in the dissolution profile of C1 when compared with the drug alone (approximately 0.12% in the time-frame shown), as C1 is poorly

water-soluble, suggesting that the Un-P-D-ANP may act as a beneficial drug carrier for the delivery of this compound. Thus, isoprenaline-induced myocardial ischemia rats were administered *i.v.* with unloaded and C1-loaded Un-P-D-ANP nanoparticles, and the effect on MAPK signaling was assessed in the endocardial layer of the left ventricle, at 4 h, 1 day (groups receiving one single dose of nanoparticles) and 3 days (groups received three doses of unloaded or C1-loaded Un-P-D-ANP nanoparticles at 0 h, 24 h, and 48 h, and were sacrificed at 72 h). Each animal received a dose of about 31.5 μg of C1 per injection.

Almost all the MAPK signaling components are activated in the end-stage human heart failure and in animal models of pathologic cardiac hypertrophy.[57, 58, 350, 351] Regarding one of these components, ERK 1/2 is characterized by phosphorylation of the ERK 1/2 proteins, which will lead to the activation of hypertrophy-related transcription factors in the nucleus. Previous studies showed that the ERK cascade plays an essential role in signaling mechanisms leading to cardiac hypertrophy, and thus, the inhibition of ERK1/2 in patients with severe myocardial remodeling and restrictive cardiomyopathy may serve as a therapeutic choice.[58, 351] The administration of C1-loaded Un-P-D-ANP nanoparticles significantly decreased ($p < 0.01$) ERK1/2 phosphorylation, particularly after repeated administration (**Figure 17B** and **17c**). The observed result suggests that the attenuation of ERK signaling cascade may lead to a therapeutic cardioprotective effect for the C1-loaded nanoparticles. The observed results suggest that the Un-P-D-ANP nanoparticles could be considered to precisely deliver relevant cargos and exert a protective effect in the endocardial layer of the ischemic heart.

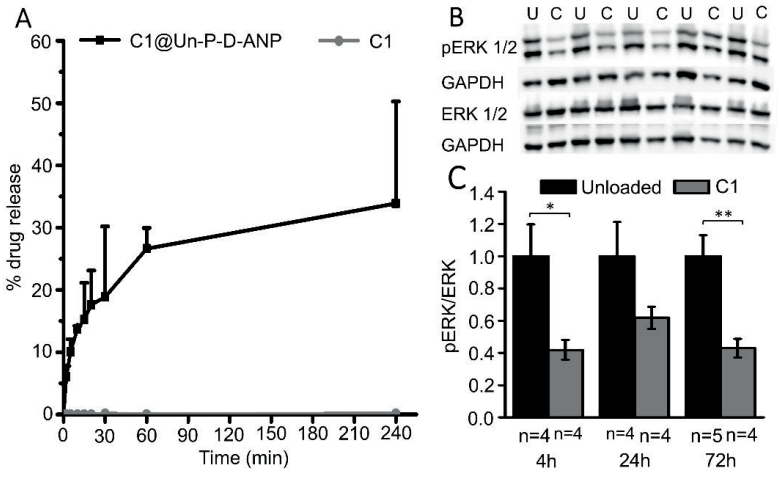

Figure 17. *In vivo* modulation of ERK1/2 MAPK signaling pathways in the endocardium after systemic administration of C1-loaded Un-P-D-ANP. (A) Release profiles of compound C1 in human plasma over 4 h. The data represent the mean ± s.d. ($n = 3$). (B) Western blots showing the total ERK1/2 and phosphorylated ERK1/2 (pERK1/2) immunoreactive bands with the corresponding GAPDH immunoreactive bands (U, unloaded nanoparticles; C, C1-loaded nanoparticles). (C) The ratio of the GAPDH-normalized optical densities for pERK and ERK in the endocardium of the left ventricle after *i.v.* administration of unloaded (U) or C1-loaded (C) Un-P-D-ANP nanoparticles in an isoprenaline-induced rat model of MI. The results are expressed as the mean ± S.E.M. (independent samples analyzed by the Student t-test set at probabilities of *$p < 0.05$ and **$p < 0.01$).

5.4. Dual drug delivery using pH-responsive spermine-acetalated dextran-based nanoparticles (IV)

In order to have an even more versatile nanosystem that would allow a precise delivery of cargos into the target cells, AcDXSp was used as a core material and was further functionalized for improvements in biocompatibility, stability, and specificity. AcDXSp presents pH-dependent degradation in physiologically relevant mildly acidic conditions, which is ideal for intracellular delivery of cargos.[31] In addition, the application of AcDX-based microparticles showed encouraging results for protein delivery to the ischemic heart, however with the drawback of invasive intramyocardial administration.[182, 183] The use of small drug molecules for cardiac reprogramming is an emerging field, and efforts towards clinical translation are still limited or even inexistent.[130, 352] Encapsulation of these compounds into particulate systems has not been addressed before for application in the direct cellular reprogramming of cardiac fibroblasts. Thus, in this thesis, AcDXSp was evaluated as a candidate for pH-triggered dual-drug delivery of relevant small molecules, CHIR99021 and SB431542, as previously described for direct fibroblast reprogramming into cardiomyocytes.[123]

5.4.1. pH-dependent dual drug release

To evaluate the pH-dependent release from AcDXSp-based nanoparticles, dissolution studies were performed at relevant physiological extracellular (pH 7.4) and intracellular (pH 5) environments, and the free drugs were used as controls. The release of the different cargos at pH 5 occurred fast due to the hydrolysis of the acetal groups, while at pH 7.4 the release was hampered by the slow degradation rate of the acetal groups present in the polymer (**Figure 18**). While the free compounds demonstrated pH-dependent dissolution profiles, their release profiles in both conditions were similar and dictated by the degradation hydrolysis of the polymeric matrix towards mildly acidic conditions.[353] As a consequence, a considerable amount of both the cargos were rapidly released in the first hour at pH 5. The dissolution rate of both drugs was, therefore, improved under mildly acidic conditions and precisely triggered only upon acidic pH stimulus, as previously described.[258] The small amounts of cargos released at pH 7.4 are justifiable by a slight degradation of dextran at this pH resulting in the release of a small percentage of the cargos, as previously reported.[354] Also, the surface functionalization of the nanoparticles made the surfaces more hydrophilic, facilitating the interaction with the solvent molecules and released the cargos entrapped closer to the surface, hence slightly higher release was observed for the functionalized nanoparticles at this pH. The degree of acetalation obtained for this polymer was 46.1% by ^{1}H NMR, which also influenced the hydrolysis rate of the polymer, and thus, the release of cargos at pH values close to neutrality.[182] Considering nanoparticles for intravenous administration, this is an optimal condition, since the cargo will only be released upon internalization into acidic subcellular compartments in the cells of the target tissue. In addition, the ischemic myocardium presents inflammation and consequently changes in the interstitial pH to 6 – 6.5,[355, 356] which makes this material highly suitable for sustained drug delivery to the injured myocardium.[182, 183]

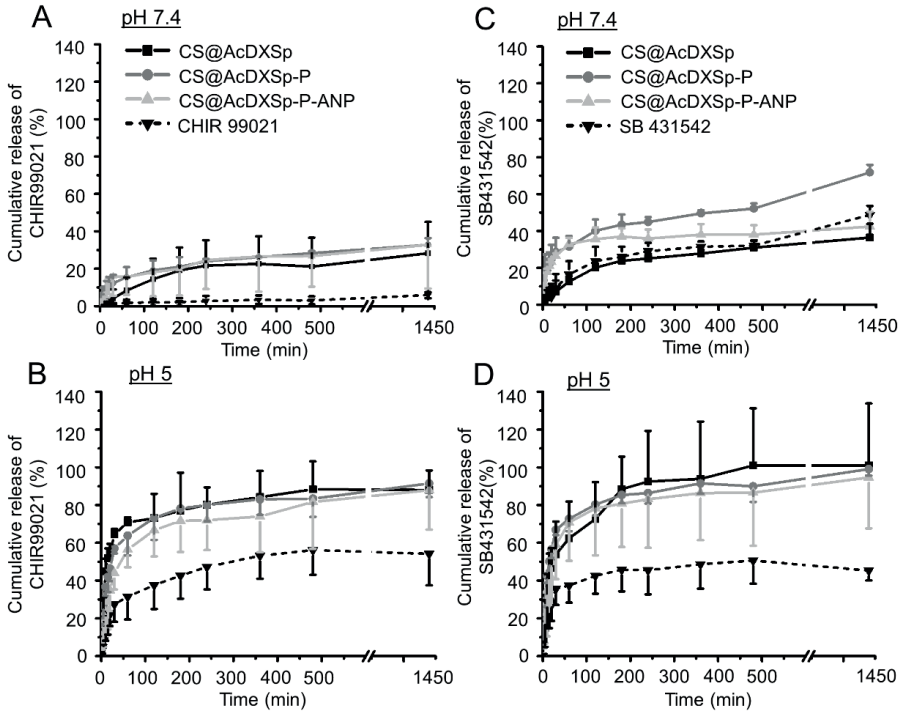

Figure 18. Drug release profiles of CHIR99021 and SB431542 in simulated extracellular (pH 7.4) and intracellular (pH 5) conditions. (A–B) The release profiles of CHIR99021 and (C–D) SB431542 from bare CS@AcDXSp and functionalized CS@AcDXSp-P and AcDXSp-P-ANP evaluated at pH 7.4 and 5.0, at 37 °C. Data represent mean ± s.d. ($n \geq 3$).

5.4.2. *In vitro* modulation of β-catenin and Smad3 for direct fibroblast reprogramming

In order to investigate whether the AcDXSp-based nanoparticles could be used for direct fibroblast reprogramming, CS@AcDXSp, CS@AcDXSp-P and CS@AcDXSp-P-ANP, and respective controls were incubated with non-myocytes for 6 h. The biological effect was assessed by quantifying the staining intensity for β-catenin and Smad3. The cells were immunostained for nuclei (DAPI), β-catenin or Smad3, and in addition, for a fibroblast marker, vimentin or α-smooth muscle actin (SMA), which demonstrated that the majority of cardiac non-myocytes were (myo)fibroblasts (**Figure 19A** and **19E**). As controls, both vehicle-loaded nanoparticles and the free compounds were used. In all the conditions where the compounds were present, 1 μM of CHIR99021 and 2.1 μM of SB431542 were used in all the tests, correspondent to a safe dose of nanoparticles given, which was calculated based on the LD of the different nanoparticles.

The nanoparticles loaded with the Wnt activator CHIR99021 successfully stabilized β-catenin in the cytoplasm, which in turn translocated to the nucleus the drug-loaded nanoparticles compared to the untreated group and the vehicle-loaded nanoparticles ($p < 0.05$) (**Figure 19B** and **19C**). Importantly, the effect of CHIR90221 on stabilization of β-catenin in the cytoplasm was significantly higher for CS@AcDXSp-P-ANP compared with the

free drug ($p < 0.05$), indicating improvement in the delivery of CHIR99021 by the ANP-functionalized nanoparticles. The nucleus to cytoplasm ratio of β-catenin did not differ significantly among groups, except for the CS group, in which to the cytoplasmic β-catenin appeared to be lower than in the drug-loaded nanoparticle groups. (**Figure 19D**).

Furthermore, the delivery of the TGF-β inhibitor SB431542 affected the intracellular Smad3 by preventing its translocation to the nucleus, while it did not seem to interfere with the amount of Smad3 already existent in the nucleus for the 6 h (**Figure 19F**). Instead, the SB431542 prevented the phosphorylation of Smad3 by the ALK and the consequent Smad complex formation for nuclear translocation, which is in agreement with the mechanism of action of the compound.[309] Although free SB431542 significantly increased the cytoplasmic Smad3 compared to its control ($p < 0.05$, CS *vs.* DMSO), this effect was more marked for the drug-loaded nanoparticles, as reflected by the statistically significant cytoplasmic increase of Smad3 compared to all the other groups, including the CS group (**Figure 19G**, $p < 0.05$), which was also noted in the ratio of nuclear/cytoplasmic Smad3 staining intensity (**Figure 19H**).

The use of nanoparticulate systems for drug delivery applications has shown numerous advantages in multidisciplinary biomedical fields. Delivery of small molecules, growth factors and nucleic acid cargos to the heart with the particulate systems using diverse strategies have been described.[182, 191, 205, 357-362] However, employment of particulate systems for the application of direct cardiac reprogramming is scarce and involves generally the delivery of microRNAs and viral vectors.[363, 364] Pharmacological induction of fibroblast reprogramming is an unexplored field in terms of the application of particulate carriers.[130, 352] Due to the poor physicochemical properties of small molecules like CHIR99021 and SB431542, in this thesis the beneficial properties of nanoparticulate systems to improve the delivery of these compounds was explored, and at the same time to overcome the drawbacks of reprogramming techniques using multiple genetic factors with low efficiency, technical and safety issues.[128, 365-371] Several reports on the combined application of CHIR99021 and SB431542 for cardiac fibroblasts reprogramming specifically justified the concomitant use of both the compounds in this study to be delivered simultaneously by a functional nanoparticulate system.[123, 372, 373] Moreover, this functional nanosystem could potentially be explored for induction of cardiomyocyte proliferation as well, since the inhibition of GSK-3 (involved in degradation of β-catenin) may induce cell proliferation and mitosis in cardiomyocytes.[374] As a proof-of-concept and for the first time, we have described the development of a biocompatible and functional nanodelivery system for pH-triggered delivery of at least two poorly-water soluble small drug molecules for applications promoting cardiac regeneration. This may be extended to other nanoparticulate-based systems and other small drug molecules.

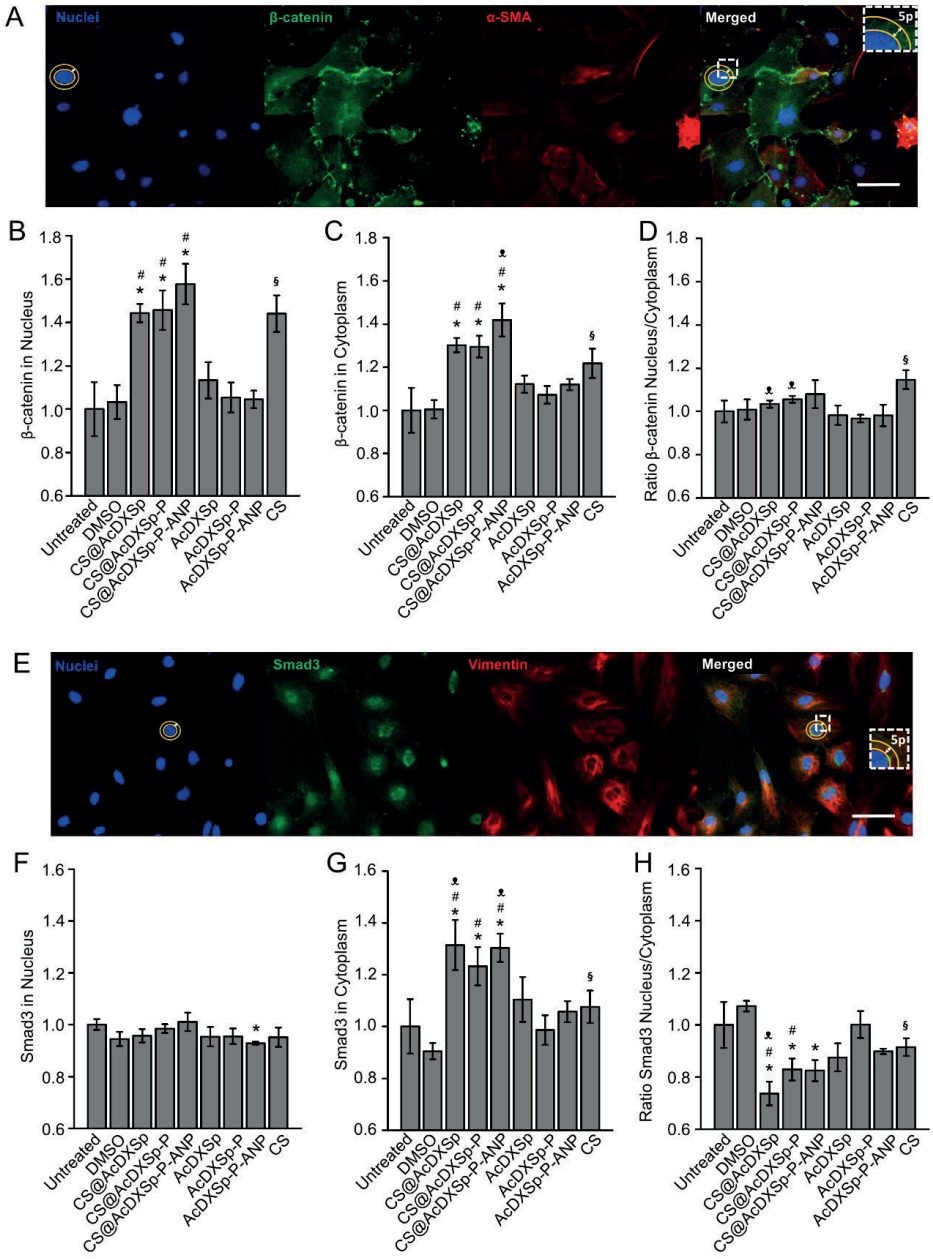

Figure 19. High-content cell imaging and quantification for the sub-cellular localization of β-catenin. (A, E) Representative images of non-myocyte cells treated with CS@AcDXSp-P-ANP at the dose of 1 μM of CHIR 99021 and 2.1 μM of SB 431542, and stained for nuclei (DAPI, blue), β-catenin or Smad3 (green) and the fibroblast marker α-smooth muscle actin (α-SMA) or vimentin (red), with a 20× magnification objective (scale bars are 50 μm). (B-D) Quantification of β-catenin and (F-H) Smad3 staining intensity: the average intensity of (B) β-catenin or (F) Smad3 staining in the nucleus, (C) β-catenin or (G) Smad3 in the cytoplasm and

the ratio of (D) β-catenin or (H) Smad3 in nucleus/cytoplasm. The different treatment conditions are stated below each bar. Fluorescence intensity in the cytoplasm was quantified from a 5-pixel ring immediately outside the nucleus defined by DAPI staining, as indicated in panels A and E. A one-way ANOVA followed by a Tukey-Kramer post hoc test was used for the statistical analysis. The significance levels of the differences were set at probabilities of $^{*}p < 0.05$ for comparison with the untreated group; $^{\#}p < 0.05$ for comparison between loaded nanoparticles *vs*. their vehicle-loaded counterparts; $^{\S}p < 0.05$ for comparison between DMSO and CS groups and $^{\bullet}p < 0.05$ for comparison of loaded nanoparticles *vs*. CS group. Values represent the mean ± s.d. ($n = 3$). All the results were normalized to the untreated control.

6. Summary and conclusions

The investigation of regenerative and protective proposed therapeutic approaches including stem cell therapy, biomaterial-based therapy or the development of gene-based and pharmacological agents do not yet tackle the urgent medical need of successfully treating MI patients. Accordingly, in this thesis, PSi-based and AcDXSp-based carriers were developed as a base for potential applications in imaging and therapy of MI, due to their intrinsic properties of small size, enhanced and pH-dependent dissolution rate of poorly-water soluble cargos, possibility for functionalization, and biocompatibility.

Firstly, the biocompatibility of PSi-based carriers was assessed in heart. Different sizes and surface chemistries of PSi were evaluated, showing that the hydrophobic THCPSi microparticles and TOPSi nanoparticles displayed better cytocompatibility *in vitro*. *In vivo*, although the THCPSi microparticles activated inflammatory and fibrotic-promoting genes, both micro- and nanoparticles showed no toxicity or impairment in cardiac function in healthy or MI rats, suggesting that the PSi materials could be a platform considered for application in the therapy of heart diseases. Secondly, PSi-based nanosystems were successfully functionalized with DOTA and 3 different peptides, for the screening of the most promising nanosystem towards targeted drug delivery and imaging. Cytocompatibility was achieved for nanoparticle concentrations up to 50 μg/mL. Further investigation of the cell–nanoparticle interactions in cardiomyocytes and non-myocytes revealed a preferential cellular interaction with ANP-functionalized nanoparticles in both the cell types. Displacement studies revealed that the ANP-functionalized PSi nanoparticles interacted with the cardiomyocytes preferentially through the NPRs present at the cell surface. These observations led to further investigations in the third study of this thesis with ANP-functionalized PSi nanoparticles, where the receptor-mediated interaction was confirmed for cardiomyocytes and disclosed for non-myocytes. Furthermore, improvement of the colloidal stability of the nanosystem was achieved upon successful PEGylation of the surface of the PSi nanoparticles. The Un-P-D-ANP showed good colloidal stability in both human plasma and the injection solution, 5.4% glucose. Radiolabeled [^{111}In]Un-P-D-ANP nanoparticles were administered to isoprenaline-treated MI rats, showing not only preferential accumulation of the nanoparticles in the heart by SPECT/CT imaging, but also regional accumulation in the endocardial layer of the MI hearts, as well as selectivity towards the MI induced hearts compared with healthy hearts. The administration of Un-P-D-ANP nanoparticles loaded with a cardioprotective small molecule (C1) significantly decreased ERK1/2 phosphorylation, particularly after repeated administration. These observations suggested that the Un-P-D-ANP loaded nanoparticles may have potential therapeutic effects by delivering a poorly water-soluble cardioprotective small molecule to attenuate the ERK signaling cascade, which has implications in the hypertrophy signaling and may promote a cardioprotective effect. Finally, in the last study, AcDXSp-functionalized nanoparticles were developed, showing pH-dependent drug delivery of two poorly water-soluble cargos, triggered under physiologically relevant mildly acidic pH conditions. In addition, *in vitro* drug delivery by the AcDXSp-P-ANP nanoparticles demonstrated superior therapeutic modulation of key signaling pathways involved in the direct fibroblast reprogramming into cardiomyocytes. The observation of dual therapeutic effect strengthens the suitability of this nanosystem for potential application in cardiac regeneration.

Overall, as a proof-of-concept, PSi and AcDXSp-based particulate systems were developed in this thesis by functionalizing their surface with stabilizing and targeting excipients, for improved and pH-triggered drug delivery of relevant poorly water-soluble cargos for the applications in MI imaging and cardioprotective and cardio restorative therapy. The work described here does not show optimal *in vivo* accumulation of PSi-functionalized

nanoparticles, nor represents an exhaustive study of the nanoparticulate systems developed regarding profound toxicologic assessment in different cell lines, bioeffects of the nanoystems themselves, or *in vivo* functional outcomes. Continuation of this work would cover the referred topics. Regarding dextran nanoparticle technology, further studies would involve investigation of the *in vitro* and *in vivo* potential applications in the direct cellular reprogramming of fibroblasts, as well as evaluation of functional outcomes upon MI treatment with dual-loaded dextran nanoparticles, as well as exploring the possibility of rescue existing cardiomyocytes back to the cell cycle and induce their proliferation with the same AcDXSp-based nanoparticles.

The search for the perfect "nanobullet" demands continuous research in the development of more stable, able to comply with biological barriers, and efficient nanocarriers for targeted drug delivery to the heart. Although new insights on the pathological features of MI provide a better understanding of the existent and possibly new therapeutic targets, there is still lack of a specific cardiac marker(s) suitable for targeting, which puts the targetability of cardiac tissue into perspective. From the material point-of-view, the increasing information about the particularities, versatility, and advantages of nanomaterials offers a panoply of opportunities for the development of adaptable tools to fight MI. Yet, limitations include the ability to overcome biological barriers, time-consuming and complex functionalization, reproducibility and scalability, factors taken into account in the clinical development and commercialization, which may impair their translation into the clinic. Despite a large body of work needed, and to put the developed work into context, this thesis contributes to enrich the knowledge regarding PSi and dextran-based nanoparticle technology as a starting point for the application in MI therapy.

References

1. Global, regional, and national age-sex specific all-cause and cause-specific mortality for 240 causes of death, 1990-2013: a systematic analysis for the Global Burden of Disease Study 2013. *Lancet (London, England)* 385, 117-171 (2015).
2. World Health Organization, Cardiovascular diseases (CVDs). *Available at: http://www.who.int/mediacentre/factsheets/fs317/en/* [8 December 2016] (2017).
3. Xin, M., Olson, E.N. & Bassel-Duby, R. Mending broken hearts: cardiac development as a basis for adult heart regeneration and repair. *Nature reviews,* 14, 529-541 (2013).
4. Sutton, M.G. & Sharpe, N. Left ventricular remodeling after myocardial infarction: pathophysiology and therapy. *Circulation* 101, 2981-2988 (2000).
5. Talman, V. & Ruskoaho, H. Cardiac fibrosis in myocardial infarction—from repair and remodeling to regeneration. *Cell and Tissue Research* 365, 563-581 (2016).
6. Shah, A.M. & Mann, D.L. In search of new therapeutic targets and strategies for heart failure: recent advances in basic science. *Lancet (London, England)* 378, 704-712 (2011).
7. Mudd, J.O. & Kass, D.A. Tackling heart failure in the twenty-first century. *Nature* 451, 919-928 (2008).
8. Cui, Z., Yang, B. & Li, R.-K. Application of Biomaterials in Cardiac Repair and Regeneration. *Engineering* 2, 141-148 (2016).
9. Suarez, S., Almutairi, A. & Christman, K.L. Micro- and Nanoparticles for Treating Cardiovascular Disease. *Biomaterials science* 3, 564-580 (2015).
10. Ferreira, M.P., Balasubramanian, V., Hirvonen, J., Ruskoaho, H. & Santos, H.A. Advanced Nanomedicines for the Treatment and Diagnosis of Myocardial Infarction and Heart Failure. *Current drug targets* 16, 1682-1697 (2015).
11. Segers, V.F.M. & Lee, R.T. Stem-cell therapy for cardiac disease. *Nature* 451, 937-942 (2008).
12. Golpanian, S. et al. Concise Review: Review and Perspective of Cell Dosage and Routes of Administration From Preclinical and Clinical Studies of Stem Cell Therapy for Heart Disease. *Stem Cells Translational Medicine* 5, 186-191 (2016).
13. Ye, L., Zimmermann, W.-H., Garry, D.J. & Zhang, J. Patching the Heart: Cardiac Repair from Within and Outside. *Circulation research* 113 (2013).
14. Anselmo, A.C. & Mitragotri, S. Nanoparticles in the clinic. *Bioengineering & Translational Medicine* 1, 10-29 (2016).
15. Ventola, C.L. The Nanomedicine Revolution: Part 2: Current and Future Clinical Applications. *Pharmacy and Therapeutics* 37, 582-591 (2012).
16. De Crozals, G., Bonnet, R., Farre, C. & Chaix, C. Nanoparticles with multiple properties for biomedical applications: A strategic guide. *Nano Today* 11, 435-463 (2016).
17. Salonen, J., Kaukonen, A.M., Hirvonen, J. & Lehto, V.-P. Mesoporous Silicon in Drug Delivery Applications. *Journal of pharmaceutical sciences* 97, 632-653 (2008).
18. Santos, H.A., Makila, E., Airaksinen, A.J., Bimbo, L.M. & Hirvonen, J. Porous silicon nanoparticles for nanomedicine: preparation and biomedical applications. *Nanomedicine (London)* 9, 535-554 (2014).
19. Bimbo, L.M. et al. Biocompatibility of Thermally Hydrocarbonized Porous Silicon Nanoparticles and their Biodistribution in Rats. *ACS Nano* 4, 3023-3032 (2010).
20. Araújo, F. et al. Microfluidic Assembly of a Multifunctional Tailorable Composite System Designed for Site Specific Combined Oral Delivery of Peptide Drugs. *ACS Nano* 9, 8291-8302 (2015).
21. Fontana, F. et al. Multistaged Nanovaccines Based on Porous Silicon@Acetalated Dextran@Cancer Cell Membrane for Cancer Immunotherapy. *Advanced Materials* 29, 1603239-n/a (2017).
22. Janoniene, A. et al. A Versatile Carbonic Anhydrase IX Targeting Ligand-Functionalized Porous Silicon Nanoplatform for Dual Hypoxia Cancer Therapy and Imaging. *ACS Applied Materials & Interfaces* 9, 13976-13987 (2017).
23. Santos, H.A. et al. Multifunctional porous silicon for therapeutic drug delivery and imaging. *Current drug discovery technologies* 8, 228-249 (2011).
24. Shahbazi, M.-A. et al. Surface chemistry dependent immunostimulative potential of porous silicon nanoplatforms. *Biomaterials* 35, 9224-9235 (2014).
25. Shrestha, N. et al. Multistage pH-responsive mucoadhesive nanocarriers prepared by aerosol flow reactor technology: A controlled dual protein-drug delivery system. *Biomaterials* 68, 9-20 (2015).
26. Wang, C.-F. et al. Multifunctional porous silicon nanoparticles for cancer theranostics. *Biomaterials* 48, 108-118 (2015).
27. Zhang, H. et al. Fabrication of a Multifunctional Nano-in-micro Drug Delivery Platform by Microfluidic Templated Encapsulation of Porous Silicon in Polymer Matrix. *Advanced Materials* 26, 4497-4503 (2014).
28. Venuta, A., Wolfram, J., Shen, H. & Ferrari, M. Post-nano strategies for drug delivery: Multistage porous silicon microvectors. *J Mater Chem B Mater Biol Med* 5, 207-219 (2017).
29. Park, J.H. et al. Biodegradable luminescent porous silicon nanoparticles for in vivo applications. *Nature materials* 8, 331-336 (2009).
30. Martinez, J.O. et al. Degradation and biocompatibility of multistage nanovectors in physiological systems. *Journal of biomedical materials research. Part A* 102, 3540-3549 (2014).
31. Bachelder, E.M., Pino, E.N. & Ainslie, K.M. Acetalated Dextran: A Tunable and Acid-Labile Biopolymer with Facile Synthesis and a Range of Applications. *Chemical reviews* 117, 1915-1926 (2017).
32. Lopez, A.D. & Murray, C.C. The global burden of disease, 1990-2020. *Nature medicine* 4, 1241-1243 (1998).
33. Organization, W.H. World Health Report 1999: Making a difference. *Available at: http://www.who.int/whr/1999/en/* [10 July 2017] (1999).
34. Writing Group, M. et al. Heart Disease and Stroke Statistics—2014 Update: A Report From the American Heart Association. *Circulation* 129, e28-e292 (2014).
35. Network, E.H. European Cardiovascular Disease Statistics 2017. *Available at: http://www.ehnheart.org/cvd-statistics.html* [26 August 2017] (2017).

36. Roger, V.L. Epidemiology of Heart Failure. *Circulation Research* 113, 646-659 (2013).
37. Official Statistics of Finland, Ischaemic heart disease still the cause of one in five deaths. *Accessed at: http://www.stat.fi/til/ksyyt/2014/ksyyt_2014_2015-12-30_kat_002_en.html* [13.7.2017] (2014).
38. Pappano, A.J. & Gil Wier, W. in Cardiovascular Physiology (10th Edition) 55-90 (2013).
39. Krenning, G., Zeisberg, E.M. & Kalluri, R. The origin of fibroblasts and mechanism of cardiac fibrosis. *Journal of cellular physiology* 225, 631-637 (2010).
40. Zeisberg, E.M. & Kalluri, R. Origins of cardiac fibroblasts. *Circ Res* 107, 1304-1312 (2010).
41. Banerjee, I., Fuseler, J.W., Price, R.L., Borg, T.K. & Baudino, T.A. Determination of cell types and numbers during cardiac development in the neonatal and adult rat and mouse. *American journal of physiology. Heart and circulatory physiology* 293, H1883-1891 (2007).
42. Deb, A. & Ubil, E. Cardiac fibroblast in development and wound healing. *Journal of molecular and cellular cardiology* 70, 47-55 (2014).
43. Pinto, A.R. et al. Revisiting Cardiac Cellular Composition. *Circ Res* 118, 400-409 (2016).
44. Thygesen, K. et al. Third Universal Definition of Myocardial Infarction. *Circulation* 126, 2020-2035 (2012).
45. Jennings, R.B. & Ganote, C.E. Structural changes in myocardium during acute ischemia. *Circ Res* 35, 156-172 (1974).
46. Thygesen, K. et al. Universal definition of myocardial infarction. *Circulation* 116, 2634-2653 (2007).
47. Duncker, D.J., Traverse, J.H., Ishibashi, Y. & Bache, R.J. Effect of NO on transmural distribution of blood flow in hypertrophied left ventricle during exercise. The American journal of physiology 276, H1305-1312 (1999).
48. Sarvari, S.I. et al. Layer-specific quantification of myocardial deformation by strain echocardiography may reveal significant CAD in patients with non-ST-segment elevation acute coronary syndrome. JACC. Cardiovascular imaging 6, 535-544 (2013).
49. Cohen, M.V., Yang, X.M., Neumann, T., Heusch, G. & Downey, J.M. Favorable remodeling enhances recovery of regional myocardial function in the weeks after infarction in ischemically preconditioned hearts. *Circulation* 102, 579-583 (2000).
50. Diwan, A. & Dorn, G.W., 2nd Decompensation of cardiac hypertrophy: cellular mechanisms and novel therapeutic targets. *Physiology (Bethesda, Md.)* 22, 56-64 (2007).
51. Selvetella, G., Hirsch, E., Notte, A., Tarone, G. & Lembo, G. Adaptive and maladaptive hypertrophic pathways: points of convergence and divergence. *Cardiovascular research* 63, 373-380 (2004).
52. McKay, R.G. et al. Left ventricular remodeling after myocardial infarction: a corollary to infarct expansion. *Circulation* 74, 693-702 (1986).
53. Rumberger, J.A., Behrenbeck, T., Breen, J.R., Reed, J.E. & Gersh, B.J. Nonparallel changes in global left ventricular chamber volume and muscle mass during the first year after transmural myocardial infarction in humans. *J Am Coll Cardiol* 21, 673-682 (1993).
54. Pfeffer, M.A. & Braunwald, E. Ventricular remodeling after myocardial infarction. Experimental observations and clinical implications. *Circulation* 81, 1161-1172 (1990).
55. Jessup , M. & Brozena , S. Heart Failure. *New England Journal of Medicine* 348, 2007-2018 (2003).
56. Konstam, M.A., Kramer, D.G., Patel, A.R., Maron, M.S. & Udelson, J.E. Left Ventricular Remodeling in Heart Failure. *JACC: Cardiovascular Imaging* 4, 98-108 (2011).
57. Rose, B.A., Force, T. & Wang, Y. Mitogen-activated protein kinase signaling in the heart: angels versus demons in a heart-breaking tale. *Physiological reviews* 90, 1507-1546 (2010).
58. Wang, Y. Mitogen-Activated Protein Kinases in Heart Development and Diseases. *Circulation* 116, 1413-1423 (2007).
59. Sugden, P.H. & Clerk, A. Cellular mechanisms of cardiac hypertrophy. *Journal of Molecular Medicine* 76, 725-746 (1998).
60. Yue, T.-L. *et al.* Extracellular Signal-regulated Kinase Plays an Essential Role in Hypertrophic Agonists, Endothelin-1 and Phenylephrine-induced Cardiomyocyte Hypertrophy. *Journal of Biological Chemistry* 275, 37895-37901 (2000).
61. Heineke, J. & Molkentin, J.D. Regulation of cardiac hypertrophy by intracellular signalling pathways. *Nature reviews. Molecular cell biology* 7, 589-600 (2006).
62. Bueno, O.F. et al. The MEK1-ERK1/2 signaling pathway promotes compensated cardiac hypertrophy in transgenic mice. *The EMBO journal* 19, 6341-6350 (2000).
63. Peng, K. et al. Novel EGFR inhibitors attenuate cardiac hypertrophy induced by angiotensin II. *Journal of Cellular and Molecular Medicine* 20, 482-494 (2016).
64. Cipolletta, E. et al. Targeting the CaMKII/ERK Interaction in the Heart Prevents Cardiac Hypertrophy. *PLoS ONE* 10, e0130477 (2015).
65. Sudoh, T., Kangawa, K., Minamino, N. & Matsuo, H. A new natriuretic peptide in porcine brain. *Nature* 332, 78-81 (1988).
66. Sudoh, T., Minamino, N., Kangawa, K. & Matsuo, H. C-type natriuretic peptide (CNP): a new member of natriuretic peptide family identified in porcine brain. *Biochemical and biophysical research communications* 168, 863-870 (1990).
67. Flynn, T.G., de Bold, M.L. & de Bold, A.J. The amino acid sequence of an atrial peptide with potent diuretic and natriuretic properties. *Biochemical and biophysical research communications* 117, 859-865 (1983).
68. Ruskoaho, H. Atrial natriuretic peptide: synthesis, release, and metabolism. *Pharmacological reviews* 44, 479-602 (1992).
69. Kato, T. et al. Atrial natriuretic peptide promotes cardiomyocyte survival by cGMP-dependent nuclear accumulation of zyxin and Akt. *J Clin Invest* 115, 2716-2730 (2005).
70. Curry, F.-R.E. Atrial natriuretic peptide: an essential physiological regulator of transvascular fluid, protein transport, and plasma volume. *Journal of Clinical Investigation* 115, 1458-1461 (2005).
71. Cao, L. & Gardner, D.G. Natriuretic Peptides Inhibit DNA Synthesis in Cardiac Fibroblasts. *Hypertension (Dallas, Tex. : 1979)* 25, 227-234 (1995).
72. Oliver, P.M. et al. Hypertension, cardiac hypertrophy, and sudden death in mice lacking natriuretic peptide receptor A. *Proc Natl Acad Sci U S A* 94, 14730-14735 (1997).

73. Mukoyama, M. et al. Augmented secretion of brain natriuretic peptide in acute myocardial infarction. *Biochemical and biophysical research communications* 180, 431-436 (1991).
74. Foy, S.G. et al. Neurohormonal changes after acute myocardial infarction. Relationships with haemodynamic indices and effects of ACE inhibition. *European heart journal* 16, 770-778 (1995).
75. Sergeeva, I.A. & Christoffels, V.M. Regulation of expression of atrial and brain natriuretic peptide, biomarkers for heart development and disease. *Biochimica et Biophysica Acta (BBA) - Molecular Basis of Disease* 1832, 2403-2413 (2013).
76. Cameron, V.A. et al. Atrial (ANP) and brain natriuretic peptide (BNP) expression after myocardial infarction in sheep: ANP is synthesized by fibroblasts infiltrating the infarct. *Endocrinology* 141, 4690-4697 (2000).
77. Ruskoaho, H. Cardiac hormones as diagnostic tools in heart failure. *Endocrine reviews* 24, 341-356 (2003).
78. Gardner, D.G. Natriuretic peptides: markers or modulators of cardiac hypertrophy? *Trends in endocrinology and metabolism: TEM* 14, 411-416 (2003).
79. Nishikimi, T., Maeda, N. & Matsuoka, H. The role of natriuretic peptides in cardioprotection. *Cardiovascular research* 69, 318-328 (2006).
80. Vanneste, Y., Michel, A., Dimaline, R., Najdovski, T. & Deschodt-Lanckman, M. Hydrolysis of alpha-human atrial natriuretic peptide in vitro by human kidney membranes and purified endopeptidase-24.11. Evidence for a novel cleavage site. *Biochem J* 254, 531-537 (1988).
81. Nakao, K. et al. The pharmacokinetics of alpha-human atrial natriuretic polypeptide in healthy subjects. *European journal of clinical pharmacology* 31, 101-103 (1986).
82. Yandle, T.G. et al. Metabolic clearance rate and plasma half life of alpha-human atrial natriuretic peptide in man. *Life sciences* 38, 1827-1833 (1986).
83. Potter, L.R., Yoder, A.R., Flora, D.R., Antos, L.K. & Dickey, D.M. Natriuretic Peptides: Their Structures, Receptors, Physiologic Functions and Therapeutic Applications. *Handbook of experimental pharmacology*, 341-366 (2009).
84. Wilcox, J.N., Augustine, A., Goeddel, D.V. & Lowe, D.G. Differential regional expression of three natriuretic peptide receptor genes within primate tissues. *Molecular and cellular biology* 11, 3454-3462 (1991).
85. Lin, X., Hänze, J., Heese, F., Sodmann, R. & Lang, R.E. Gene Expression of Natriuretic Peptide Receptors in Myocardial Cells. *Circulation Research* 77, 750-758 (1995).
86. Nunez, D.J., Dickson, M.C. & Brown, M.J. Natriuretic peptide receptor mRNAs in the rat and human heart. *The Journal of Clinical Investigation* 90, 1966-1971 (1992).
87. Santhekadur, P.K., Kumar, D.P., Seneshaw, M., Mirshahi, F. & Sanyal, A.J. The multifaceted role of natriuretic peptides in metabolic syndrome. *Biomedicine & Pharmacotherapy* 92, 826-835 (2017).
88. Kumar, M. et al. Animal models of myocardial infarction: Mainstay in clinical translation. *Regulatory Toxicology and Pharmacology* 76, 221-230 (2016).
89. Hashmi, S. & Al-Salam, S. Acute myocardial infarction and myocardial ischemia-reperfusion injury: a comparison. *International Journal of Clinical and Experimental Pathology* 8, 8786-8796 (2015).
90. Hou, Y., Huang, C., Cai, X., Zhao, J. & Guo, W. Improvements in the establishment of a rat myocardial infarction model. *The Journal of international medical research* 39, 1284-1292 (2011).
91. Rona, G., Chappel, C.I., Balazs, T. & Gaudry, R. An infarct-like myocardial lesion and other toxic manifestations produced by isoproterenol in the rat. *A.M.A. archives of pathology* 67, 443-455 (1959).
92. Nirmala, C. & Puvanakrishnan, R. Protective role of curcumin against isoproterenol induced myocardial infarction in rats. *Molecular and cellular biochemistry* 159, 85-93 (1996).
93. Lobo Filho, H.G. et al. Modelo experimental de infarto do miocárdio induzido por isoproterenol em ratos. *Brazilian Journal of Cardiovascular Surgery* 26, 469-476 (2011).
94. Marx, S.O. et al. PKA phosphorylation dissociates FKBP12.6 from the calcium release channel (ryanodine receptor): defective regulation in failing hearts. *Cell* 101, 365-376 (2000).
95. Goldspink, D.F., Burniston, J.G., Ellison, G.M., Clark, W.A. & Tan, L.B. Catecholamine-induced apoptosis and necrosis in cardiac and skeletal myocytes of the rat in vivo: the same or separate death pathways? *Experimental physiology* 89, 407-416 (2004).
96. Reiken, S. et al. Protein kinase A phosphorylation of the cardiac calcium release channel (ryanodine receptor) in normal and failing hearts. Role of phosphatases and response to isoproterenol. *The Journal of biological chemistry* 278, 444-453 (2003).
97. Shizukuda, Y. et al. beta-adrenergic stimulation causes cardiocyte apoptosis: influence of tachycardia and hypertrophy. *The American journal of physiology* 275, H961-968 (1998).
98. Zaafan, M.A., Zaki, H.F., El-Brairy, A.I. & Kenawy, S.A. Protective effects of atorvastatin and quercetin on isoprenaline-induced myocardial infarction in rats. *Bulletin of Faculty of Pharmacy, Cairo University* 51, 35-41 (2013).
99. Dvir, T. et al. Nanoparticles Targeting the Infarcted Heart. *Nano Letters* 11, 4411-4414 (2011).
100. Opie, L.H., Commerford, P.J., Gersh, B.J. & Pfeffer, M.A. Controversies in ventricular remodelling. *The Lancet* 367, 356-367 (2006).
101. Krum, H. & Teerlink, J.R. Medical therapy for chronic heart failure. *The Lancet* 378, 713-721 (2011).
102. Braunwald, E. The war against heart failure: the Lancet lecture. *Lancet (London, England)* 385, 812-824 (2015).
103. Givertz, M.M. Ventricular Assist Devices. *Important Information for Patients and Families* 124, e305-e311 (2011).
104. American Heart Association, Devices and Surgical Procedures to Treat Heart Failure. *http://www.heart.org/HEARTORG/Conditions/HeartFailure/TreatmentOptionsForHeartFailure/Devices-and-Surgical-Procedures-to-Treat-Heart-Failure_UCM_306354_Article.jsp#.WWsfHGchFec* [16 July 2017] (2017).
105. Mahmoudi, M. et al. Multiscale technologies for treatment of ischemic cardiomyopathy. *Nat Nano* 12, 845-855 (2017).
106. Soonpaa, M.H. & Field, L.J. Assessment of cardiomyocyte DNA synthesis in normal and injured adult mouse hearts. *The American journal of physiology* 272, H220-226 (1997).
107. Senyo, S.E. et al. Mammalian heart renewal by pre-existing cardiomyocytes. *Nature* 493, 433-436 (2013).
108. Bergmann, O. et al. Evidence for cardiomyocyte renewal in humans. *Science* 324, 98-102 (2009).

109. Hosoda, T., Rota, M., Kajstura, J., Leri, A. & Anversa, P. Role of stem cells in cardiovascular biology. *Journal of thrombosis and haemostasis : JTH* 9 Suppl 1, 151-161 (2011).
110. Laflamme, M.A. & Murry, C.E. Heart regeneration. *Nature* 473, 326-335 (2011).
111. Beltrami, A.P. et al. Adult cardiac stem cells are multipotent and support myocardial regeneration. *Cell* 114, 763-776 (2003).
112. Orlic, D. et al. Bone marrow cells regenerate infarcted myocardium. *Nature* 410, 701-705 (2001).
113. Senyo, S.E. et al. Mammalian heart renewal by pre-existing cardiomyocytes. *Nature* 493, 433-436 (2013).
114. Marx, S.O. & Marks, A.R. Dysfunctional ryanodine receptors in the heart: new insights into complex cardiovascular diseases. *Journal of molecular and cellular cardiology* 58, 225-231 (2013).
115. Cleland, J.G. et al. The effects of the cardiac myosin activator, omecamtiv mecarbil, on cardiac function in systolic heart failure: a double-blind, placebo-controlled, crossover, dose-ranging phase 2 trial. *Lancet (London, England)* 378, 676-683 (2011).
116. Murakoshi, M., Saiki, K., Urayama, K. & Sato, T.N. An Anthelmintic Drug, Pyrvinium Pamoate, Thwarts Fibrosis and Ameliorates Myocardial Contractile Dysfunction in a Mouse Model of Myocardial Infarction. *PLOS ONE* 8, e79374 (2013).
117. Jung, D.W. & Williams, D.R. Reawakening atlas: chemical approaches to repair or replace dysfunctional musculature. *ACS chemical biology* 7, 1773-1790 (2012).
118. Hsueh, Y.C., Wu, J.M., Yu, C.K., Wu, K.K. & Hsieh, P.C. Prostaglandin E(2) promotes post-infarction cardiomyocyte replenishment by endogenous stem cells. *EMBO molecular medicine* 6, 496-503 (2014).
119. Engel, F.B., Hsieh, P.C.H., Lee, R.T. & Keating, M.T. FGF1/p38 MAP kinase inhibitor therapy induces cardiomyocyte mitosis, reduces scarring, and rescues function after myocardial infarction. *Proceedings of the National Academy of Sciences of the United States of America* 103, 15546-15551 (2006).
120. Kuhn, B. et al. Periostin induces proliferation of differentiated cardiomyocytes and promotes cardiac repair. *Nature medicine* 13, 962-969 (2007).
121. Bersell, K., Arab, S., Haring, B. & Kuhn, B. Neuregulin1/ErbB4 signaling induces cardiomyocyte proliferation and repair of heart injury. *Cell* 138, 257-270 (2009).
122. Xie, M., Cao, N. & Ding, S. Small Molecules for Cell Reprogramming and Heart Repair: Progress and Perspective. *ACS chemical biology* 9, 34-44 (2014).
123. Wang, H. et al. Small molecules enable cardiac reprogramming of mouse fibroblasts with a single factor, Oct4. *Cell reports* 6, 951-960 (2014).
124. Hodgkinson, C.P., Kang, M.H., Dal-Pra, S., Mirotsou, M. & Dzau, V.J. MicroRNAs and cardiac regeneration. *Circulation research* 116, 1700-1711 (2015).
125. Melman, Y.F., Shah, R. & Das, S. MicroRNAs in heart failure: is the picture becoming less miRky? *Circulation. Heart failure* 7, 203-214 (2014).
126. Care, A. et al. MicroRNA-133 controls cardiac hypertrophy. *Nature medicine* 13, 613-618 (2007).
127. Castaldi, A. et al. MicroRNA-133 modulates the beta1-adrenergic receptor transduction cascade. *Circ Res* 115, 273-283 (2014).
128. Jayawardena, T.M. et al. MicroRNA-mediated in vitro and in vivo direct reprogramming of cardiac fibroblasts to cardiomyocytes. *Circ Res* 110, 1465-1473 (2012).
129. Nam, Y.J. et al. Reprogramming of human fibroblasts toward a cardiac fate. *Proc Natl Acad Sci U S A* 110, 5588-5593 (2013).
130. Hastings, C.L. et al. Drug and cell delivery for cardiac regeneration. *Advanced Drug Delivery Reviews* 84, 85-106 (2015).
131. Orlic, D. et al. Bone marrow cells regenerate infarcted myocardium. *Nature* 410, 701-705 (2001).
132. Kudo, M. et al. Implantation of bone marrow stem cells reduces the infarction and fibrosis in ischemic mouse heart. *Journal of molecular and cellular cardiology* 35, 1113-1119 (2003).
133. Tomita, S. et al. Autologous transplantation of bone marrow cells improves damaged heart function. *Circulation* 100, Ii247-256 (1999).
134. Tang, J., Xie, Q., Pan, G., Wang, J. & Wang, M. Mesenchymal stem cells participate in angiogenesis and improve heart function in rat model of myocardial ischemia with reperfusion. *European journal of cardio-thoracic surgery : official journal of the European Association for Cardio-thoracic Surgery* 30, 353-361 (2006).
135. Kajstura, J. et al. Bone marrow cells differentiate in cardiac cell lineages after infarction independently of cell fusion. *Circ Res* 96, 127-137 (2005).
136. Zhang, S. et al. Long-term effects of bone marrow mononuclear cell transplantation on left ventricular function and remodeling in rats. *Life sciences* 74, 2853-2864 (2004).
137. Tang, Y.L. et al. Autologous mesenchymal stem cell transplantation induce VEGF and neovascularization in ischemic myocardium. *Regulatory peptides* 117, 3-10 (2004).
138. Zhang, D.Z. et al. Transplantation of autologous adipose-derived stem cells ameliorates cardiac function in rabbits with myocardial infarction. *Chinese medical journal* 120, 300-307 (2007).
139. Bolli, R. et al. Cardiac stem cells in patients with ischaemic cardiomyopathy (SCIPIO): initial results of a randomised phase 1 trial. *Lancet (London, England)* 378, 1847-1857 (2011).
140. Makkar, R.R. et al. Intracoronary cardiosphere-derived cells for heart regeneration after myocardial infarction (CADUCEUS): a prospective, randomised phase 1 trial. *Lancet (London, England)* 379, 895-904 (2012).
141. Malliaras, K. et al. Intracoronary cardiosphere-derived cells after myocardial infarction: evidence of therapeutic regeneration in the final 1-year results of the CADUCEUS trial (CArdiosphere-Derived aUtologous stem CElls to reverse ventricULar dySfunction). *J Am Coll Cardiol* 63, 110-122 (2014).
142. Chugh, A.R. et al. Administration of cardiac stem cells in patients with ischemic cardiomyopathy: the SCIPIO trial: surgical aspects and interim analysis of myocardial function and viability by magnetic resonance. *Circulation* 126, S54-64 (2012).
143. Bartunek, J. et al. Cardiopoietic stem cell therapy in heart failure: the C-CURE (Cardiopoietic stem Cell therapy in heart failURE) multicenter randomized trial with lineage-specified biologics. *J Am Coll Cardiol* 61, 2329-2338 (2013).

144. Templin, C., Luscher, T.F. & Landmesser, U. Cell-based cardiovascular repair and regeneration in acute myocardial infarction and chronic ischemic cardiomyopathy-current status and future developments. *The International journal of developmental biology* 55, 407-417 (2011).
145. Robey, T.E., Saiget, M.K., Reinecke, H. & Murry, C.E. Systems approaches to preventing transplanted cell death in cardiac repair. *Journal of molecular and cellular cardiology* 45, 567-581 (2008).
146. Hare, J.M. et al. A Randomized, Double-Blind, Placebo-Controlled, Dose-Escalation Study of Intravenous Adult Human Mesenchymal Stem Cells (Prochymal) After Acute Myocardial Infarction. *Journal of the American College of Cardiology* 54, 2277-2286 (2009).
147. Wollert, K.C. et al. Intracoronary autologous bone-marrow cell transfer after myocardial infarction: the BOOST randomised controlled clinical trial. *The Lancet* 364, 141-148 (2004).
148. Venugopal, J.R. et al. Biomaterial strategies for alleviation of myocardial infarction. *Journal of the Royal Society, Interface* 9, 1-19 (2012).
149. Russo, V., Young, S., Hamilton, A., Amsden, B.G. & Flynn, L.E. Mesenchymal stem cell delivery strategies to promote cardiac regeneration following ischemic injury. *Biomaterials* 35, 3956-3974 (2014).
150. Zhang, G., Hu, Q., Braunlin, E.A., Suggs, L.J. & Zhang, J. Enhancing efficacy of stem cell transplantation to the heart with a PEGylated fibrin biomatrix. *Tissue engineering. Part A* 14, 1025-1036 (2008).
151. Christman, K.L. et al. Injectable fibrin scaffold improves cell transplant survival, reduces infarct expansion, and induces neovasculature formation in ischemic myocardium. *J Am Coll Cardiol* 44, 654-660 (2004).
152. Martens, T.P. et al. Percutaneous Cell Delivery Into the Heart Using Hydrogels Polymerizing In Situ. *Cell transplantation* 18, 297-304 (2009).
153. Habib, M. et al. A combined cell therapy and in-situ tissue-engineering approach for myocardial repair. *Biomaterials* 32, 7514-7523 (2011).
154. Wang, T. et al. Bone marrow stem cells implantation with alpha-cyclodextrin/MPEG-PCL-MPEG hydrogel improves cardiac function after myocardial infarction. *Acta Biomater* 5, 2939-2944 (2009).
155. Yu, J. et al. The use of human mesenchymal stem cells encapsulated in RGD modified alginate microspheres in the repair of myocardial infarction in the rat. *Biomaterials* 31, 7012-7020 (2010).
156. Liu, Z. et al. The influence of chitosan hydrogel on stem cell engraftment, survival and homing in the ischemic myocardial microenvironment. *Biomaterials* 33, 3093-3106 (2012).
157. Li, J. et al. A chitosan-glutathione based injectable hydrogel for suppression of oxidative stress damage in cardiomyocytes. *Biomaterials* 34, 9071-9081 (2013).
158. Zhang, Y. et al. Collagen-based matrices improve the delivery of transplanted circulating progenitor cells: development and demonstration by ex vivo radionuclide cell labeling and in vivo tracking with positron-emission tomography. *Circulation. Cardiovascular imaging* 1, 197-204 (2008).
159. Suuronen, E.J. et al. Tissue-engineered injectable collagen-based matrices for improved cell delivery and vascularization of ischemic tissue using CD133+ progenitors expanded from the peripheral blood. *Circulation* 114, I138-144 (2006).
160. Wang, H. et al. Promotion of cardiac differentiation of brown adipose derived stem cells by chitosan hydrogel for repair after myocardial infarction. *Biomaterials* 35, 3986-3998 (2014).
161. Ravichandran, R. et al. Mimicking native extracellular matrix with phytic acid-crosslinked protein nanofibers for cardiac tissue engineering. *Macromolecular bioscience* 13, 366-375 (2013).
162. Eniola-Adefeso, O., Heslinga, M.J. & Porter, T.M. Design of Nano Vectors for Therapy and Imaging of Cardiovascular Diseases. *Methodist DeBakey Cardiovascular Journal* 8, 13-17 (2012).
163. Paulis, L.E. et al. Distribution of lipid-based nanoparticles to infarcted myocardium with potential application for MRI-monitored drug delivery. *Journal of Controlled Release* 162, 276-285 (2012).
164. Sun, W., Hu, Q., Ji, W., Wright, G. & Gu, Z. Leveraging Physiology for Precision Drug Delivery. *Physiological reviews* 97, 189-225 (2017).
165. Bozzuto, G. & Molinari, A. Liposomes as nanomedical devices. *International Journal of Nanomedicine* 10, 975-999 (2015).
166. Erathodiyil, N. & Ying, J.Y. Functionalization of Inorganic Nanoparticles for Bioimaging Applications. *Accounts of chemical research* 44, 925-935 (2011).
167. Li, S.D. & Huang, L. Pharmacokinetics and biodistribution of nanoparticles. *Molecular pharmaceutics* 5, 496-504 (2008).
168. Suk, J.S., Xu, Q., Kim, N., Hanes, J. & Ensign, L.M. PEGylation as a strategy for improving nanoparticle-based drug and gene delivery. *Advanced Drug Delivery Reviews* 99, 28-51 (2016).
169. Jokerst, J.V., Lobovkina, T., Zare, R.N. & Gambhir, S.S. Nanoparticle PEGylation for imaging and therapy. *Nanomedicine (London, England)* 6, 715-728 (2011).
170. Sisco, P.N. et al. The Effect of Gold Nanorods on Cell-Mediated Collagen Remodeling. *Nano letters* 8, 3409-3412 (2008).
171. Bunjes, H. Lipid nanoparticles for the delivery of poorly water-soluble drugs. *The Journal of pharmacy and pharmacology* 62, 1637-1645 (2010).
172. Santos, H.A., Peltonen, L., Limnell, T. & Hirvonen, J. Mesoporous materials and nanocrystals for enhancing the dissolution behavior of poorly water-soluble drugs. *Current pharmaceutical biotechnology* 14, 926-938 (2013).
173. McCarthy, J.R. Nanomedicine and Cardiovascular Disease. *Current cardiovascular imaging reports* 3, 42-49 (2010).
174. Chang, M.Y. et al. Functionalized nanoparticles provide early cardioprotection after acute myocardial infarction. *Journal of controlled release : official journal of the Controlled Release Society* 170, 287-294 (2013).
175. Formiga, F.R. et al. Sustained release of VEGF through PLGA microparticles improves vasculogenesis and tissue remodeling in an acute myocardial ischemia-reperfusion model. *Journal of controlled release : official journal of the Controlled Release Society* 147, 30-37 (2010).
176. Qi, Q. et al. Spatiotemporal delivery of nanoformulated liraglutide for cardiac regeneration after myocardial infarction. *International Journal of Nanomedicine* 12, 4835-4848 (2017).

177. Binsalamah, Z.M., Paul, A., Khan, A.A., Prakash, S. & Shum-Tim, D. Intramyocardial sustained delivery of placental growth factor using nanoparticles as a vehicle for delivery in the rat infarct model. *Int J Nanomedicine* 6, 2667-2678 (2011).
178. Hwang, H. et al. Peptide-loaded nanoparticles and radionuclide imaging for individualized treatment of myocardial ischemia. *Radiology* 273, 160-167 (2014).
179. Iwakura, A. et al. Intramyocardial sustained delivery of basic fibroblast growth factor improves angiogenesis and ventricular function in a rat infarct model. *Heart and vessels* 18, 93-99 (2003).
180. Cittadini, A. et al. Complementary therapeutic effects of dual delivery of insulin-like growth factor-1 and vascular endothelial growth factor by gelatin microspheres in experimental heart failure. *European journal of heart failure* 13, 1264-1274 (2011).
181. Foronjy, R.F., Sun, J., Lemaitre, V. & D'Armiento, J.M. Transgenic expression of matrix metalloproteinase-1 inhibits myocardial fibrosis and prevents the transition to heart failure in a pressure overload mouse model. *Hypertension research : official journal of the Japanese Society of Hypertension* 31, 725-735 (2008).
182. Suarez, S.L. et al. Degradable Acetalated Dextran Microparticles for Tunable Release of an Engineered Hepatocyte Growth Factor Fragment. *ACS Biomaterials Science & Engineering* 2, 197-204 (2016).
183. Suarez, S., Grover, G.N., Braden, R.L., Christman, K.L. & Almutairi, A. Tunable Protein Release from Acetalated Dextran Microparticles: A Platform for Delivery of Protein Therapeutics to the Heart Post-MI. *Biomacromolecules* 14, 3927-3935 (2013).
184. Somasuntharam, I. et al. Delivery of Nox2-NADPH oxidase siRNA with polyketal nanoparticles for improving cardiac function following myocardial infarction. *Biomaterials* 34, 7790-7798 (2013).
185. Liu, J. et al. Functionalized Dendrimer-Based Delivery of Angiotensin Type 1 Receptor siRNA for Preserving Cardiac Function Following Infarction. *Biomaterials* 34, 3729-3736 (2013).
186. Tranter, M. et al. In Vivo Delivery of Nucleic Acids via Glycopolymer Vehicles Affords Therapeutic Infarct Size Reduction In Vivo. *Molecular Therapy* 20, 601-608 (2012).
187. Nguyen, M.M. et al. Enzyme-Responsive Nanoparticles for Targeted Accumulation and Prolonged Retention in Heart Tissue after Myocardial Infarction. *Advanced Materials* 27, 5547-5552 (2015).
188. Verma, D.D., Hartner, W.C., Levchenko, T.S., Bernstein, E.A. & Torchilin, V.P. ATP-loaded liposomes effectively protect the myocardium in rabbits with an acute experimental myocardial infarction. *Pharmaceutical research* 22, 2115-2120 (2005).
189. Lundy, D.J., Chen, K.-H., Toh, E.K.W. & Hsieh, P.C.H. Distribution of Systemically Administered Nanoparticles Reveals a Size-Dependent Effect Immediately following Cardiac Ischaemia-Reperfusion Injury. *Scientific Reports* 6, 25613 (2016).
190. Lukyanov, A.N., Hartner, W.C. & Torchilin, V.P. Increased accumulation of PEG-PE micelles in the area of experimental myocardial infarction in rabbits. *Journal of controlled release : official journal of the Controlled Release Society* 94, 187-193 (2004).
191. Takahama, H. et al. Prolonged targeting of ischemic/reperfused myocardium by liposomal adenosine augments cardioprotection in rats. *J Am Coll Cardiol* 53, 709-717 (2009).
192. Geelen, T., Paulis, L.E., Coolen, B.F., Nicolay, K. & Strijkers, G.J. Passive targeting of lipid-based nanoparticles to mouse cardiac ischemia-reperfusion injury. *Contrast media & molecular imaging* 8, 117-126 (2013).
193. Hiller, K.H., Waller, C., Nahrendorf, M., Bauer, W.R. & Jakob, P.M. Assessment of cardiovascular apoptosis in the isolated rat heart by magnetic resonance molecular imaging. *Molecular imaging* 5, 115-121 (2006).
194. Sanders, H.M. et al. Morphology, binding behavior and MR-properties of paramagnetic collagen-binding liposomes. *Contrast media & molecular imaging* 4, 81-88 (2009).
195. Zhang, S., Wang, J. & Pan, J. Baicalin-loaded PEGylated lipid nanoparticles: characterization, pharmacokinetics, and protective effects on acute myocardial ischemia in rats. *Drug Delivery* 23, 3696-3703 (2016).
196. Torchilin, V.P., Khaw, B.A., Smirnov, V.N. & Haber, E. Preservation of antimyosin antibody activity after covalent coupling to liposomes. *Biochemical and biophysical research communications* 89, 1114-1119 (1979).
197. Khaw, B.A., DaSilva, J. & Hartner, W.C. Cytoskeletal-antigen specific immunoliposome-targeted in vivo preservation of myocardial viability. *Journal of controlled release : official journal of the Controlled Release Society* 120, 35-40 (2007).
198. Scott, R.C. et al. Targeted delivery of antibody conjugated liposomal drug carriers to rat myocardial infarction. *Biotechnology and bioengineering* 96, 795-802 (2007).
199. Verma, D.D., Levchenko, T.S., Bernstein, E.A., Mongayt, D. & Torchilin, V.P. ATP-loaded immunoliposomes specific for cardiac myosin provide improved protection of the mechanical functions of myocardium from global ischemia in an isolated rat heart model. *Journal of drug targeting* 14, 273-280 (2006).
200. Ko, Y.T., Hartner, W.C., Kale, A. & Torchilin, V.P. Gene delivery into ischemic myocardium by double-targeted lipoplexes with anti-myosin antibody and TAT peptide. *Gene therapy* 16, 52-59 (2009).
201. Harel-Adar, T. et al. Modulation of cardiac macrophages by phosphatidylserine-presenting liposomes improves infarct repair. *Proc Natl Acad Sci U S A* 108, 1827-1832 (2011).
202. Cheng, B. et al. Biomimicking Platelet-Monocyte Interactions as a Novel Targeting Strategy for Heart Healing. *Advanced healthcare materials* 5, 2686-2697 (2016).
203. Dasa, S.S.K. et al. Development of target-specific liposomes for delivering small molecule drugs after reperfused myocardial infarction. *Journal of Controlled Release* 220, 556-567 (2015).
204. Dong, Z. et al. RGD modified and PEGylated lipid nanoparticles loaded with puerarin: Formulation, characterization and protective effects on acute myocardial ischemia model. *Biomedicine & Pharmacotherapy* 89, 297-304 (2017).
205. Huang, Z. et al. Targeted delivery of thymosin beta 4 to the injured myocardium using CREKA-conjugated nanoparticles. *International Journal of Nanomedicine* 12, 3023-3036 (2017).
206. Vinodhini, A., Govindaraju, K., Singaravelu, G., Mohamed Sadiq, A. & Kumar, V.G. Cardioprotective potential of biobased gold nanoparticles. *Colloids and Surfaces B: Biointerfaces* 117, 480-486 (2014).
207. Galagudza, M. et al. Passive targeting of ischemic-reperfused myocardium with adenosine-loaded silica nanoparticles. *International Journal of Nanomedicine* 7, 1671-1678 (2012).

208. Cheng, K. et al. Magnetic antibody-linked nanomatchmakers for therapeutic cell targeting. *Nature Communications* 5, 4880 (2014).
209. Yilmaz, A. et al. Imaging of myocardial infarction using ultrasmall superparamagnetic iron oxide nanoparticles: a human study using a multi-parametric cardiovascular magnetic resonance imaging approach. *European heart journal* 34, 462-475 (2013).
210. Florian, A. et al. Positive effect of intravenous iron-oxide administration on left ventricular remodelling in patients with acute ST-elevation myocardial infarction - a cardiovascular magnetic resonance (CMR) study. *International journal of cardiology* 173, 184-189 (2014).
211. Weissleder, R., Lee, A.S., Khaw, B.A., Shen, T. & Brady, T.J. Antimyosin-labeled monocrystalline iron oxide allows detection of myocardial infarct: MR antibody imaging. *Radiology* 182, 381-385 (1992).
212. Shevtsov, M.A. et al. Detection of experimental myocardium infarction in rats by MRI using heat shock protein 70 conjugated superparamagnetic iron oxide nanoparticle. *Nanomedicine: Nanotechnology, Biology and Medicine* 12, 611-621 (2016).
213. Swyer, T., Strom, J. & Larson, D. Nanoparticle oxygen delivery to the ischemic heart. *Perfusion* 29, 539-543 (2014).
214. Caride, V. & Zaret, B. Liposome accumulation in regions of experimental myocardial infarction. *Science* 198, 735-738 (1977).
215. Levchenko, T.S., Hartner, W.C. & Torchilin, V.P. Liposomes in diagnosis and treatment of cardiovascular disorders. *Methodist DeBakey Cardiovascular Journal* 8, 36-41 (2012).
216. Xu, G.X. et al. Adenosine triphosphate liposomes: encapsulation and distribution studies. *Pharmaceutical research* 7, 553-557 (1990).
217. Hirsjarvi, S., Passirani, C. & Benoit, J.P. Passive and active tumour targeting with nanocarriers. *Current drug discovery technologies* 8, 188-196 (2011).
218. Fang, J., Nakamura, H. & Maeda, H. The EPR effect: Unique features of tumor blood vessels for drug delivery, factors involved, and limitations and augmentation of the effect. *Adv Drug Deliv Rev* 63, 136-151 (2011).
219. Weis, S.M. Vascular permeability in cardiovascular disease and cancer. *Current opinion in hematology* 15, 243-249 (2008).
220. Prabhakar, U. et al. Challenges and key considerations of the enhanced permeability and retention effect for nanomedicine drug delivery in oncology. *Cancer research* 73, 2412-2417 (2013).
221. Palmer, T.N., Caride, V.J., Caldecourt, M.A., Twickler, J. & Abdullah, V. The mechanism of liposome accumulation in infarction. *Biochimica et biophysica acta* 797, 363-368 (1984).
222. Heusch, G. Cardioprotection: chances and challenges of its translation to the clinic. *Lancet (London, England)* 381, 166-175 (2013).
223. Cung, T.T. et al. Cyclosporine before PCI in Patients with Acute Myocardial Infarction. *The New England journal of medicine* 373, 1021-1031 (2015).
224. Skelton, R.J. et al. SIRPA, VCAM1 and CD34 identify discrete lineages during early human cardiovascular development. *Stem cell research* 13, 172-179 (2014).
225. Andreev, O.A., Engelman, D.M. & Reshetnyak, Y.K. pH-sensitive membrane peptides (pHLIPs) as a novel class of delivery agents. *Molecular membrane biology* 27, 341-352 (2010).
226. Sosunov, E.A. et al. pH (low) insertion peptide (pHLIP) targets ischemic myocardium. *Proceedings of the National Academy of Sciences* 110, 82-86 (2013).
227. Scott, R.C. et al. Targeting VEGF-encapsulated immunoliposomes to MI heart improves vascularity and cardiac function. *FASEB journal : official publication of the Federation of American Societies for Experimental Biology* 23, 3361-3367 (2009).
228. Bietenbeck, M., Florian, A., Sechtem, U. & Yilmaz, A. The diagnostic value of iron oxide nanoparticles for imaging of myocardial inflammation – quo vadis? *Journal of Cardiovascular Magnetic Resonance* 17, 54 (2015).
229. Seko, Y. et al. Expression of costimulatory molecule CD40 in murine heart with acute myocarditis and reduction of inflammation by treatment with anti-CD40L/B7-1 monoclonal antibodies. *Circ Res* 83, 463-469 (1998).
230. Uhlir, A. Electrolytic Shaping of Germanium and Silicon. *Bell System Technical Journal* 35, 333-347 (1956).
231. Turner, D.R. Electropolishing Silicon in Hydrofluoric Acid Solutions. *Journal of The Electrochemical Society* 105, 402-408 (1958).
232. Watanabe Y., S.T. Application of a thick anode film to semiconductor devices. *Review of Electrical Communication Laboratories* 19, 899 (1971).
233. Canham, L.T. Silicon quantum wire array fabrication by electrochemical and chemical dissolution of wafers. *Applied Physics Letters* 57, 1046-1048 (1990).
234. Canham, L.T. Bioactive silicon structure fabrication through nanoetching techniques. *Advanced Materials* 7, 1033-1037 (1995).
235. Canham, L.T. in Porous Silicon for Biomedical Applications 3-20 (Woodhead Publishing, 2014).
236. McInnes, S.J.P. & Lowe, R.D. in Electrochemically Engineered Nanoporous Materials: Methods, Properties and Applications. (eds. D. Losic & A. Santos) 117-162 (Springer International Publishing, Cham; 2015).
237. Tzur-Balter, A., Shtenberg, G. & Segal, E. in Reviews in Chemical Engineering, Vol. 31 193 (2015).
238. Santos, H.A. & Hirvonen, J. Nanostructured porous silicon materials: potential candidates for improving drug delivery. *Nanomedicine (Lond)* 7, 1281-1284 (2012).
239. Canham, L. in Handbook of Porous Silicon. (ed. L. Canham) 733-740 (Springer International Publishing, Cham; 2014).
240. Savage, D., Liu, X., Curley, S., Ferrari, M. & Serda, R.E. Porous silicon advances in drug delivery and immunotherapy. *Current opinion in pharmacology* 13, 834-841 (2013).
241. Salonen, J. & Lehto, V.-P. Fabrication and chemical surface modification of mesoporous silicon for biomedical applications. *Chemical Engineering Journal* 137, 162-172 (2008).
242. Anglin, E.J., Cheng, L., Freeman, W.R. & Sailor, M.J. Porous silicon in drug delivery devices and materials. *Adv Drug Deliv Rev* 60, 1266-1277 (2008).
243. Bomchil, G., Halimaoui, A. & Herino, R. Porous silicon: The material and its applications to SOI technologies. *Microelectronic Engineering* 8, 293-310 (1988).

244. Jarvis, K.L., Barnes, T.J. & Prestidge, C.A. Surface chemistry of porous silicon and implications for drug encapsulation and delivery applications. *Advances in Colloid and Interface Science* 175, 25-38 (2012).
245. Petrova, E.A., Bogoslovskaya, K.N., Balagurov, L.A. & Kochoradze, G.I. Room temperature oxidation of porous silicon in air. *Materials Science and Engineering: B* 69, 152-156 (2000).
246. Salonen, J., Björkqvist, M., Laine, E. & Niinistö, L. Stabilization of porous silicon surface by thermal decomposition of acetylene. *Applied Surface Science* 225, 389-394 (2004).
247. Kovalainen, M. et al. Mesoporous silicon (PSi) for sustained peptide delivery: effect of psi microparticle surface chemistry on peptide YY3-36 release. *Pharmaceutical research* 29, 837-846 (2012).
248. Chiappini, C. et al. Tailored porous silicon microparticles: fabrication and properties. *Chemphyschem : a European journal of chemical physics and physical chemistry* 11, 1029-1035 (2010).
249. Nissinen, T., Ikonen, T., Lama, M., Riikonen, J. & Lehto, V.-P. Improved production efficiency of mesoporous silicon nanoparticles by pulsed electrochemical etching. *Powder Technology* 288, 360-365 (2016).
250. Godin, B. et al. Discoidal Porous Silicon Particles: Fabrication and Biodistribution in Breast Cancer Bearing Mice. *Advanced functional materials* 22, 4225-4235 (2012).
251. Mares, J.W., Fain, J.S., Beavers, K.R., Duvall, C.L. & Weiss, S.M. Shape-engineered multifunctional porous silicon nanoparticles by direct imprinting. *Nanotechnology* 26, 271001 (2015).
252. Alhmoud, H. et al. Porous Silicon Nanodiscs for Targeted Drug Delivery. *Advanced functional materials* 25, 1137-1145 (2015).
253. Qin, Z., Joo, J., Gu, L. & Sailor, M.J. Size Control of Porous Silicon Nanoparticles by Electrochemical Perforation Etching. *Particle & Particle Systems Characterization* 31, 252-256 (2014).
254. Wang, F., Hui, H., Barnes, T.J., Barnett, C. & Prestidge, C.A. Oxidized Mesoporous Silicon Microparticles for Improved Oral Delivery of Poorly Soluble Drugs. *Molecular pharmaceutics* 7, 227-236 (2010).
255. Salonen, J. et al. Mesoporous silicon microparticles for oral drug delivery: Loading and release of five model drugs. *Journal of Controlled Release* 108, 362-374 (2005).
256. Wang, C.-F. et al. Dual-drug delivery by porous silicon nanoparticles for improved cellular uptake, sustained release, and combination therapy. *Acta Biomaterialia* 16, 206-214 (2015).
257. Shahbazi, M.-A. et al. Intracellular responsive dual delivery by endosomolytic polyplexes carrying DNA anchored porous silicon nanoparticles. *Journal of Controlled Release* 249, 111-122 (2017).
258. Liu, D. et al. Microfluidic assisted one-step fabrication of porous silicon@acetalated dextran nanocomposites for precisely controlled combination chemotherapy. *Biomaterials* 39, 249-259 (2015).
259. Shrestha, N. et al. Chitosan-modified porous silicon microparticles for enhanced permeability of insulin across intestinal cell monolayers. *Biomaterials* 35, 7172-7179 (2014).
260. Araújo, F. et al. The impact of nanoparticles on the mucosal translocation and transport of GLP-1 across the intestinal epithelium. *Biomaterials* 35, 9199-9207 (2014).
261. Shahbazi, M.-A. et al. A prospective cancer chemo-immunotherapy approach mediated by synergistic CD326 targeted porous silicon nanovectors. *Nano Research* 8, 1505-1521 (2015).
262. Balasubramanian, V. et al. Biomimetic Engineering Using Cancer Cell Membranes for Designing Compartmentalized Nanoreactors with Organelle-Like Functions. *Advanced Materials* 29, 1605375-n/a (2017).
263. Sarparanta, M.P. et al. The mucoadhesive and gastroretentive properties of hydrophobin-coated porous silicon nanoparticle oral drug delivery systems. *Biomaterials* 33, 3353-3362 (2012).
264. Shrestha, N. et al. Oral hypoglycaemic effect of GLP-1 and DPP4 inhibitor based nanocomposites in a diabetic animal model. *Journal of Controlled Release* 232, 113-119 (2016).
265. Liu, D. et al. Nanostructured Porous Silicon-Solid Lipid Nanocomposite: Towards Enhanced Cytocompatibility and Stability, Reduced Cellular Association, and Prolonged Drug Release. *Advanced functional materials* 23, 1893-1902 (2013).
266. Correia, A. et al. Cyclodextrin-Modified Porous Silicon Nanoparticles for Efficient Sustained Drug Delivery and Proliferation Inhibition of Breast Cancer Cells. *ACS Applied Materials & Interfaces* 7, 23197-23204 (2015).
267. Herranz-Blanco, B. et al. On-Chip Self-Assembly of a Smart Hybrid Nanocomposite for Antitumoral Applications. *Advanced functional materials* 25, 1488-1497 (2015).
268. Kinnari, P.J. et al. Tumour homing peptide-functionalized porous silicon nanovectors for cancer therapy. *Biomaterials* 34, 9134-9141 (2013).
269. Meraz, I.M. et al. Activation of the Inflammasome and Enhanced Migration of Microparticle-Stimulated Dendritic Cells to the Draining Lymph Node. *Molecular pharmaceutics* 9, 2049-2062 (2012).
270. Naessens, M., Cerdobbel, A., Soetaert, W. & Vandamme, E.J. Leuconostoc dextransucrase and dextran: production, properties and applications. *Journal of Chemical Technology & Biotechnology* 80, 845-860 (2005).
271. Bachelder, E.M., Beaudette, T.T., Broaders, K.E., Dashe, J. & Frechet, J.M. Acetal-derivatized dextran: an acid-responsive biodegradable material for therapeutic applications. *J Am Chem Soc* 130, 10494-10495 (2008).
272. Sun-Wada, G.H., Wada, Y. & Futai, M. Lysosome and lysosome-related organelles responsible for specialized functions in higher organisms, with special emphasis on vacuolar-type proton ATPase. *Cell structure and function* 28, 455-463 (2003).
273. Helmlinger, G., Sckell, A., Dellian, M., Forbes, N.S. & Jain, R.K. Acid production in glycolysis-impaired tumors provides new insights into tumor metabolism. *Clinical cancer research : an official journal of the American Association for Cancer Research* 8, 1284-1291 (2002).
274. Cohen, J.L. et al. Acid-Degradable Cationic Dextran Particles for the Delivery of siRNA Therapeutics. *Bioconjugate chemistry* 22, 1056-1065 (2011).
275. Manchanda, R., Fernandez-Fernandez, A., Nagesetti, A. & McGoron, A.J. Preparation and characterization of a polymeric (PLGA) nanoparticulate drug delivery system with simultaneous incorporation of chemotherapeutic and thermo-optical agents. *Colloids and surfaces. B, Biointerfaces* 75, 260-267 (2010).
276. Keum, C.-G. et al. Practical preparation procedures for docetaxel-loaded nanoparticles using polylactic acid-co-glycolic acid. *International Journal of Nanomedicine* 6, 2225-2234 (2011).

277. Broaders, K.E., Cohen, J.A., Beaudette, T.T., Bachelder, E.M. & Fréchet, J.M.J. Acetalated dextran is a chemically and biologically tunable material for particulate immunotherapy. *Proceedings of the National Academy of Sciences* 106, 5497-5502 (2009).
278. Bilati, U., Allémann, E. & Doelker, E. Sonication Parameters for the Preparation of Biodegradable Nanocapsulesof Controlled Size by the Double Emulsion Method. *Pharmaceutical Development and Technology* 8, 1-9 (2003).
279. Bachelder, E.M. et al. In vitro analysis of acetalated dextran microparticles as a potent delivery platform for vaccine adjuvants. *Molecular pharmaceutics* 7, 826-835 (2010).
280. Kauffman, K.J. et al. Optimization of rapamycin-loaded acetalated dextran microparticles for immunosuppression. *Int J Pharm* 422, 356-363 (2012).
281. Paine, A. & Davan, A.D. Defining a tolerable concentration of methanol in alcoholic drinks. *Human & experimental toxicology* 20, 563-568 (2001).
282. Cui, L., Cohen, J.A., Broaders, K.E., Beaudette, T.T. & Fréchet, J.M.J. Mannosylated Dextran Nanoparticles: A pH-Sensitive System Engineered for Immunomodulation through Mannose Targeting. *Bioconjugate Chemistry* 22, 949-957 (2011).
283. Bauleth-Ramos, T. et al. Nutlin-3a and Cytokine Co-loaded Spermine-Modified Acetalated Dextran Nanoparticles for Cancer Chemo-Immunotherapy. *Advanced functional materials*, 1703303.
284. Kong, F. et al. Biodegradable Photothermal and pH Responsive Calcium Carbonate@Phospholipid@Acetalated Dextran Hybrid Platform for Advancing Biomedical Applications. *Advanced functional materials* 26, 6158-6169 (2016).
285. Zhang, H. et al. Microfluidic Encapsulation of Prickly Zinc-Doped Copper Oxide Nanoparticles with VD1142 Modified Spermine Acetalated Dextran for Efficient Cancer Therapy. *Advanced healthcare materials* 6, 1601406-n/a (2017).
286. Wang, Z., Gupta, S.K. & Meenach, S.A. Development and physicochemical characterization of acetalated dextran aerosol particle systems for deep lung delivery. *International Journal of Pharmaceutics* 525, 264-274 (2017).
287. Meenach, S.A. et al. Synthesis, Optimization, and Characterization of Camptothecin-Loaded Acetalated Dextran Porous Microparticles for Pulmonary Delivery. *Molecular pharmaceutics* 9, 290-298 (2012).
288. Liu, D., Yang, F., Xiong, F. & Gu, N. The Smart Drug Delivery System and Its Clinical Potential. *Theranostics* 6, 1306-1323 (2016).
289. Vllasaliu, D., Fowler, R. & Stolnik, S. PEGylated nanomedicines: recent progress and remaining concerns. *Expert opinion on drug delivery* 11, 139-154 (2014).
290. Abuchowski, A., McCoy, J.R., Palczuk, N.C., van Es, T. & Davis, F.F. Effect of covalent attachment of polyethylene glycol on immunogenicity and circulating life of bovine liver catalase. *The Journal of biological chemistry* 252, 3582-3586 (1977).
291. Yang, Q. & Lai, S.K. Anti-PEG immunity: emergence, characteristics, and unaddressed questions. *Wiley Interdisciplinary Reviews: Nanomedicine and Nanobiotechnology* 7, 655-677 (2015).
292. Vonarbourg, A., Passirani, C., Saulnier, P. & Benoit, J.-P. Parameters influencing the stealthiness of colloidal drug delivery systems. *Biomaterials* 27, 4356-4373 (2006).
293. Xie, J., Lee, S. & Chen, X. Nanoparticle-based theranostic agents. *Advanced drug delivery reviews* 62, 1064-1079 (2010).
294. Stendahl, J.C. & Sinusas, A.J. Nanoparticles for Cardiovascular Imaging and Therapeutic Delivery, Part 2: Radiolabeled Probes. *Journal of nuclear medicine : official publication, Society of Nuclear Medicine* 56, 1637-1641 (2015).
295. Deb, S., Ghosh, K. & Shetty, S.D. Nanoimaging in cardiovascular diseases: Current state of the art. *The Indian Journal of Medical Research* 141, 285-298 (2015).
296. Sarparanta, M. et al. (1)(8)F-labeled modified porous silicon particles for investigation of drug delivery carrier distribution in vivo with positron emission tomography. *Molecular pharmaceutics* 8, 1799-1806 (2011).
297. Sosabowski, J.K. & Mather, S.J. Conjugation of DOTA-like chelating agents to peptides and radiolabeling with trivalent metallic isotopes. *Nature protocols* 1, 972-976 (2006).
298. Salonen, J., Kaukonen, A.M., Hirvonen, J. & Lehto, V.P. Mesoporous silicon in drug delivery applications. *Journal of pharmaceutical sciences* 97, 632-653 (2008).
299. Bimbo, L.M. et al. Drug permeation across intestinal epithelial cells using porous silicon nanoparticles. *Biomaterials* 32, 2625-2633 (2011).
300. Knor, S. et al. Synthesis of novel 1,4,7,10-tetraazacyclodecane-1,4,7,10-tetraacetic acid (DOTA) derivatives for chemoselective attachment to unprotected polyfunctionalized compounds. *Chemistry (Weinheim an der Bergstrasse, Germany)* 13, 6082-6090 (2007).
301. Kinnunen, S.T., M.; Välimäki, M.; Jumppanen, M.; Boije af Gennäs, G.; Yli-Kauhaluoma, J.; Ruskoaho, H. Pharmaceutical compounds. *Patent Application No.: 20165712* (2016).
302. Välimäki, M.J. et al. Discovery of Small Molecules Targeting the Synergy of Cardiac Transcription Factors GATA4 and NKX2-5. *Journal of Medicinal Chemistry* (2017).
303. Pikkarainen, S. et al. GATA-4 is a nuclear mediator of mechanical stretch-activated hypertrophic program. *The Journal of biological chemistry* 278, 23807-23816 (2003).
304. Polinger, I.S. Separation of cell types in embryonic heart cell cultures. *Experimental cell research* 63, 78-82 (1970).
305. Takahashi, K., Ohyabu, Y., Schaffer, S.W. & Azuma, J. Cellular characterization of an in-vitro cell culture model of seal-induced cardiac ischaemia. *The Journal of pharmacy and pharmacology* 53, 379-386 (2001).
306. Vengellur, A. & LaPres, J.J. The role of hypoxia inducible factor 1alpha in cobalt chloride induced cell death in mouse embryonic fibroblasts. *Toxicological sciences : an official journal of the Society of Toxicology* 82, 638-646 (2004).
307. Wu, D. & Yotnda, P. Induction and testing of hypoxia in cell culture. *Journal of visualized experiments : JoVE* (2011).
308. Weber, W., Fischli, W., Hochuli, E., Kupfer, E. & Weibel, E.K. Anantin--a peptide antagonist of the atrial natriuretic factor (ANF). I. Producing organism, fermentation, isolation and biological activity. *The Journal of antibiotics* 44, 164-171 (1991).
309. Inman, G.J. et al. SB-431542 is a potent and specific inhibitor of transforming growth factor-beta superfamily type I activin receptor-like kinase (ALK) receptors ALK4, ALK5, and ALK7. *Molecular pharmacology* 62, 65-74 (2002).

310. Tenhunen, O. et al. p38 Kinase rescues failing myocardium after myocardial infarction: evidence for angiogenic and anti-apoptotic mechanisms. *FASEB journal : official publication of the Federation of American Societies for Experimental Biology* 20, 1907-1909 (2006).
311. Ellison, G.M. et al. Acute beta-adrenergic overload produces myocyte damage through calcium leakage from the ryanodine receptor 2 but spares cardiac stem cells. *The Journal of biological chemistry* 282, 11397-11409 (2007).
312. Chirgwin, J.M., Przybyla, A.E., MacDonald, R.J. & Rutter, W.J. Isolation of biologically active ribonucleic acid from sources enriched in ribonuclease. *Biochemistry* 18, 5294-5299 (1979).
313. Bai, B., Bading, J. & Conti, P.S. Tumor quantification in clinical positron emission tomography. *Theranostics* 3, 787-801 (2013).
314. Bimbo, L.M., Peltonen, L., Hirvonen, J. & Santos, H.A. Toxicological profile of therapeutic nanodelivery systems. *Current drug metabolism* 13, 1068-1086 (2012).
315. Elsaesser, A. & Howard, C.V. Toxicology of nanoparticles. *Advanced drug delivery reviews* 64, 129-137 (2012).
316. Martinez, J.O. et al. Short and long term, in vitro and in vivo correlations of cellular and tissue responses to mesoporous silicon nanovectors. *Small* 9, 1722-1733 (2013).
317. Hudson, S.P., Padera, R.F., Langer, R. & Kohane, D.S. The biocompatibility of mesoporous silicates. *Biomaterials* 29, 4045-4055 (2008).
318. Du, Z. et al. Cardiovascular Toxicity of Different Sizes Amorphous Silica Nanoparticles in Rats After Intratracheal Instillation. *Cardiovasc Toxicol* 13, 194-207 (2013).
319. Nian, M., Lee, P., Khaper, N. & Liu, P. Inflammatory cytokines and postmyocardial infarction remodeling. *Circ Res* 94, 1543-1553 (2004).
320. Weber, K.T., Sun, Y., Tyagi, S.C. & Cleutjens, J.P. Collagen network of the myocardium: function, structural remodeling and regulatory mechanisms. *Journal of molecular and cellular cardiology* 26, 279-292 (1994).
321. Godin, B. et al. Tailoring the degradation kinetics of mesoporous silicon structures through PEGylation. *Journal of biomedical materials research. Part A* 94, 1236-1243 (2010).
322. Linde, C. et al. Long-term benefits of biventricular pacing in congestive heart failure: results from the MUltisite STimulation in cardiomyopathy (MUSTIC) study. *Journal of the American College of Cardiology* 40, 111-118 (2002).
323. Abraham , W.T. et al. Cardiac Resynchronization in Chronic Heart Failure. *New England Journal of Medicine* 346, 1845-1853 (2002).
324. Rose , E.A. et al. Long-Term Use of a Left Ventricular Assist Device for End-Stage Heart Failure. *New England Journal of Medicine* 345, 1435-1443 (2001).
325. Alrefai, M.T. et al. Cardiac tissue engineering and regeneration using cell-based therapy. *Stem Cells and Cloning : Advances and Applications* 8, 81-101 (2015).
326. Pascual-Gil, S., Garbayo, E., Diaz-Herraez, P., Prosper, F. & Blanco-Prieto, M.J. Heart regeneration after myocardial infarction using synthetic biomaterials. *Journal of controlled release : official journal of the Controlled Release Society* 203, 23-38 (2015).
327. Santos, H.A. et al. In vitro cytotoxicity of porous silicon microparticles: Effect of the particle concentration, surface chemistry and size. *Acta Biomaterialia* 6, 2721-2731 (2010).
328. Leroueil, P.R. et al. Nanoparticle interaction with biological membranes: does nanotechnology present a Janus face? *Accounts of chemical research* 40, 335-342 (2007).
329. Verma, A. & Stellacci, F. Effect of surface properties on nanoparticle-cell interactions. *Small (Weinheim an der Bergstrasse, Germany)* 6, 12-21 (2010).
330. Gaihre, B., Hee Lee, Y., Khil, M.S., Yi, H.K. & Kim, H.Y. In-vitro cytotoxicity and cell uptake study of gelatin-coated magnetic iron oxide nanoparticles. *Journal of microencapsulation* 28, 240-247 (2011).
331. Deol, S., Weerasuriya, N. & Shon, Y.-S. Stability, Cytotoxicity and Cell Uptake of Water-Soluble Dendron-Conjugated Gold Nanoparticles with 3, 12 and 17 nm Core. *Journal of materials chemistry. B, Materials for biology and medicine* 3, 6071-6080 (2015).
332. Bhattacharjee, S. et al. Cytotoxicity and cellular uptake of tri-block copolymer nanoparticles with different size and surface characteristics. *Particle and Fibre Toxicology* 9, 11 (2012).
333. Verma, A. & Stellacci, F. Effect of Surface Properties on Nanoparticle–Cell Interactions. *Small (Weinheim an der Bergstrasse, Germany)* 6, 12-21 (2010).
334. Jin, H., Heller, D.A., Sharma, R. & Strano, M.S. Size-dependent cellular uptake and expulsion of single-walled carbon nanotubes: single particle tracking and a generic uptake model for nanoparticles. *ACS Nano* 3, 149-158 (2009).
335. Nunez, D.J., Dickson, M.C. & Brown, M.J. Natriuretic peptide receptor mRNAs in the rat and human heart. *Journal of Clinical Investigation* 90, 1966-1971 (1992).
336. Lin, X., Hanze, J., Heese, F., Sodmann, R. & Lang, R.E. Gene expression of natriuretic peptide receptors in myocardial cells. *Circ Res* 77, 750-758 (1995).
337. Cao, L. & Gardner, D.G. Natriuretic peptides inhibit DNA synthesis in cardiac fibroblasts. *Hypertension (Dallas, Tex. : 1979)* 25, 227-234 (1995).
338. Moro, C. et al. Functional and pharmacological characterization of the natriuretic peptide-dependent lipolytic pathway in human fat cells. *J Pharmacol Exp Ther* 308, 984-992 (2004).
339. Wyss, D.F., Lahm, H.W., Manneberg, M. & Labhardt, A.M. Anantin--a peptide antagonist of the atrial natriuretic factor (ANF). II. Determination of the primary sequence by NMR on the basis of proton assignments. *The Journal of antibiotics* 44, 172-180 (1991).
340. Kanki, S. et al. Identification of targeting peptides for ischemic myocardium by in vivo phage display. *Journal of molecular and cellular cardiology* 50, 841-848 (2011).
341. Ruoslahti, E., Mackenna D. Heart homing peptides and methods of using same. *U.S. Patent #6303573 B1* (October 16, 2001).
342. Ferreira, M.P.A. et al. In vitro and in vivo assessment of heart-homing porous silicon nanoparticles. *Biomaterials* 94, 93-104 (2016).
343. Buglioni, A. & Burnett, J.C., Jr. New Pharmacological Strategies to Increase cGMP. *Annual review of medicine* 67, 229-243 (2016).
344. Kuhn, M. Molecular Physiology of Membrane Guanylyl Cyclase Receptors. *Physiological reviews* 96, 751-804 (2016).

345. Owens, D.E., 3rd & Peppas, N.A. Opsonization, biodistribution, and pharmacokinetics of polymeric nanoparticles. *Int J Pharm* 307, 93-102 (2006).
346. Monopoli, M.P. et al. Physical–Chemical Aspects of Protein Corona: Relevance to in Vitro and in Vivo Biological Impacts of Nanoparticles. *Journal of the American Chemical Society* 133, 2525-2534 (2011).
347. Shahbazi, M.-A. et al. Augmented cellular trafficking and endosomal escape of porous silicon nanoparticles via zwitterionic bilayer polymer surface engineering. *Biomaterials* 35, 7488-7500 (2014).
348. Cedervall, T. et al. Understanding the nanoparticle-protein corona using methods to quntify exchange rates and affinities of proteins for nanoparticles. *P Natl Acad Sci USA* 104, 2050-2055 (2007).
349. Horio, T. et al. Inhibitory regulation of hypertrophy by endogenous atrial natriuretic peptide in cultured cardiac myocytes. *Hypertension (Dallas, Tex. : 1979)* 35, 19-24 (2000).
350. Kim, N. et al. Site specific differential activation of ras/raf/ERK signaling in rabbit isoproterenol-induced left ventricular hypertrophy. *Biochimica et Biophysica Acta (BBA) - Molecular Cell Research* 1763, 1067-1075 (2006).
351. van Berlo, J.H., Maillet, M. & Molkentin, J.D. Signaling effectors underlying pathologic growth and remodeling of the heart. *The Journal of Clinical Investigation* 123, 37-45 (2013).
352. Kamps, J.A.A.M. & Krenning, G. Micromanaging cardiac regeneration: Targeted delivery of microRNAs for cardiac repair and regeneration. *World Journal of Cardiology* 8, 163-179 (2016).
353. Bachelder, E.M., Beaudette, T.T., Broaders, K.E., Dashe, J. & Fréchet, J.M.J. Acetal-Derivatized Dextran: An Acid-Responsive Biodegradable Material for Therapeutic Applications. *Journal of the American Chemical Society* 130, 10494-10495 (2008).
354. Cohen, J.A. et al. Acetal-Modified Dextran Microparticles with Controlled Degradation Kinetics and Surface Functionality for Gene Delivery in Phagocytic and Non-Phagocytic Cells. *Advanced materials (Deerfield Beach, Fla.)* 22, 3593-3597 (2010).
355. Garlick, P.B., Radda, G.K. & Seeley, P.J. Studies of acidosis in the ischaemic heart by phosphorus nuclear magnetic resonance. *Biochemical Journal* 184, 547-554 (1979).
356. Khabbaz, K.R., Zankoul, F. & Warner, K.G. Intraoperative metabolic monitoring of the heart: II. Online measurement of myocardial tissue pH. *The Annals of thoracic surgery* 72, S2227-2233; discussion S2233-2224, S2267-2270 (2001).
357. Ferreira, M.P.A. et al. Drug-Loaded Multifunctional Nanoparticles Targeted to the Endocardial Layer of the Injured Heart Modulate Hypertrophic Signaling. *Small 13(33), 1701276 (*2017).
358. Ferreira, M.P.A. et al., Advanced Nanomedicines for the Treatment and Diagnosis of Myocardial Infarction and Heart Failure. *Current Drug Targets* 16, 1682-1697 (2015).
359. Yan Teck Ho, B.P., Hames Chen Yong Kah Nanoparticle drug delivery systems and their use in cardiac tissue therapy. *Nanomedicine* 11, 693-714 (2016).
360. Formiga, F.R. et al. Controlled delivery of fibroblast growth factor-1 and neuregulin-1 from biodegradable microparticles promotes cardiac repair in a rat myocardial infarction model through activation of endogenous regeneration. *Journal of Controlled Release* 173, 132-139 (2014).
361. Formiga, F.R. et al. Sustained release of VEGF through PLGA microparticles improves vasculogenesis and tissue remodeling in an acute myocardial ischemia–reperfusion model. *Journal of Controlled Release* 147, 30-37 (2010).
362. Chang, M.-Y. et al. Functionalized nanoparticles provide early cardioprotection after acute myocardial infarction. *Journal of Controlled Release* 170, 287-294 (2013).
363. Di Mauro, V. et al. Bioinspired negatively charged calcium phosphate nanocarriers for cardiac delivery of MicroRNAs. *Nanomedicine (Lond)* 11, 891-906 (2016).
364. Ma, H., Wang, L., Liu, J. & Qian, L. Direct Cardiac Reprogramming as a Novel Therapeutic Strategy for Treatment of Myocardial Infarction. *Methods in molecular biology (Clifton, N.J.)* 1521, 69-88 (2017).
365. Efe, J.A. et al. Conversion of mouse fibroblasts into cardiomyocytes using a direct reprogramming strategy. *Nature cell biology* 13, 215-222 (2011).
366. Ifkovits, J.L., Addis, R.C., Epstein, J.A. & Gearhart, J.D. Inhibition of TGFβ Signaling Increases Direct Conversion of Fibroblasts to Induced Cardiomyocytes. *PLOS ONE* 9, e89678 (2014).
367. Zhao, Y. et al. High-efficiency reprogramming of fibroblasts into cardiomyocytes requires suppression of pro-fibrotic signalling. *Nature communications* 6, 8243 (2015).
368. Inagawa, K. et al. Induction of cardiomyocyte-like cells in infarct hearts by gene transfer of Gata4, Mef2c, and Tbx5. *Circulation research* 111, 1147-1156 (2012).
369. Qian, L. & Srivastava, D. Direct Cardiac Reprogramming: From Developmental Biology to Cardiac Regeneration. *Circulation research* 113, 10.1161/CIRCRESAHA.1112.300625 (2013).
370. Raso, A. & Dirkx, E. Cardiac regenerative medicine: At the crossroad of microRNA function and biotechnology. *Non-coding RNA Research* 2, 27-37 (2017).
371. Fu, J.D. et al. Direct reprogramming of human fibroblasts toward a cardiomyocyte-like state. *Stem cell reports* 1, 235-247 (2013).
372. Cao, N. et al. Conversion of human fibroblasts into functional cardiomyocytes by small molecules. *Science* 352, 1216-1220 (2016).
373. Ifkovits, J.L., Addis, R.C., Epstein, J.A. & Gearhart, J.D. Inhibition of TGFbeta signaling increases direct conversion of fibroblasts to induced cardiomyocytes. *PLoS One* 9, e89678 (2014).
374. Tseng, A.S., Engel, F.B. & Keating, M.T. The GSK-3 inhibitor BIO promotes proliferation in mammalian cardiomyocytes. *Chemistry & biology* 13, 957-963 (2006).

Recent Publications in this Series

47/2017 Eeva Suvikas-Peltonen
Lääkkeiden turvallisen käyttökuntoon saattamisen edistäminen sairaaloiden osastoilla
48/2017 Pedro Alexandre Bento Pereira
The Human Microbiome in Parkinson's Disease and Primary Sclerosing Cholangitis
49/2017 Mira Sundström
Urine Testing and Abuse Patterns of Drugs and New Psychoactive Substances — Application of Comprehensive Time-of-Flight Mass Spectrometry
50/2017 Anna-Maija Penttinen
GDNF and Neurturin Isoforms in an Experimental Model of Parkinson's Disease
51/2017 Jenni Lehtonen
New Tools for Mitochondrial Disease Diagnosis: FGF21, GDF15 and Next-Generation Sequencing
52/2017 Jenni Pessi
Insights into Particle Formation and Analysis
53/2017 Stefan Björkman
Parturition and Subsequent Uterine Health and Fertility in Sows
54/2017 Elina Isokuortti
Non-alcoholic Fatty Liver Disease - Studies on Pathogenesis and Diagnosis
55/2017 Joni Nikkanen
Tissue-Specific Implications of Mitochondrial DNA Maintenance in Health and Disease
56/2017 Kiran Hasygar
Physiological Adaptation to Nutrient Starvation: A Key Role for ERK7 in Regulation of Insulin Secretion and Metabolic Homeostasis
57/2017 Miina Ruokolainen
Imitation of Biologically Relevant Oxidation Reactions by Titanium Dioxide Photocatalysis: Advances in Understanding the Mimicking of Drug Metabolism and the Oxidation of Phosphopeptides
58/2017 Tiia Maria Luukkonen
Consequences of Balanced Translocations and Loss-of-function Mutations
59/2017 Karoliina Hirvonen
Adenoid Cystic Carcinoma of Salivary Glands - Diagnostic and Prognostic Factors and Treatment Outcome
60/2017 John Liljestrand
Systemic Exposure to Oral Infections — a Cardiometabolic Risk
61/2017 Hanna Dyggve
Doberman Hepatitis — Role of Immunological and Genetic Mechanisms
62/2017 Tiina A. Lantto
Cytotoxic and Apoptotic Effects of Selected Phenolic Compounds and Extracts from Edible Plants
63/2017 Niina Laine
Use of Antimicrobials in a Tertiary Children's Hospital
64/2017 Jenni Hyysalo
Prevalence and Genetics of Non-alcoholic Fatty Liver Disease
65/2017 Agnieszka Szwajda
Bioinformatic Identification of Disease Driver Networks Using Functional Profiling Data
66/2017 Henri A. J. Puttonen
Neuropharmacological Properties of the Histaminergic System in the Zebrafish

Helsinki 2017 ISSN 2342-3161 ISBN 978-951-51-3863-7